

**SEDIMENTARY RECORD OF MEDITERRANEAN INFLOW EFFECT ON
REDOX CONDITIONS OF ISTANBUL STRAIT OUTLET AREA OF
BLACK SEA**

**M.Sc. Thesis by
Zeynep ERDEM**

Department : Climate and Marine Sciences

Programme : Earth System Science

June, 2011

**SEDIMENTARY RECORD OF MEDITERRANEAN INFLOW EFFECT ON
REDOX CONDITIONS OF ISTANBUL STRAIT OUTLET AREA OF
BLACK SEA**

**M.Sc. Thesis by
Zeynep ERDEM
601081007**

**Date of submission : 06/05/2011
Date of defence examination: 08/06/2011**

**Supervisor (Chairman) : Prof. Dr. M.Namık ÇAĞATAY (ITU)
Members of the Examining Committee : Prof. Dr. Naci GÖRÜR (ITU)
Prof. Dr. Mehmet KARACA (ITU)**

June, 2011

İSTANBUL TEKNİK ÜNİVERSİTESİ ★ AVRASYA YERBİLİMLERİ
ENSTİTÜSÜ

AKDENİZ AKINTISININ KARADENİZ'DE İSTANBUL BOĞAZI
ÇIKIŞINDAKİ REDOKS KOŞULLARI ÜZERİNE ETKİSİNİN SEDİMAN
KAYITLARININ İNCELENMESİ

YÜKSEK LİSANS TEZİ
Zeynep ERDEM
601081007

Tezin Enstitüye Verildiği Tarih : 06/05/2011

Tezin Savunulduğu Tarih : 08/06/2011

Tez Danışmanı : Prof. Dr.M.Namık ÇAĞATAY (İTÜ)
Diğer Jüri Üyeleri : Prof. Dr. Naci GÖRÜR(İTÜ)
Prof. Dr. Mehmet KARACA(İTÜ)

Haziran, 2011

FOREWORD

I would like to thank to;

My advisor Prof. Dr. Namık Çağatay for his continuous support, effort and guidance since my undergraduate years, and for giving me the opportunity to be a part of the EC FP7 project “HYPOX: In situ monitoring of oxygen depletion in hypoxic ecosystems of coastal and open seas and land locked bodies” and ITU EMCOL,

ITU EMCOL’s members, Umut Barış Ülgen, Dr. Ümmühan Sancar, Dr. Demet Biltekin, Sena Akçer Ön, Emre Damcı and Dursun Acar for their help and guidance with patience during the two cruises in the Black Sea and in the laboratory work,

Colleagues from partner institutes of the HYPOX project, who participated in the Black Sea cruises and the crew members of the RV Arar and RV MS Merian,

My ‘classmates’ and dear friends; Seden Baltacıbaşı, Gönenç Göçmengil, Emir Altıntaş, Semih Can Ülgen, Doğuşhan Kılıç, Esra Çetin, Nalan Lom, Pınar Gutsuz for their support and help whenever I needed,

My mother İlfan Erdem for her limitless patience and support,

Prof.Dr. A.M. Celal Şengör for his encouragement and support during the time of my M.Sc. studies.

I would like to dedicate this thesis study to my father, Nevzat Erdem, who passed away.

May, 2011

Zeynep ERDEM
ITU EMCOL

TABLE OF CONTENTS

	<u>Page</u>
FOREWORD	v
ABBREVIATIONS	ix
LIST OF TABLES	xi
LIST OF FIGURES	xiii
SUMMARY	xix
ÖZET	xxi
1. INTRODUCTION	1
1.1 Background	1
1.1.1 Basin history	1
1.1.2 Holocene stratigraphy	4
1.1.3 Redox sensitive elements: Mn, Br, I and Fe-S-Organic Carbon system.....	5
1.2 Study Area.....	8
1.2.1 Morphology and bathymetry.....	8
1.2.2 Oceanography	9
1.3 Scientific Problems, Thesis Objectives and Scope of the Study	11
2. MATERIALS AND METHODOLOGY	13
2.1 Sediment Cores and Sampling Methods	13
2.2 Multi Sensor Core Logger (MSCL)	14
2.3 Itrax XRF (X-Ray Fluorescence) Core Scanner	17
2.4 Total Organic and Total Inorganic Carbon Analysis	19
2.5 AMS Radiocarbon (¹⁴ C) Dating	20
3. RESULTS	21
3.1 Lithostratigraphy and Chronostratigraphy	21
3.1.1 Seismic Line 1 (SL1) cores	22
3.1.2 Seismic Line 8 (SL8) cores	29
3.2 MSCL Results	35
3.2.1 Seismic Line 1 (SL1) cores	35
3.2.2 Seismic Line 8 (SL8) cores	37
3.3 XRF Results	40
3.3.1 Seismic Line 1 (SL1) cores	40
3.3.2 Seismic Line 8 (SL8) cores	44
3.4 Total Organic Carbon and Total Inorganic Carbon Results.....	49
3.4.1 Seismic Line 1 (SL1) cores	49
3.4.2 Seismic Line 8 (SL8) cores	51
4. DISCUSSION	53
4.1 Changes in the Oxic/Anoxic Boundary.....	53
4.2 Mediterranean Water (MW) Effect	63
5. CONCLUSIONS	67
REFERENCES	69
APPENDICES	73
CURRICULUM VITAE	77

ABBREVIATIONS

AMS	: Accelerator Mass Spectrometry
App	: Appendix
B/A	: Bolling Allerod
CIL	: Cold Intermediate Layer
CTD	: Conductivity, Temperature, Depth
DOP	: Degree of Pyritization
EMCOL	: Eastern Mediterranean Centre for Oceanography and Limnology
LGM	: Last Glacial Maximum
MSCL	: Multi Sensor Core Logger
MW	: Mediterranean Water
OMZ	: Oxygen Minimum Zone
TC	: Total Carbon
TIC	: Total Inorganic Carbon
TOC	: Total Organic Carbon
XRF	: X-Ray Fluorescence
YD	: Younger Dryas

LIST OF TABLES

	<u>Page</u>
Table 3.1 : AMS C14 dating results, age errors and calibrated age data with error margins of selected core depths from selected cores.	21
Table A.1 : Sample table in appendix.	75

LIST OF FIGURES

	<u>Page</u>
Figure 1.1 : Location and the multibeam bathymetry of the study area, showing the main sampling transects; SL8 and SL1 and CTD profile locations; CTD4, CTD5 and CTD9.	2
Figure 1.2 : General Holocene stratigraphic section of Black Sea sediment, showing the evidence of anoxia and transitions of boundaries with calendar age; modified using the data of the previous studies (Degens and Ross, 1974; Arthur and Dean, 1998; Çağatay, 1999; Ryan et al., 2003; Major et al., 2006; and the references therein).....	3
Figure 1.3 :Elements of the surface circulation of the Black Sea (Oğuz et al.,1993).	8
Figure 1.4 : Bathymetry map of the study area, MW creates a delta fan structure with its channel-levée complex, bifurcation is seen in area in the square.	10
Figure 1.5 : Two way current system in the Istanbul Strait (Bosphorus) area and a graph showing the water column structure of Black Sea (Özsoy and Ünlüata, 1997).	11
Figure 1.6 : CTD cast profiles obtained durin R/V Arar cruise in November 2009. Fluctuations of temperature, conductivity and O ₂ at CTD9 and CTD5 indicate the active Mediterranean inflow in the area whereas at CTD4 there is no active inflow observed in the water column (Holtappels et al., in prep.). For locations of the CTD casts see Fig. 1.1.	12
Figure 2.1 : The locations of the seismic lines SL1 and SL8 and studied cores.....	14
Figure 2.2 : A typical MSCL configuration for soft sediments.	15
Figure 2.3 : Front view of the Itrax core scanner with open hoods (Croudace et al, 2006).	18
Figure 3.1 : Lithological description and radiographic image of MSM015-300 core located at -82m in eastern side (SL1) above present anoxic/oxic boundary. See Fig. 2.1 for core location.	23
Figure 3.2 : Lithological description and radiographic image of HBS09-G04C core located at -120m at eastern side (SL1) above the present anoxic/oxic boundary. Bioturbation and abundance of in situ shells are observed from radiographic image. See Fig. 2.1 for core location.	25
Figure 3.3 : Lithological description and radiographic image of the MSM015-245 core obtained from -152 m at eastern side (SL1) below the present anoxic/oxic boundary. There is an abrupt lithological change at 41 cm depth that is dated as 6.8 ka BP. See Fig. 2.1 for core location.....	27
Figure 3.4 : Lithological description and radiographic image of the MSM015-192 core obtained from -307 m at eastern side (SL1) below the present	

anoxic/oxic boundary showing no sharp lithological change. See Fig. 2.1 for core location.	28
Figure 3.5 : Lithological description and radiographic image of the HBS09-G18 core obtained from -93m at western side (SL8) above the present anoxic/oxic boundary. Decrease in the amount of shells are observed through the top part of the core whereas a distinct change in color is observed. See Fig. 2.1 for core location.	30
Figure 3.6 : Lithological description and radiographic image of the HBS09-G17B core obtained from -120 m at western side (SL8) above the present anoxic/oxic boundary. Sharp change of the amount of the shells gives an age of 6.8 ka BP. See Fig. 2.1 for core location.....	31
Figure 3.7 : Lithological description and radiographic image of the HBS09-G15B core obtained from -160m at western slope area (SL8) below the present anoxic/oxic boundary. 5.5 ka BP calibrated age determined is shown in the figure. See Fig. 2.1 for core location.	33
Figure 3.8 : Lithological description and radiographic image of the MSM015-311 core obtained at -307m from western slope area (SL8) below the present anoxic/oxic boundary. Sharp lithological change is dated as 5.3 ka BP. See Fig. 2.1 for core location.....	34
Figure 3.9 : Physical properties (MSCL results) of the MSM015-300 core located at -82m in the eastern side of the area (SL1). See Fig.2.1 for core location.	35
Figure 3.10 : Physical properties (MSCL results) of HBS09-G04C core collected from -120m at eastern side of the area (SL1). See Fig. 2.1 for core location.	36
Figure 3.11 : Physical properties (MSCL results) of the MSM015-245 core collected from -152m from eastern slope area (SL1). There is an abrupt change observed at 40-45 cm interval. See Fig. 2.1 for core location.	36
Figure 3.12 : Physical properties (MSCL results) of the MSM015-192 core collected from -307m on eastern slope area (SL1). Uppermost distinct fluctuation is because of the gas (H ₂ S) content. See Fig.2.1 for core location.	37
Figure 3.13 : Physical properties (MSCL results) of the HBS09-G18 core collected from -93m at western side (SL8). See Fig.2.1 for core location.	38
Figure 3.14 : Physical properties (MSCL results) of the HBS09-G17B core collected from -120m at western side (SL8). See Fig.2.1 for core location.	38
Figure 3.15 : Physical properties (MSCL results) of the HBS09-G15B core collected from -160m at the western slope area (SL8). See Fig.2.1 for core location.	39
Figure 3.16 : Physical properties (MSCL results) of the MSM015-311 core collected from -307m at western slope area. See Fig.2.1 for core location.	39
Figure 3.17 : XRF/depth profiles of K, Ti, Mn, Fe, S, Ca, Br and I in the MSM015-300 core located at -82m at eastern side (SL1), Ca peaks are due to shell content and Mn shows no changes. See Fig.2.1 for core location.	40

Figure 3.18 :XRF/depth profiles of K, Ti, Mn, Fe, S, Ca, Br and I in the HBS09-G04C located at -120m at the eastern side (SL1), showing Mn decrease above 23 cm core depth in association with increased Fe-S values. See Fig.2.1 for core location.....	41
Figure 3.19 :XRF/depth profiles of K, Ti, Mn, Fe, S, Ca, Br and I in the MSM015-245 core located at -152m, at eastern slope area. Sharp change in the amounts of elements at 40 cm core depth indicate presence of two different units. Above the boundary Mn shows fluctuations. See Fig.2.1 for core location.	43
Figure 3.20 :XRF/depth profiles of K, Ti, Mn, Fe, S, Ca, Br and I in the MSM015-192 core collected from -307m at eastern slope area (SL1), Mn shows fluctuations throughout the core beside Mn, the other measured elements do not show distinct changes. See Fig.2.1 for core location.....	44
Figure 3.21 :XRF/depth profiles of K, Ti, Mn, Fe, S, Ca, Br and I in the HBS09-G18 core collected from -93m at western side (SL8), show distinct increase in the amount of Mn, S and Br values at 7-13cm interval. See Fig.2.1 for core location.....	45
Figure 3.22 :XRF/depth profiles of K, Ti, Mn, Fe, S, Ca, Br and I in the HBS09-G17B core collected from -120m at western side (SL8), show sharp changes at 30 cm core depth and Mn shows distinct decrease at 3-7cm interval in association with Fe-S enrichment. See Fig.2.1 for core location.....	46
Figure 3.23 :XRF/depth profiles of K, Ti, Mn, Fe, S, Ca, Br and I in the HBS09-G15B core collected from -160m at western slope area (SL8), Mn values fluctuate below the depth of 8 cm, Fe-S enrichments are observed at the topmost 8 cm of the core where Mn is depleted. See Fig.2.1 for core location.....	47
Figure 3.24 :XRF/depth profiles of K, Ti, Mn, Fe, S, Ca, Br and I in the MSM015-311 core collected from -307m at western slope area (SL8), show a sharp change of the elemental data at around 40 cm core depth, Mn depletion observed above the boundary. See Fig.2.1 for core location.	48
Figure 3.25 :Depth (cm)/TOC and TIC profiles of Seismic Line 1(SL1)cores located at eastern part of the area. (a) MSM015-300 core from -83m, (b) HBS09-G04C core from -122m, (c) MSM015-245 core from -158m, (d) MSM015-197 core from -307m water depth. See Fig.2.1 for core locations.	50
Figure 3.26 :Depth (cm)/TOC and TIC profiles of Seismic Line 8 (SL8)cores located at western part of the area. (a) HBS09-G18 core from -93m, (b) HBS09-G17B core from -120m, (c) HBS09-G15B core from -160m, (d) MSM015-311 core from -307m water depth. See Fig.2.1 for core locations.	52
Figure 4.1 : MSCL, XRF and TOC/TIC results of MSM015-300 core collected from -93m in eastern side (SL1) above the present anoxic/oxic boundary. Yellow shaded areas indicate the intervals without shell, shell fragments and transported material. Elemental concentrations are in cps. See Fig. 2.1 for core location.....	54

- Figure 4.2 :** MSCL, XRF and TOC/TIC results of HBS09-G04C core collected from -120m in eastern side (SL1) above the present anoxic/oxic boundary. Green shaded areas indicate the distinct decrease in Mn-Fe-S values, yellow shaded area indicate reducing conditions by depleted Mn and enriched Fe-S values with increasing TOC values. Elemental concentrations are in cps. See Fig. 2.1 for core location.....55
- Figure 4.3 :** MSCL, XRF and TOC/TIC results of MSM015-245 core collected from -152m in eastern slope area (SL1) below the present anoxic/oxic boundary. Green shaded area indicate bottom water oxic conditions by high values of Mn, Ca and TIC and shell abundance. Sharp boundary is dated as 6.8 ka BP. Above the boundary Mn fluctuations show the MW ventilation effect. Elemental concentrations are in cps. See Fig. 2.1 for core location.....57
- Figure 4.4 :** MSCL, XRF and TOC/TIC results of HBS09-G17B core collected from -120m in western side (SL8) above the present anoxic/oxic boundary. Green shaded area indicate a different unit with shell abundant oxygenated bottom water conditions. Sharp boundary is dated as 6.8 ka BP. Yellow shaded area indicate anoxic to suboxic bottom water conditions. Elemental concentrations are in cps. See Fig. 2.1 for the core location..... 58
- Figure 4.5 :** MSCL, XRF and TOC/TIC results of MSM015-192 core collected from -307m in eastern slope area (SL1) below the present anoxic/oxic boundary. MW ventilation effect indicated by Mn fluctuations. Elemental concentrations are in cps. See Fig. 2.1 for the core location.....60
- Figure 4.5 :** MSCL, XRF and TOC/TIC results of HBS09-G18 core collected from -93m in western side above the present anoxic/oxic boundary. Upward decrease in the amount of oxygen is recorded. Yellow shaded area indicate the recent shoaling of oxic/anoxic boundary (See also Fig. 4.7). Elemental concentrations are in cps. See Fig. 2.1 for the core location.....62
- Figure 4.7 :** Ti normalized Fe-Mn-S element profiles of HBS09-G18 core located at -93m western side above the present anoxic/oxic boundary. Yellow shaded shows enrichment of Mn-Fe-S record of oxic/anoxic shoaling. Elemental concentrations are in cps. See Fig. 2.1 for the core location.....63
- Figure 4.8 :** MSCL, XRF and TOC/TIC results of HBS09-G15B core located at -160m western upper slope area below the present anoxic/oxic boundary. Oxic bottom water conditions prevailed during 5.5 ka BP indicated by in situ shells observed radiographic image below 20 cm. Yellow shaded area indicated the anoxic bottom water conditions with depleted Mn values in association with Fe-S enrichments. Elemental concentrations are in cps. See Fig. 2.1 for the core location.....65
- Figure 4.9 :** MSCL, XRF and TOC/TIC results of MSM015-311 core located at -307m in western slope area below the present anoxic/oxic boundary. Green shaded area shows the past oxic bottom water conditions before 5.3 ka BP. Lighter green area shows the transition zone from oxic to anoxic bottom conditions. Present MW ventilation effect not

recorded. Elemental concentrations are in cps. See Fig. 2.1 for the
core location.....66

SEDIMENTARY RECORD OF MEDITERRANEAN INFLOW EFFECT ON REDOX CONDITIONS OF ISTANBUL STRAIT OUTLET AREA OF BLACK SEA

SUMMARY

The İstanbul Strait (Bosphorus) outlet area of the Black Sea (ISBS) is the only connection of the anoxic Black Sea basin with the world ocean. This area is characterized by the Mediterranean inflow which has played a major role in forming a fan delta with channel-levée complex. This inflow is also responsible for the ventilation and sluggish deep circulation the anoxic Black Sea basin. The oxic-anoxic boundary is presently at 100-150 m depth, but may have varied in the past as result of the changes in the amounts of the Mediterranean inflow, of riverine water input and global sea level. The cores obtained from the study area were analyzed for physical properties, XRF elemental analysis and total organic (TOC) and inorganic (TIC) contents, and dated by AMS C14 analysis.

Cores located in the oxic zone above -150 m are green gray to gray mud without any distinct lamination whereas the cores in the anoxic zone are laminated and banded dark gray to black mud. Cores below -150 m show the presence of the suboxic to anoxic sediments of dark green to gray Sapropel and dark gray to black Coccolith units.

The anoxia development started after the latest connection with Mediterranean waters at 9.4 ka BP as known from the previous works. The anoxic/oxic boundary and increasing suboxic-anoxic bottom water conditions in the whole slope area are detectable by Mn, S and Fe anomalies in the cores at -150 m and -120 m, which is tentatively dated 6.8 ka BP. Mediterranean inflow used the main channel towards to NW transporting oxygenated waters to the western side of the area and this transportation stopped at 5.3 ka BP. Bottom water anoxic conditions started to prevail in the area at that time as a result of this change in the direction of the inflow. The ventilation effect of Mediterranean waters on the seafloor can be followed at the eastern side of the outlet area down to -307 m (depth limit of the transects) by high Mn counts on the XRF scanner profiles, whereas on the western side of the area no active ventilation effect observed in the sedimentary record. Such Mn anomalies in upper slope cores, unassociated with Fe and S anomalies, are probably formed by deposition of Mn(II) from the water column. In addition to Mn anomalies the transition from oxic to anoxic conditions are shown by changes in mud colour from gray green through gray and dark gray to black and by the disappearance of the euryhaline bivalves.

AKDENİZ AKINTISININ KARADENİZ'DE İSTANBUL BOĞAZI ÇIKIŞINDA REDOKS KOŞULLARI ÜZERİNE OLAN ETKİSİNİN SEDİMANTER KAYITLARININ İNCELENMESİ

ÖZET

Karadeniz'in dünya okyanus sistemi ile tek birleşim kanalı olan İstanbul Boğazı'nın çıkışı, kıtasal şelf ile kıtasal yamaçların üst kesimlerinden oluşmaktadır. Bölgenin karakteristik özelliği olan ağır dip Akdeniz akıntısı, anoksik Karadeniz havzasına girerek havzanın oksijenle havalanmasından sorumludur. Günümüz koşullarında oksik-anoksik sınırı su kolonunda 100-150 metre arasındadır ancak global deniz seviyesi değişimleri, havzaya gelen Akdeniz akıntısının ve nehir girdisinin miktarına bağlı olarak bu sınır geçmişte değişiklikler göstermiştir. İstanbul Boğazı'nın Karadeniz ile bulunduğu bölgeden oluşan çalışma alanından alınan karotlarının fiziksel özellikleri, XRF (X-Ray Floresans) yöntemi ile elementer analizleri ve toplam organik karbon (TOC) ve toplam inorganik karbon (TIC) değerleri ölçülmüştür ve bu ölçümlere dayanarak belirli seviyelerde AMS C14 yaş tayini yapılmıştır.

-150 metreden daha sığ ve oksik alandan alınan karotlar belirgin laminasyon göstermeyen kavkı içerikli yeşil gri ve gri renkte çamur, anoksik ortamdan alınan karotlar laminalı ve bantlı koyu gri-siyah renkli çamur özelliği göstermektedir. -150 metreden daha derinden alınan karotlarda suboksik ve anoksik koyu yeşil – gri renkli Sapropel birimi ile koyu gri-siyah renkli Kokolit birimi gözlenmektedir.

Havzaya Akdeniz suyunun girmesinden sonra, günümüzden 9,4 binyıl öncesinde anoksik koşullar gelişmeye başlamıştır. Mn, Fe ve S anomalileri ve değişen kavkı içerikleri göz önünde bulundurularak, anoksik/oksik sınırı ve yükselen suboksik-anoksik dip su koşullarının sedimanter kayıtları -120m ve -150m karotlarında gözlenebilmektedir ve yapılan yaş tayinleri neticesinde bu seviye GÖ 6,8 binyıl olarak yaşlandırılmışlardır. Akdeniz akıntısı, GÖ 5.3 binyıl öncesine kadar, KD yönlü ana kanalı kullanarak bölgesinin batısında oksik dip su koşullarını sağlamıştır. Şelf alanının doğusunu oluşturan bölgede -307metre derinlikten alınan karotlarda yüksek Mn değerleri göz önünde bulundurularak Akdeniz akıntısının etkisi gözlenebilmektedir. Şelfin daha sığ bölgelerinden alınan karotlarda gözlenen Fe ve S anomalileri ile ilişkilendirilmemiş bu tarz Mn değişimleri büyük olasılıkla su kolonunda oluşmuş Mn(II)'nin çökelişi sonucudur. Mn anomalilerine ek olarak karotlarda gözlenen yeşil griden koyu gri-siyah renge geçiş ve kavkı içeriği de oksik koşullardan anoksik koşullara geçişi simgeleyen özelliklerden bir diğeridir.

1. INTRODUCTION

Black Sea is the largest anoxic basin in the world today and İstanbul Strait (Bosphorus) is the only connection of Black Sea to the world ocean via Sea of Marmara and Dardanelles Strait. Warm and saline Mediterranean inflow enters to Black Sea basin as an undercurrent, creates a delta fan structure with its levée-channel system and mixes with Black Sea deep waters (Özsoy and Ünlüata, 1997). Shallow sill depth of the İstanbul Strait together with the oxygen consumption by organic matter mineralization is responsible for the establishment of a permanent oxic-anoxic boundary (chemocline). Today the oxic-anoxic interface is at around 100-150m water depth. The Black Sea surface circulation is characterized by the cyclonic rim current that follows the shelf edge and upper slope areas.

The amount of the Mediterranean inflow and velocity of the rim current are function of the climate that are the major controlling parameters of the oxic/anoxic boundary level. Variations in the amount of riverine water input and global sea level also affect the amount of the Mediterranean Water (MW) input which enters through the İstanbul Strait (Bosphorus). The İstanbul Strait outlet area is therefore believed to be a sensitive recorder of the past changes in climatic and environmental conditions in the Black Sea (Fig. 1.1).

1.1 Background

1.1.1 Basin history

Black Sea sediments have recorded important changes of the oceanographic and environmental conditions since the Last Glacial Maximum (LGM), including the sea level, salinity, anoxic and climatic changes. The shallow sill depth at the İstanbul Strait has caused the connection of the Black Sea with the world ocean system to be cut off during the glacial low stands, exposing the strait and the shelf. Multi-proxy data by Bahr et al. (2008) provide evidence of environmental changes in the Black Sea during the late glacial-early Holocene interval. The Black Sea was a stable fresh water lake until about 16.5 ka BP when melting ice sheets provided large amount of

melt waters to the basin and deposited the brown clays rich in radiogenic Sr. During the Bolling Allerod (B/A) (15-13 ka BP) there was lowering of the lake level as a result of evaporation. High lake levels are recorded as a result of cold and wet climate of Younger Dryas (YD) (ca. 13-12 ka BP) period (Ryan et al., 2003; Major et al. 2006). During the lake period of the basin lacustrine Lutite Unit (Unit 3) was deposited (Fig. 1.2; Degens and Ross, 1974; Çağatay et al, 1999 and the references therein).

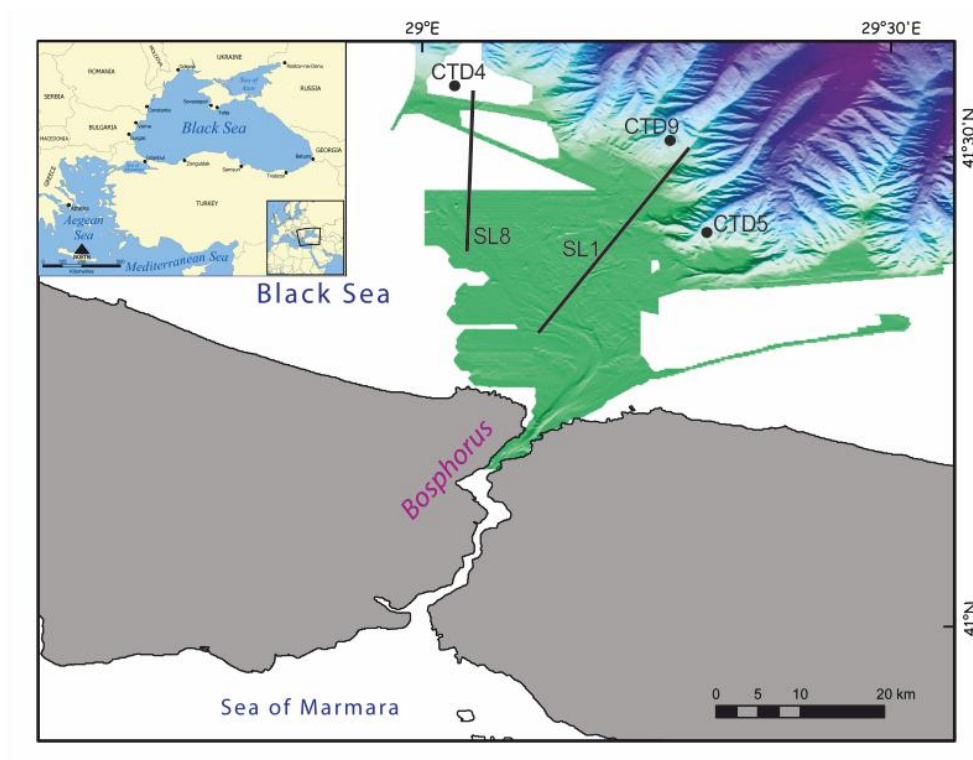


Figure 1.1 : Location and the multibeam bathymetry of the study area, showing the main sampling transects; SL8 and SL1 and CTD profile locations; CTD4, CTD5 and CTD9.

The beginning of the inflow of marine waters at 9.4 ka BP is clearly indicated by sudden increases in the Sr- and O-isotope data (Ryan et al, 2003; Major et al, 2006). There is a consensus that the anoxia in the Black Sea has developed as a result of the restricted circulation due to sharp density stratification, weak vertical circulation and organic matter degradation (e.g., Ross and Degens, 1970; Arthur and Dean, 1998; Çağatay, 1999). After the connection, high organic productivity and restricted circulation conditions caused deposition of a Sapropel Unit (Unit 2) and development of anoxia starting at 7-8 ka BP. (Degens and Ross, 1974; Calvert, 1990; Arthur and Dean, 1998; Çağatay, 1999).

The onset of the Holocene anoxia and sapropel deposition has generally been assumed to be coeval in the Black Sea, although this issue is still a matter of debate. According to some workers the Black Sea Holocene Sapropel Unit (Unit 2) was deposited under oxic bottom-water conditions (Calvert et al., 1990; Calvert and Pedersen, 1993). Another issue is the rate of development of the anoxia and the rise of the oxic/anoxic boundary in the water column. Considering that the start of the marine transgression of the Black Sea at 9.4 ka (Ryan et al, 2003; Major et al, 2006) and sapropel deposition at ca 7.5-8 ka BP (Jones and Gagnon, 1994; Arthur and Dean, 1998; Bahr et al, 2006; 2008), there appears to be time lag of about 1.5 ka between the two events (Fig. 1.2).

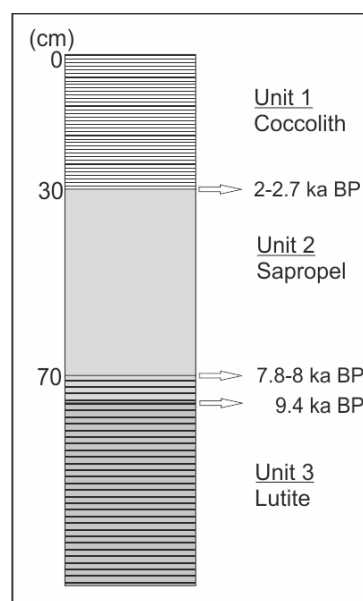


Figure 1.2 : General Holocene stratigraphic section of Black Sea sediment, showing the evidence of anoxia and transitions of boundaries with calendar age; modified using the data of the previous studies (Degens and Ross, 1974; Arthur and Dean, 1998; Çağatay, 1999; Ryan et al., 2003; Major et al., 2006; and the references therein)

With the invasion of the basin by the coccolithophore *Emiliana huxleyi* at about 3 ka BP (Ross and Degens, 1970) a microlaminated Coccolith Mud Unit (Unit 1) started to deposit in the basin establishing the present oceanographic conditions (Fig. 1.2). These three units can be traced over most of the deep Black Sea basin and reflect the basin evolution during Holocene.

Over the last several decades Black Sea has been severally affected by natural and environmental degradation mainly because of riverine input of contaminants and nutrients (Oğuz et al, 2002; 2005). There have been claims of oxic/anoxic boundary

shoaling and/or thickening of anoxic zone by several tens of meters in recent years (Murray et al, 1989; Codispoti et al, 1991; Lyons, 1993; Oğuz et al, 2002; 2005). Others indicate, however, the structure and position of the interface has been reasonably stable within the last several decades, especially when compared to existing density stratification (Tuğrul et al, 1992; Baştürk et al, 1994; Özsoy and Ünlüata, 1997). According to Lyons (1993) Fe-Mn-S profiles of cores in the Istanbul Strait outlet area of the Black Sea show enrichments of pyrite-Fe and Mn that strongly suggest chemocline shoaling in this region by 40-50 m about 250-300 a BP. During about the same period, Güngör and Çağatay (2006) found high CaCO₃ deposition of coccolithophore origin in the Black Sea during 1750-1650 AD, which corresponds to the Late Maunder Minimum, the coldest period of the Little Ice Age.

1.1.2 Holocene stratigraphy

The Holocene stratigraphic sequence of the Black Sea consists of 3 units, Unit 1, 2 and 3 (Ross and Degens, 1974).

Unit 1 is the most recent sediment unit with ~30 cm thick coccolith marl, consisting of alternations of light and dark colored microlaminae. The dark-light laminae couplets in Unit 1 are ~0.2 mm thick and consist of white, coccolith-rich material alternating with dark organic-and clay-rich material containing diatoms (Çağatay, 1999). Unit 1 contains 1%-10% organic carbon and 10%-75% CaCO₃ consisting almost entirely of remains of *Emiliana huxleyi*, and a remainder dominated by detrital clay (Arthur and Dean, 1998). The clay minerals consist predominantly of chlorite, smectite and illite. Pyrite formation is limited mainly by iron availability in the Unit 1 sediments (Wilkin and Arthur, 2001).

Unit 2 is ~40 cm thick sapropel, consisting mainly of gelatinous organic matter with some coccolith remains, clays, inorganically precipitated aragonite, iron monosulfides and pyrite. Chlorite/illite and smectite/illite ratios are lower than the other two units, suggesting a warmer climate during its deposition than the present one. The sapropel unit was deposited during a period of high plankton productivity after the flooding of the lacustrine Black Sea basin by the Mediterranean waters via Istanbul Strait, (Çağatay, 1999). Unit 2 contains 3%-20% organic carbon and 5%-15% CaCO₃.

The transition between Unit 2 and Unit 3 is marked by a sharp downward decrease in organic carbon content to values that are generally <1.0% in unit 3 and a change downward from laminated sapropel typical of Unit 2 to macrobioturbated clay typical to Unit 3. This transition in organic carbon content and bioturbation occurs over a stratigraphic interval of 2-5 cm, equivalent to a time interval of <1.0 kyr (Arthur and Dean, 1998).

The oldest Pleistocene – Holocene sediments, Unit 3, are composed of laminated organic carbon-poor clays (<1% organic carbon). It includes dark laminae that are formed by high concentrations of unstable iron mono-sulfides. The chlorite/illite and smectite/illite ratios in this unit are as high as in Unit 1 (Çağatay, 1999). The upper part of Unit 3 consists predominantly of greenish-gray to olive-gray clay that is homogeneous, coarsely banded, or marked with black streaks, pods, and laminae relatively enriched in iron monosulfides (Arthur and Dean, 1998). Unit 3 was deposited under freshwater lacustrine conditions during ~30000 – 7000 yr BP when the water level of Black Sea was about 100 m lower the present sea level (Çağatay, 1999).

1.1.3 Redox sensitive elements: Mn, Br, I and Fe-S-organic carbon system

In modern marine environments, early diagenesis proceeds in a general sequence by redox reactions in which the oxidants are used in the order: oxygen > nitrate > manganese oxides > iron oxides > sulphate (e.g., Chester, 2000), but the diagenetic processes are not always sequential, i.e. in anoxic environments the sediment interstitial water does not contain dissolved oxygen so anaerobic metabolism occurs and diagenesis has to proceed via secondary oxidants. During diagenesis, elements are mobilized into solution and migrate through the interstitial water. Although some of the elements are incorporated into newly formed minerals, the others can be released into the overlying seawater. Diagenetic processes are intimately related to the interstitial water chemistries of many trace metals, including those transported down the water column and those associated with the secondary oxidants (Chester, 2000).

Previous studies on black shales and diagenetic processes on modern sediments show that some trace metals are redox sensitive elements. They are good indicators of changes in oxic, suboxic or anoxic conditions. Variations in the oxygenation of water

column and of the bottom water (along with the uppermost 1-2 cm of sediment) affect the concentrations of the redox sensitive elements in marine sediments. The concentrations are affected also by the amount of refractory detrital inventory (Yarincik et al., 2000). Authigenic metal fluxes increase and get enriched closer to the sediment-water interface as oxygen penetration becomes shallower and reducing conditions intensify (Klinkhammer and Palmer, 1991; Crusius et al, 1996; Morford and Emerson, 1999).

Black Sea Basin with its similarity to Cariaco Basin, Venezuela, has been subject for several studies for prevailing redox conditions. Manganese exists as Mn (IV) oxide in the oxic and as dissolved Mn (II) in the anoxic water layers of the Black Sea Basin (Çağatay, 1999). In the water column, Mn maximum is often observed at the level of oxygen minimum zones wherever oxygen concentrations fall below 100 μM (Calvert and Pedersen, 1993). Dissolved Mn (II) accumulates in the deep sulphidic waters of anoxic basins due to the downward migration and reduction of Mn (IV) oxides from oxic layers above the redox boundary. In the suboxic zone, the concentrations of dissolved Mn get higher than the deeper parts of the water column whereas immediately above the suboxic zone upward diffusing Mn^{2+} gets oxidized settling a particle concentration maximum (Calvert and Pedersen, 1993 and the references therein). Both Fe and Mn are more soluble in their reduced states (Calvert and Pedersen, 1993; Thomson et al, 1995; Crusius et al, 1996; Morford and Emerson, 1999; Yarincik, 2000 and the references therein) and thus during periods of water column anoxia the amounts of Fe and Mn in the bulk sediment should be lower (Yarincik, 2000). Authigenic enrichment of Mn occurs under oxic conditions and as the conditions become reducing, Mn is released to the overlying seawater.

Fe-S-Organic C system has been a subject for previous workers to understand the early diagenesis in marine sediments. In the presence of labile organic material, hydrogen sulphide is formed microbially in the sulphate reduction zone that consumes reactive iron which is delivered by detrital sediment (Lyons and Severmann, 2006). As a result of these reactions, sedimentary pyrite forms. There has been a debate about the limiting factors for sedimentary pyrite formation. According to the study of Berner and Raiswell (1983), in modern normal marine settings organic matter is the limiting factor whereas under freshwater to brackish conditions sulphate is the limiting factor. Under euxinic (anoxic) conditions, which

are defined as having free H₂S in the water column, pyrite forms with higher degrees of pyritization (DOP). According to work of Canfield et al, (1992) based on the total Fe content and the relationship between Fe present in sulphide minerals of Black Sea sediments, the microlaminated Unit 1 of Black Sea is relatively more enriched in reactive Fe compared to highly reactive Fe concentrations in sediments from normal marine environments. These enrichments are described by the syngenetic pyrite formation by rapid bacterial sulphate reduction and scavenging of dissolved Fe in water column. According to Wilkin et al, (1997); change in the size distributions of framboidal pyrite in Holocene Black Sea sediments exhibits a change from deposition under an oxic water column to deposition under an anoxic and sulfidic water column. Framboids in sediments of modern euxinic basins, including Black Sea, are characteristically smaller and less variable in size than those contained in sediments deposited under oxic water columns. Under oxic to suboxic conditions, all pyrite forms diagenetically in the sediments and larger framboids form. A reactive Fe shuttle mechanism is described by Lyons and Severmann (2006), which operates in euxinic basins. According to this shuttle system; as a result of suboxic diagenesis of lithogenous Fe bearing shelf sediments, Fe(II) diffuses into the overlying bottom waters. Most of the Fe is likely to be reoxidized at/near the sediment-water interface and recycled to the sediment as Fe-oxyhydroxides, whereas during water column precipitation of Fe sulphide under anoxic conditions, high amount of exported Fe from the oxic shelf is sequestered in the deep basin. In chemocline, Fe(II)_{aq} is exported to deep basin as pyrite without oxidative recycling.

The behaviours of bromine (Br) and Iodine (I) in marine sediments are associated with the diagenetic reactions involving organic matter remineralization. Their concentrations are related to the organic matter content in marine sediments and under anoxic conditions I is depleted relative to Br (Calvert and Pedersen, 1993 and the references therein). According to the study on Mediterranean S1 sapropel, only Br is systematically related to the highest amounts of C_{org} or S in the sapropel unit (Thomson et al, 1995).

1.2 Study Area

The study area is located at south western part of Black Sea at the northern coast of Istanbul (Turkey) where the Istanbul Strait (Bosphorus) forms an outlet connecting Black Sea to Sea of Marmara (Fig. 1.1). The area affected by the ventilation of Mediterranean inflow and the active surface circulation by the rim current transporting input of major rivers of Black Sea (i.e. Danube, Dniester; Fig. 1.3). The area is also a good evidence of the latest marine connection and resulting anoxia.

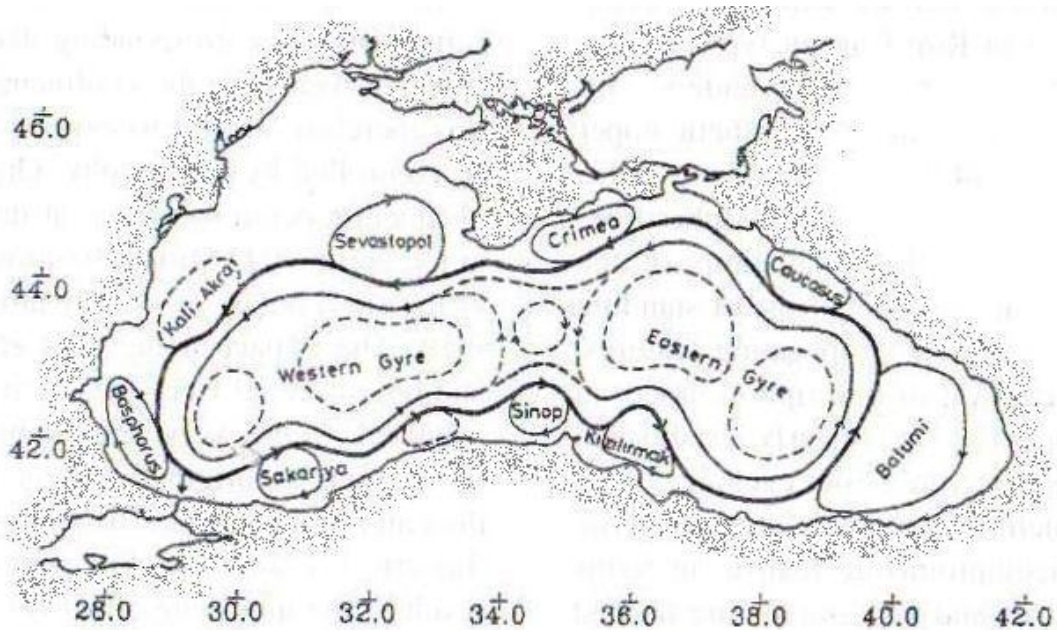


Figure 1.3 : Elements of the surface circulation of the Black Sea (Oğuz et al.,1993).

1.2.1 Morphology and bathymetry

Today the Black Sea represents the largest anoxic basin with its 5×10^5 area and 5.4×10^5 volume (Jones and Gagnon, 1994) with ~2200 m maximum depth (Özsoy and Ünlüata, 1997). The Black Sea basin consists of continental shelf, continental slope, basin apron and abyssal plain. The shelf is wider in northwest where Danube River meets the Black Sea whereas the southern shelf is narrow (<20 km) along the Anatolian coastline. The only connection between the basin and world ocean system takes place in southern part of the basin which is the Istanbul Strait (Bosphorus) with 31 km length, 0.7-3.5 km width and -35 m shallow sill depth.

The Istanbul Strait outlet area of the Black Sea includes the shelf and upper slope areas north of the strait. The shelf break occurs at around 100-150 m water depth.

The continental slope off Anatolids generally steep (5-9%), and cut by numerous submarine canyons and gullies, lead to the deep Black Sea basin (Duman et al, 2006). The multibeam bathymetry mapping of the region was carried out by Di Iorio and Yüce (1998) and Flood et al, (2009).

The bathymetry map of the area shows the extension of the Bosphorus channel from the coast towards northeast (Fig. 1.4). The channel which is formed by the Mediterranean inflow makes a turn toward northwest about 10 km from the coast where it is blocked by a bend caused by the Upper Cretaceous volcanic rocks in the area. Between the coast and the bend, the channel is up to 35 m below the seafloor with a rough topography. After the bend the channel spreads out to become <10 m deep and forms a fan delta on the mid and outer shelf areas with anastomosed distributary channels, 5-8 m high levées, in channel stream lined bars, crevasse splays, and NW-SE oriented linear to wavy sedimentary structures in between the channel-levée complexes. The outer shelf channel bifurcation increases (Fig. 1.4; Di Iorio and Yüce, 1998; Flood et al., 2009).

1.2.2 Oceanography

The bulk of the riverine runoff (up to 80%) is delivered to the northwestern part of the Black Sea by the major rivers such as Danube (200 km³/yr), the Dnieper (50 km³/yr), and the Dniester (10 km³/yr). The only connection of the basin to the world ocean system is via İstanbul (Bosphorus) and Dardanelle Straits, respectively. The İstanbul Strait with its 31 km length, 0.7-3.5 km width and -35 m sill depth, is a pathway of a two way exchange of surface Black Sea waters (salinity 17-18‰) and deep saline Mediterranean inflow (salinity 22‰) at rates 605 km³/yr and 305 km³/yr respectively (Özsoy and Ünlüata, 1997).

The Mediterranean Water (MW) which is the carrier of oxygen to the deep basin, with a 14.5°C and thickness of 10 m, overflows a -60 m sill then follows a steep bottom channel towards NE, and reach flat mid-shelf region where it spreads forming 2-3 m thick saline sheet (Di Iorio and Yüce, 1998; Di Iorio et al., 1999; Özsoy et al., 2001). At depths of 50-75 m it mixes with the Cold Intermediate Layer (CIL) and its salinity and temperature decrease to 31‰ and 8°C at the shelf edge (Fig. 1.5).

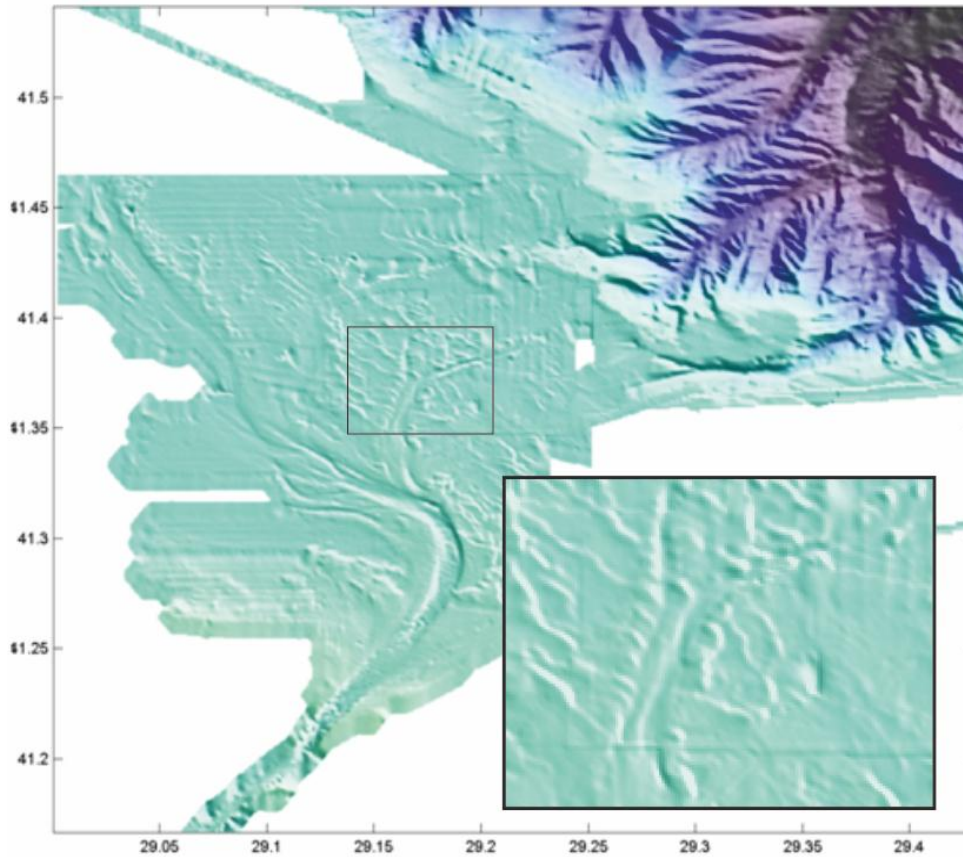


Figure 1.4 : Bathymetry map of the study area, MW creates a delta fan structure with its channel-levée complex, bifurcation is seen in area in the square.

With its high density it sinks along the continental slope forming a series of lateral intermediate depth intrusions (Özsoy and Ünlüata, 1997). The Mediterranean Water is the important driver of bottom water circulation below the halocline. The stratified water column structure of the Black Sea is a result of warm and saline Mediterranean inflow through the basin.

A strong pycnocline-chemocline is produced at -100 to -150 m depth in the Black Sea, separating the aerated brackish waters (17-18‰) from anaerobic, H₂S-rich more saline waters (22‰; 8.9°C) (Özsoy and Ünlüata, 1997). The chemocline depth is ~100 m and the suboxic zone is at 85-120 m near the head of the Bosphorus canyon.

During the cruises in November 2009 and April 2010 CTD studies were carried out. According to the CTD data, around -100 m depth there occurs an oxygen minimum zone (OMZ) and below 100 - 150 m water column becomes totally sulphidic and more saline. The surface circulation in the İstanbul Strait outlet area is characterized

by a cyclonic rim current and Bosphorus anticyclonic current (Fig. 1.3; Oğuz et al., 1993).

1.3 Scientific Problems, Thesis Objectives and Scope of the Study

Main scientific questions in the İstanbul Strait outlet area of Black Sea are;

- Did the anoxic/oxic interface change during decadal to millennial time scales?
- How are the vertical changes in the position of the oxic-anoxic interface related to the climate and other environmental changes?
- What are the useful proxies in determination of the long term sedimentary records of anoxia in the Black Sea?
- What is the role of the Mediterranean water in the ventilation of the deep Black Sea basin? Has this role changed with time?

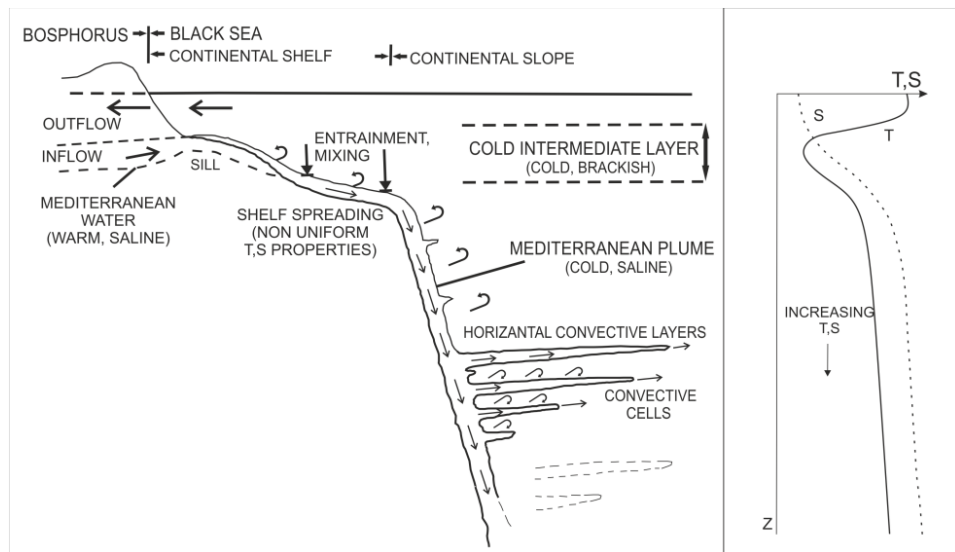


Figure 1.5 : Two way current system in the Istanbul Strait (Bosphorus) area and a graph showing the water column structure of Black Sea (Özsoy and Ünlüata, 1997).

The objectives of this thesis are to answer these questions using geochemical and physical analysis of cores recovered along depth transects in the İstanbul Strait outlet area of the Black Sea (Fig. 1.1). The transects were selected on the basis of CTD casts in the area at the time of core collection during R/V Arar cruise in November 2009, which showed that the NE-SW SL1 transect is affected by the Mediterranean

Water (MW), all the way to the depths of 300 m measurement depth, whereas transect SL8 located at western part of the study area was not influenced by the MW (Fig. 1.6; Holtappels et al, in prep.).

The cores are analyzed for multi-element analysis using XRF core scanner, for physical properties using MSCL and TOC/TIC analysis using a TOC analyzer. In situ benthic bivalves and foraminifera are selected for AMS ^{14}C dating.

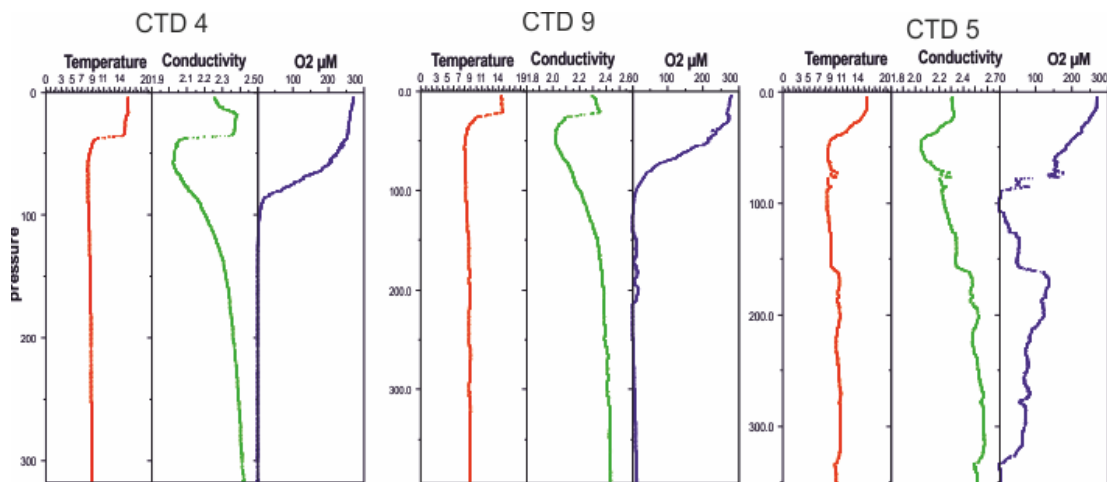


Figure 1.6 : CTD cast profiles obtained during R/V Arar cruise in November 2009. Fluctuations of temperature, conductivity and O₂ at CTD9 and CTD5 indicate the active Mediterranean inflow in the area whereas at CTD4 there is no active inflow observed in the water column (Holtappels et al., in prep.). For locations of the CTD casts see Fig. 1.1.

2. MATERIALS AND METHODOLOGY

In this chapter, details about the field trips took place in the study area; materials, equipments and methodology for the analysis are described. This thesis study includes the work that is carried out by İTÜ EMCOL as a part of European Commission 7th framework project called “Hypox: In situ monitoring of oxygen depletion in hypoxic ecosystems of coastal and open seas and land-locked water bodies”. Within the Hypox Project, two cruises took place in the study area, which are Turkish R/V Arar in November 2009 and German R/V M.S. Merian in April 2010. High resolution seismic reflection survey, sediment coring and CTD studies are carried out during these cruises. In total, over 80 short sediment cores with 7 cm diameter liners are collected by piston-interface corer. From the eight seismic profiles obtained from the study area, seismic lines 1 and 8 are considered to be the most important ones due to their locations. Seismic Line 1 (SL1) and Seismic Line 8 (SL8) starts at -75m water depth from the shallow area of the continental shelf and continues until the continental slope area to -300m water depth. These two transects give detailed information about the delta fan structure, channel-levée complex and the morphological details. Cores studied in this thesis are located along depth transects on seismic lines SL1 and SL8 on the continental shelf (Fig. 2.1). There is also long gravity cores obtained which is out of this thesis studies’ main subject.

2.1 Sediment Cores and Sampling Methods

The analysis which take place in this study are obtained with the equipments in the laboratories of İTÜ EMCOL. After recovery, physical properties of all cores are measured by Geotek Multi Sensor Core Logger (MSCL) with 0.5 cm resolution; they are split into two halves as archive and samples parts. From sample part of the cores, 2 cm thick sediment samples are obtained with 5 cm intervals for TOC/TIC analysis and for observations of benthic populations. X-Ray Fluorescence (XRF) analyses are done with archive sections by Itrax XRF Core Scanner with 0.05mm resolution.

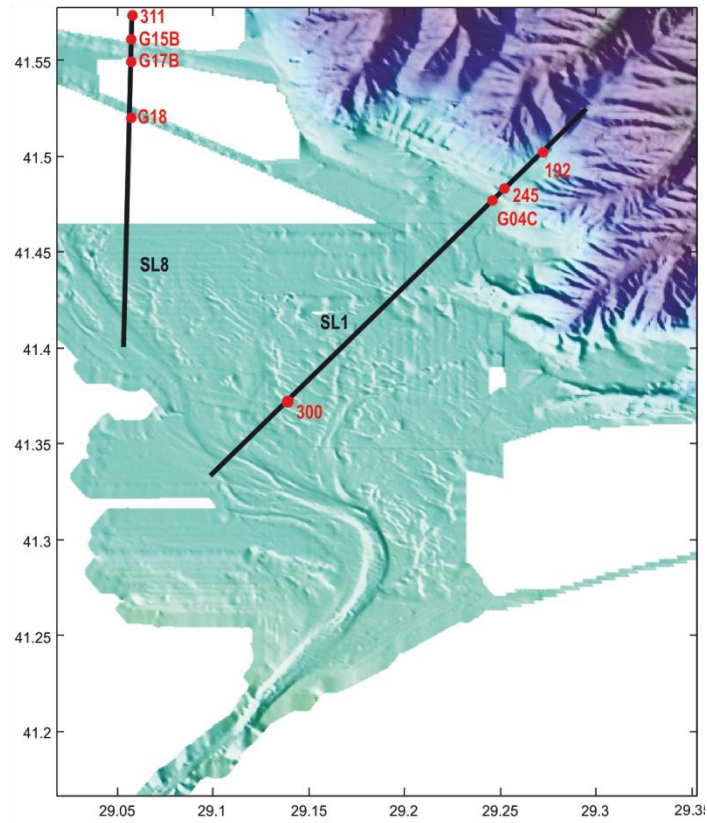


Figure 2.1 :The locations of the seismic lines SL1 and SL8 and studied cores.

All the graphical images are obtained by using free license program called PanPlot which is accessible through pangaea.de web address. From the preliminary results, some levels are identified for AMS (Accelerated Mass Spectrometer) radiocarbon dating and samples are obtained from these levels to be washed with 63 μm sieve. Both archive and sample sections of the cores are stored in İTÜ EMCOL cold storage.

2.2 Multi Sensor Core Logger (MSCL)

MSCL, located in İTÜ EMCOL's laboratories, is an equipment used for analysing high resolution physical properties of the soft sediment and rock core samples in automatic, accurate and quality controlled way using geophysical methods. It contains gamma density, magnetic susceptibility, P-wave velocity and electric resistivity sensors mounted on to measure different physical properties (Fig. 2.2). MSCL can measure up to 1.5 long samples with 50-150 mm diameter. Both the whole core samples and split ones can be scanned without disturbing the sample. The analysis is done automatically using software based on "Windows" operating system

prepared for this equipment. Core sections get pushed towards to the mounted sensors by an automatic pusher driven by a stepper motor with a user defined resolution. Each section gets measured as it passes the sensors. Stepper motor is controlled by computer which also controls the sensors, so that all the data including the length of each core section are correlated and saved automatically and also the sections can follow sequentially without breaking stream of data (webpage of Geotek MSCL, 2011).

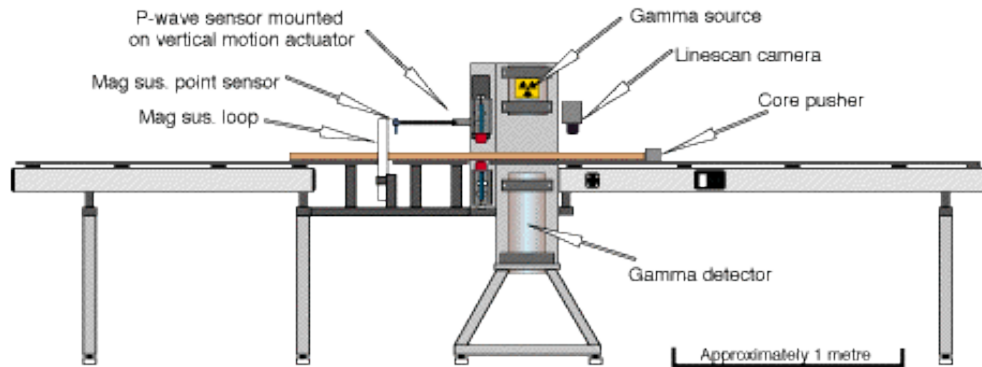


Figure 2.2 :A typical MSCL configuration for soft sediments.

MSCL measures length of the samples by line scan camera, gamma density by radioactive gamma source and detector, P-wave velocity by P-wave sensor mounted on horizontally, thickness of samples by a mechanic sensor which takes place on P-wave sensor, electric resistivity by resistivity sensor and magnetic susceptibility by magnetic susceptibility loop sensor.

According to the calibration measurements, graphs and formulas are created by the software, and these data are used for the whole analysis until the equipment is turned off. Created calibration file and formulas are used to evaluate the raw data. During the measurements for this study, sediment core samples are used as whole sections with a resolution of 0.5 cm. The main measurements of Geotek MSCL are briefly summarized below (webpage of Geotek MSCL, 2011):

1. Temperature: Both the temperature of the room and the cores can be measured with 0.01°C sensitivity by a PRT probe. Temperature data is used for calibration files.
2. Gama Density (GD): A gamma ray source and a detector are mounted on instrument in which core sections pass through the centre of them. A beam of collimated gamma rays are emitted from Cs-137 source and these emitted

gamma rays – photons – pass through the core and meet the detector. By measuring the number of transmitted gamma photons that pass through the core unattenuated the density of the core material can be determined. Calibration for this measurement is done with a cylindrical piece of aluminium of varying thickness surrounded completely by water in a sealed liner which is the same type of liner of cores.

3. Core Sample Thickness: There are two sensors in motion with a mechanic spring mounted on P-wave sensor. As the sample passes these sensors move horizontally and measures the thickness with 0.01 mm sensitivity.
4. P-wave Velocity: Measurements of almost any composition cores are obtained by the Acoustic Rolling Contact (ARC) transducers. This system is operated for core section measurements and its centre frequency is 230 kHz. The ARC transducer uses an active transducer element with a material which combines high coupling with relatively low acoustic impedance. Precise repeatable timing measurements can be obtained with the high signal to noise (S/N) ratio resulting from the use of the lower frequency and good coupling with the wide bandwidth. Large contact area and lower frequency provide improved S/N enabling accurate velocity measurement even through coarse sand.
5. Non-Contact (Electric) Resistivity (NCR): A transmitter coil induces electrical currents in the core which are inversely proportional to the resistivity. This way a high frequency magnetic field in the core is induced as a part of NCR technique. Along the core of approximately 2 cm, resistivities between 0.1 and 10 ohm-meters can be measured at spatial resolutions. Calibration for this measurement is done by measuring the different percentage salt-water solutions in a sealed liner which is the same type of liner of cores.
6. Magnetic Susceptibility (MS): Magnetic susceptibility is the degree of magnetization of a material in response to an applied magnetic field. In the sensor there is an oscillator circuit which produces a low intensity, non-saturating, alternating magnetic field. Any material having a magnetic susceptibility cause a change in the oscillator frequency when it gets closer of the sensor. The electronics convert this pulsed frequency information into magnetic susceptibility values. For whole core sections Bartington loop

sensor (MS2C) and for split cores Bartington point sensor (MS2E) can be used. Calibration for this measurement is done by measuring a single standard sample of a stable iron oxide which has been tested and analysed by the manufacturer (The Bartington). The magnetic susceptibility sensor is electronically set to measure this standard sample.

2.3 Itrax XRF (X-Ray Fluorescence) Core Scanner

Itrax Core Scanner used for the analyses for this study takes place in İTU EMCOL's laboratories. The instrument provides radiographic images and elemental profiles of sediment half core sections using a flat beam X-ray sources and also provides an optical image with an optical line-scanning camera incorporated within the system. A range of sensors including an optical-line camera, a laser topographic scanner, an X-ray line camera for measuring the transmitted X-rays and a high count-rate XRF detection system with an X-ray focusing unit within the central measuring tower constitute the instrument (Fig. 2.3). The operation uses two separate X-ray detection systems to obtain simultaneous acquisition of density (radiography) and compositional variations (XRF). X-ray transmission image information is recorded to display the samples chemical and density features as a radiographic image. Optical image displays the sample surface at high resolution. XRF, radiographic, and optical measurements are obtained without disturbing the sample and are performed without contact to the sample surface. Core sections with a length of up to 180 cm and a diameter of 2-12 cm can be analysed. Samples can be scanned in their entire length with a resolution from centimetre to 200µm (Croudace et al, 2006).

Depending on the requirements; user can define the duration of the analyses as short as 1 second per point or longer at each step. These step by step analyses together build up element profiles that show the changes in composition throughout the sample. Analyses reaching ppm sensitivity in a second for wide range of elements from Al to U can be obtained with Itrax Core Scanner. Analyses reaching ppm sensitivity in a second for wide range of elements from Al to U can be obtained with Itrax Core Scanner.



Figure 2.3 :Front view of the Itrax core scanner with open hoods (Croudace et al, 2006).

The instrument is controlled from a central computer and user can control the system by a graphical interface based on Windows XP Platform where standard operation procedures can be monitored. There is a second program called Q-Spec which interacts with the interface is used for both and on the fly analysis of XRF spectral data and refining the X-ray spectral analysis after scanning (Croudace et al, 2006). Instrumental components and detection systems of Itrax XRF Core Scanner are listed below:

1. Optical camera system: A good quality RGB digital images of the sediment surfaces are generated before the X-ray scan by an optical line camera with a maximum resolution of $50\mu\text{m pixel}^{-1}$.
2. X-ray source and focusing: The current system uses 3kW Mo target tube that can operate up to 60 kV and 50 mA, but according to the selected elements voltage-current can be optimized. During the analyses of samples of this study 45 kV and 30 mA voltage-current settings are used.
3. X-ray line camera: A digital line camera is used for recording the intensity of X-radiation transmitted through the sample. The low density areas appear light and high density areas appear darker as the images produced by the Itrax are 'radiographic positive'.
4. XRF detection system: Itrax achieves to keep the sample detector distance constant as reliable XRF analyses require, by using a laser system to measure

the topography of the sample surface. The detector moves vertically adjusting itself according to the topographic scan data previously obtained. Count rates of up to 200,000 cps can be processed by digital signal processing which provides energy dispersive spectrometry.

During this study, all the core sections are measured with Itrax Core Scanner with an optical image resolution of 0.1 mm pixel⁻¹, and X-ray analysis with a step size of 0.5mm, counting for 10 seconds at each step with the selected elements of Al, Si, P, S, Cl, Ar, K, Ca, Ti, V, Cr, Mn, Fe, Ni, Cu, Zn, As, Se, Br, Rb, Sr, Y, Zr, Nb, Pd, Sn, I, Ba, Ce, W, Pb, U, Th. Evaluation of the raw data is obtained by Q-Spec program using USGS standards for marine samples.

2.4 Total Organic and Total Inorganic Carbon Analysis

Shimadzu TOC/TIC Analyzer is used to obtain total organic carbon and inorganic carbon in the sediment samples. Split cores are sampled in every 5 cm. Sampled sediments are dried using freezer dryer after freezing. Dried samples are pounded for into finest size for the analysis. For every sampled section around 50 mg material is weighed. The TOC percentage is calculated using Total carbon (TC) – total inorganic carbon (TIC) = TOC equation. For the calibration of total carbon analysis, potassium hydrogen ftalat [C₆H₄(COOK)(COOH)] with 204.22 mollecule weight and 47.05 weight percentage is used. Calibration curves for total carbon are created by burning 10, 20 and 40 mg of potassium hydrogen ftalat. For the total inorganic carbon analysis, sodium hydrogen carbonate (NaHCO₃) with 1200 mollecule weight and 14.28 weight percentage is used. Calibration curves for total inorganic carbon are created by burning 20, 40 and 80 mg of carbonate. For further analysis methods are created using these calibration curves. According to the method, the difference between the percentages of total carbon and inorganic carbon gives the the measured percentage of total organic carbon. Analysis for Total Carbon (TC) depends on the burning process of pounded material with 900 °C and for Total Inorganic Carbon (TIC) it depends on using 85% phosphoric acid first and burning the material with 200°C and calculating the amount of CO₂ by the equipment. These analysis are obtaines with 95% precision.

2.5 AMS Radiocarbon (^{14}C) Dating

Accelerator Mass Spectrometry (AMS) method uses the naturally occurring radiocarbon isotope (^{14}C) to estimate the age of the carbonaceous materials (such as shells etc.) up to about 58,000 to 62,000 years (Plastino et al, 2001). Organisms create their soft tissues and shells taking radiocarbon isotope from the ocean and/or from the atmosphere. When they die, they stop taking more carbon from the environment therefore ^{14}C isotope starts to decrease with radioactive decay (Siani et al., 2001). Measurements counting the amount of ^{14}C of the materials give an uncalibrated age result. For this study, ^{14}C Radiocarbon dating of the selected sections and levels is done by NOSAMS laboratories of Woods Hole Oceanographic Institution. 2 cm thick (~20 g) sediment materials from the certain levels of the cores are sampled washed and sieved using a 63 μm sieve. After drying, remaining material is examined using a microscope and benthic molluscs and foraminifers are sorted out and identified for analysis. After the results arrive from Woods Hole Oceanographic Institutions, calibration process is obtained using CALIB program. Calibrated ages are calculated as Before Present (BP) ^{14}C age with an error margin of $\pm\sigma$. According to the calendar age calibrated results correspond to ~400-500 for Western Black Sea as known. (Table 3.1).

3. RESULTS

In this chapter, all the results of the analysis, which are described in the previous chapter, are detailed and plotted in graphs by using PanPlot software. First part of this chapter includes the detailed lithological properties of the cores with the age results of selected levels. Further on in this chapter, geophysical properties measured by MSCL, XRF elemental data and TOC/TIC results are studied in an order. All the cores are obtained from the southern western shelf area where İstanbul strait connects Black Sea basin with world ocean system as indicated before. The selected cores are divided into two groups due to their locations in an order starting from the shallow parts to the deeper areas. First group of the cores are located on the Seismic Line 1 (SL1) in the eastern side of the area, the second group is at the Seismic Line 8 (SL8) in the western side (Fig. 2.1). The detailed information about the core samples is listed in Appendix A.

3.1 Lithostratigraphy and Chronostratigraphy

The description of the selected cores and their lithological properties are summarized in this section. Descriptions of the cores are obtained as soon as the cores are split. The images are drawn using Corel Draw software according to the primary investigations such as length of the sample; colour and characteristics of the sediment, and the mollusc content within. Radiographical images are obtained during the XRF analyses by Itrax core scanner. Chronostratigraphical data is explained due to the AMS ^{14}C results that are obtained from selected depths of four cores described in this study. The selected cores are MSM015-245, HBS09-G18, HBS09-G17B, HBS09-G15B and HBS09-311. Unbroken medium and large size in situ *Mytilus sp.* shells were chosen for the cores MSM015-245, HBS09-G17B and HBS09-G15B, in situ *Cardium sp.* for the HBS09-G18 core whereas foraminifers (*Ammonia sp.*) are collected for dating in core MSM015-311. The samples were chosen on the basis of the redox-sensitive element profiles and lithological changes. Selected samples with their age, dating material (i.e. *Mytilus*, *Cardium* etc.), uncalibrated and calibrated

ages with error margins are listed in the Table 3.1. The radiocarbon age determined for the core HBS09-G18 is too recent so that calibration method is not used for this sample and the ^{14}C age is reported as the uncalibrated age. According to the calibrated BP age results, the redox and lithological boundaries observed at MSM015-245 and HBS09-G17B cores are dated as 6.8 ka BP. Calibrated age of the abrupt change observed at MSM015-311 core is 5.3 ka BP. In situ large *Mytilus sp.* shell sampled from 26-28 cm core depth of HBS09-G15B provides a calibrated age of 5.5 ka BP.

Table 3.1 : AMS C14 dating results, age errors and calibrated age data with error margins of selected core depths from selected cores.

AMS C14						
Core Name	Core Depth	Type	Age	Age Err	Cal Age BP	$\pm\sigma$
MSM015-245	42-44 cm	Mytilus	6370	40	6810	84
HBS09-G17B	31-33 cm	Mytilus	6400	35	6847	83
HBS09-G15B	26-28 cm	Mytilus	5230	35	5554	69
MSM015-311	42-44 cm	Ammonia sp.	5280	70	5325	98
HBS09-G18	21-23cm	Cardium sp.	505	25	-	-

3.1.1 Seismic Line 1 (SL1) cores

- MSM015-300

Sedimentary core MSM015-300 is obtained from the continental shelf at -82 m water depth during the German R/V MS Merian Leg15/1. As it is a shallow depth deposition unit, it is bioturbated green gray mud with abundant euryhaline molluscs. The mollusc shells and bioturbation structures are observed in the radiography image of the core (Fig. 3.1). Although there is no abrupt lithological change, there are levels with darker colours with dense mollusc population. The lighter intervals in radiographic image indicate less dense material. No dating is obtained from this core.

The uppermost 0.5 cm of the core shows an oxidized brown colour with concentration of Mn and Fe oxides. From the top of the core until the depth of 17 cm, the colour of the material changes progressively from green gray with a brown tint to green gray-dark gray. This very first section consists of large shells and shell fragments of mostly *Mytilus sp.* From 17 cm to 23 cm, sediment shows no shells and shell fragments and at this interval the colour of the sediment changes into dark gray green with black tint. 23-30 cm interval is green gray mud with coarser material and shell fragments. Shell fragments are dominantly accumulated at the 28-30 cm

interval with coarse particles as they arrive up to gravel size showing darker colour in the radiographic image. 30 cm to 33 cm interval shows green gray to dark gray colour without any shell or shell fragment content. Below 33 cm core depth material again becomes green gray dominated by molluscs. Around 37 cm large and whole shells are recognized, around 40 cm core depth shell sizes get smaller and fragments become dominant. Around the interval 50 cm to 52 cm large shells and shell fragments become abundant again. Sedimentological changes are observed throughout the core from the radiographic image. 2 cm thick sieved material indicate the shells belong to *Cardium sp.* (mostly *Cardium edule*), *Dreissena rostriformis*,

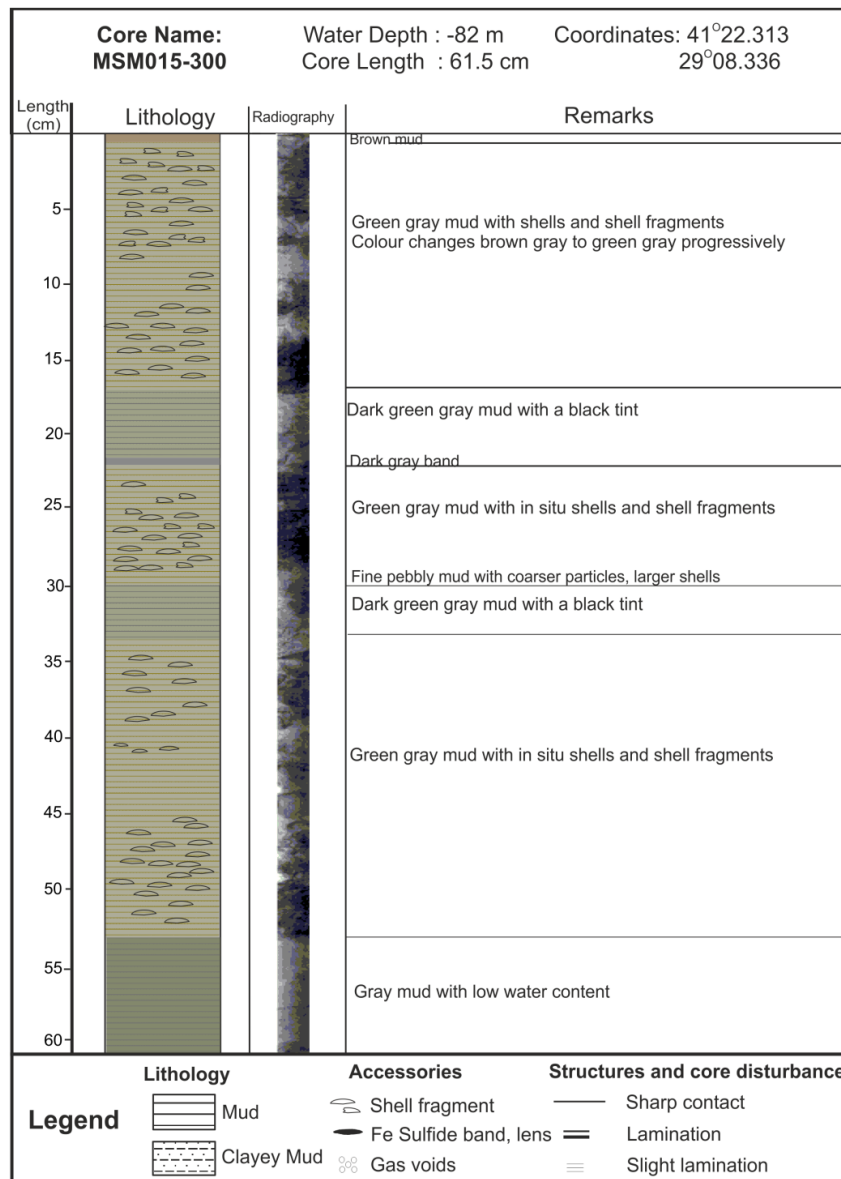


Figure 3.1 :Lithological description and radiographic image of MSM015-300 core located at -82m in eastern side (SL1) above present anoxic/oxic boundary. See Fig. 2.1 for core location.

Mytilus sp. and fragments; indicating an inflow effect at the area which has brought mollusc shells and fragments from older sediments of Black Sea. Below 52 cm the sediment is dense and devoid of shells with distinct laminations.

- HBS09-G04C

Core sample HBS09-G04C is obtained during the Turkish R/V Arar cruise in 2009. It is located at -122 m on totally oxic shelf zone of the research area and is 71.5 cm long consisting of mainly bioturbated green-gray mud without any sharp lithological change. Medium to big sized *Mytilus sp.* are abundant throughout the core. Bioturbation structures and shells of these molluscs are easily recognized in the radiography image (Fig. 3.2.). No dating is obtained from this core. 0 – 10 cm of the core consists of gray clay mud with a distinct yellow brown tint without mollusc shells or fragments. 10 – 20 cm interval consists of gray mud with <1% sand content. From 20 cm to 25 cm, the colour of mud changes into lighter gray progressively.

At 23-25 cm depth, white species of fossil fragments are recognized. 2 cm thick sediment samples are sieved from 23-25 cm and 25-27 cm intervals and they consist of broken shell fragments of *Mytilus sp.* with coarser material and broken large fragments of *Mytilus sp.*, respectively. From 25 cm depth until to the end of the core (71.5 cm) is green gray clay mud with lots of shell fragments. Shells are abundantly visible on the surface (of the split sections) between the depths of 36-39 cm and 62-71.5 cm consisting of *Mytilus sp.* and *Cardium sp.* 50-52 cm interval indicates a level of mud with yellow brown tint. Lithological properties suggest that HBS09-G04C shows the typical characteristics of oxic shelf sediments of Black Sea. *Mytilus sp.* and *Cardium sp.* are euryhaline bivalves that are widespread under oxic conditions at the shelf areas of Black Sea.

- MSM015-245

Core MSM015-245 is obtained during the German R/V MS Merian cruise Leg 15/1 in 2010. The core is located on the uppermost continental slope at eastern side (SL1) from -152 m. There is material transport from upper slope indicated by two shell hash levels in this core. These core sediments are dark gray to gray and green gray mud. There is a sharp lithological change at 41 cm. AMS ¹⁴C dating from *Mytilus sp.* shell obtained from this interval, immediately below the boundary, gives a calibrated age of 6810 BP ± 84 years. The lithological change and the bioturbation structures in

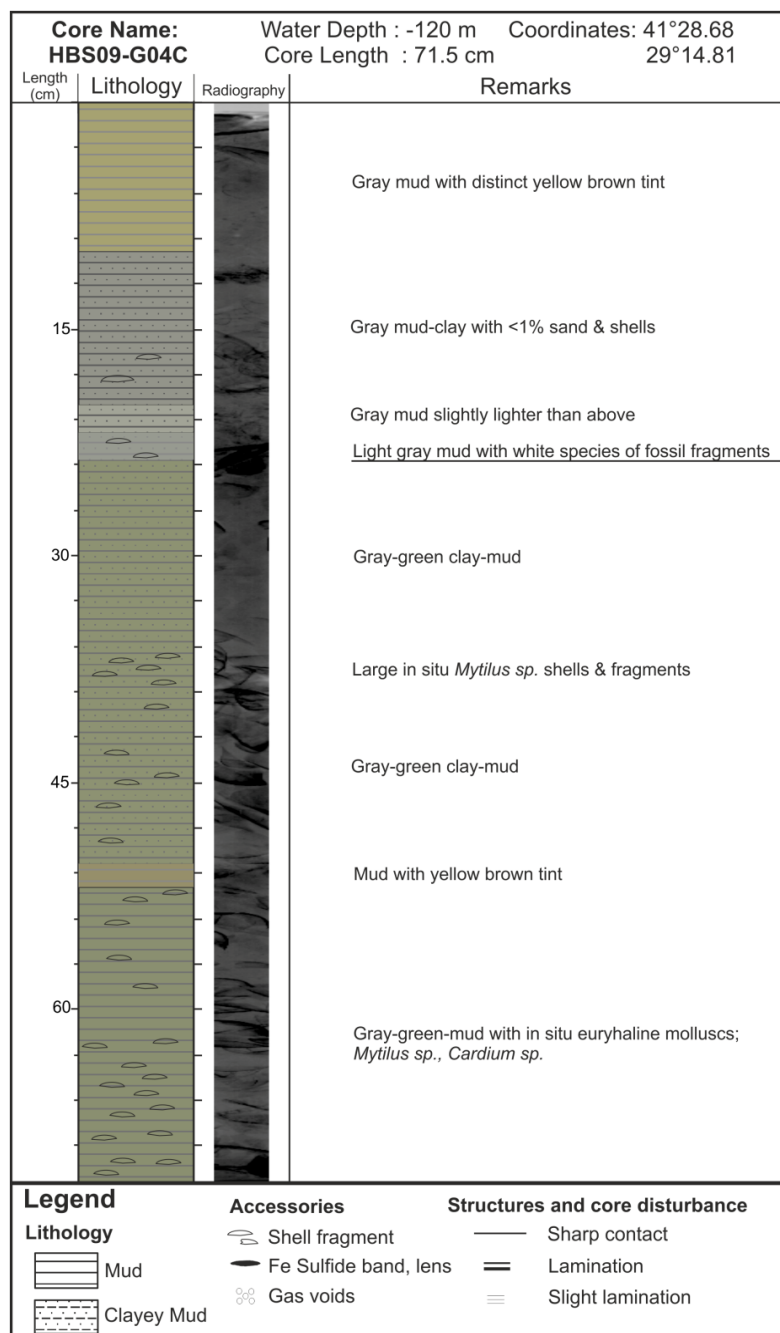


Figure 3.2 :Lithological description and radiographic image of HBS09-G04C core located at -120m at eastern side (SL1) above the present anoxic/oxic boundary. Bioturbation and abundance of in situ shells are observed from radiographic image. See Fig. 2.1 for core location.

the lower part are easily recognized from the radiographic image of the core (Fig. 3.3). First 1 cm is unconsolidated brown mud indicating microbial nitrate reduction by oxidation of Mn (II) and Fe (II) oxides. Until the depth of 37 cm, the core consist of dark gray to green gray banded mud with irregular FeS lenses and mottling structures. The colour of this first unit shows a progressive change from dark gray to gray towards to the sharp boundary at 41 cm. Two shell hash layers mentioned above

are present at 3-5 cm and 13-15 cm. These layers contain shells and shell fragments from both recent and older units of Black Sea which include *Dreissena rostriformis*, *Trochonopsis sp.*, *Turricaspia lincta* and *Mytilus sp.* These shells indicate a mixture of both marine and lacustrine environments derived from the edge of the continental shelf and upper continental slope. From 36 cm to the sharp boundary at 41 cm there is a transition zone consisting of laminated green gray mud. From 41 cm to the end of the core (70.5 cm), sediment has a colour of green gray to gray beige. Material is shell dominated mud; mainly consisting of *Mytilus sp.* 50-54 cm interval is devoid of shells. Below 54 cm whole large *Mytilus sp.* shells are abundant in the sediment.

- MSM015-192

The sediment core MSM015-192 is obtained during the German R/V MS Merian Leg 15/1 from the continental slope on the eastern side of the area (SL1) at a water depth of -307m where the water column is anoxic today. MSM015-192 is the longest core in this study with its 111 cm length. Although the sediment at this depth contains high amount of gas, the top of the core is successfully preserved with interface piston coring method. The only disturbance occurred after splitting the core. At around 6 cm core depth there is a gas void and a disturbance zone recognizable in the radiographic image of the core (Fig. 3.4.). There is no ¹⁴C dating available for this core. Although MSM015-192 shows no sharp lithological change throughout the core, it consists of changes in colour. The core sediments belong to the Coccolith Unit (Unit 1; Degens and Ross, 1974; Çağatay, 1999) with light gray-gray to black laminated and banded mud. Light gray bands and laminations indicate the Coccolith-rich levels. Two thick bands are observed at 14-17 cm and 85-89 cm intervals. At these levels, sediment consists of light gray mud without distinct laminations. As radiographic image shows these levels are observed as in black colour indicating denser material.

First 14 cm of the core consists of very dark to black laminated mud. Sediment is disturbed at around 6 cm core depth because of the gas content. From 17 cm to 51 cm material is gray-dark gray to black mud with distinct lamination and bands. This level is dominantly gray in colour. Below 51 cm until the end of the core (111 cm), material is dark gray to black laminated and banded mud having predominantly black colour.

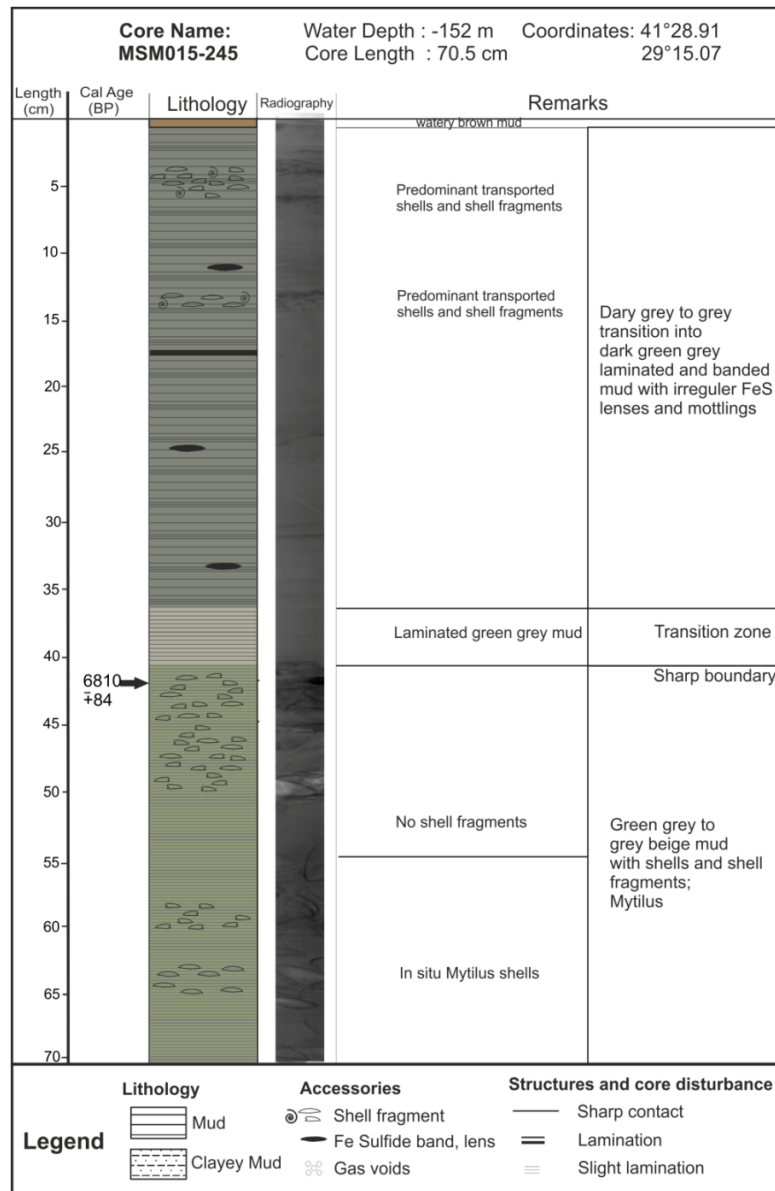


Figure 3.3 :Lithological description and radiographic image of the MSM015-245 core obtained from -152 m at eastern side (SL1) below the present anoxic/oxic boundary. There is an abrupt lithological change at 41 cm depth that is dated as 6.8 ka BP. See Fig. 2.1 for core location.

A thick gray coloured band is observed at 85-89 cm interval as indicated above. Below this band the colour of the sediment is darker gray and black showing more lamination rather than bands. Core does not show changes in colour but the density changes can be observed in radiographic image of the core; at around 60 cm the density starts to increase towards the base of the core. Sedimentological properties show no distinct environmental change during the accumulation of MSM015-192 core. No shell is identified or observed from this core.

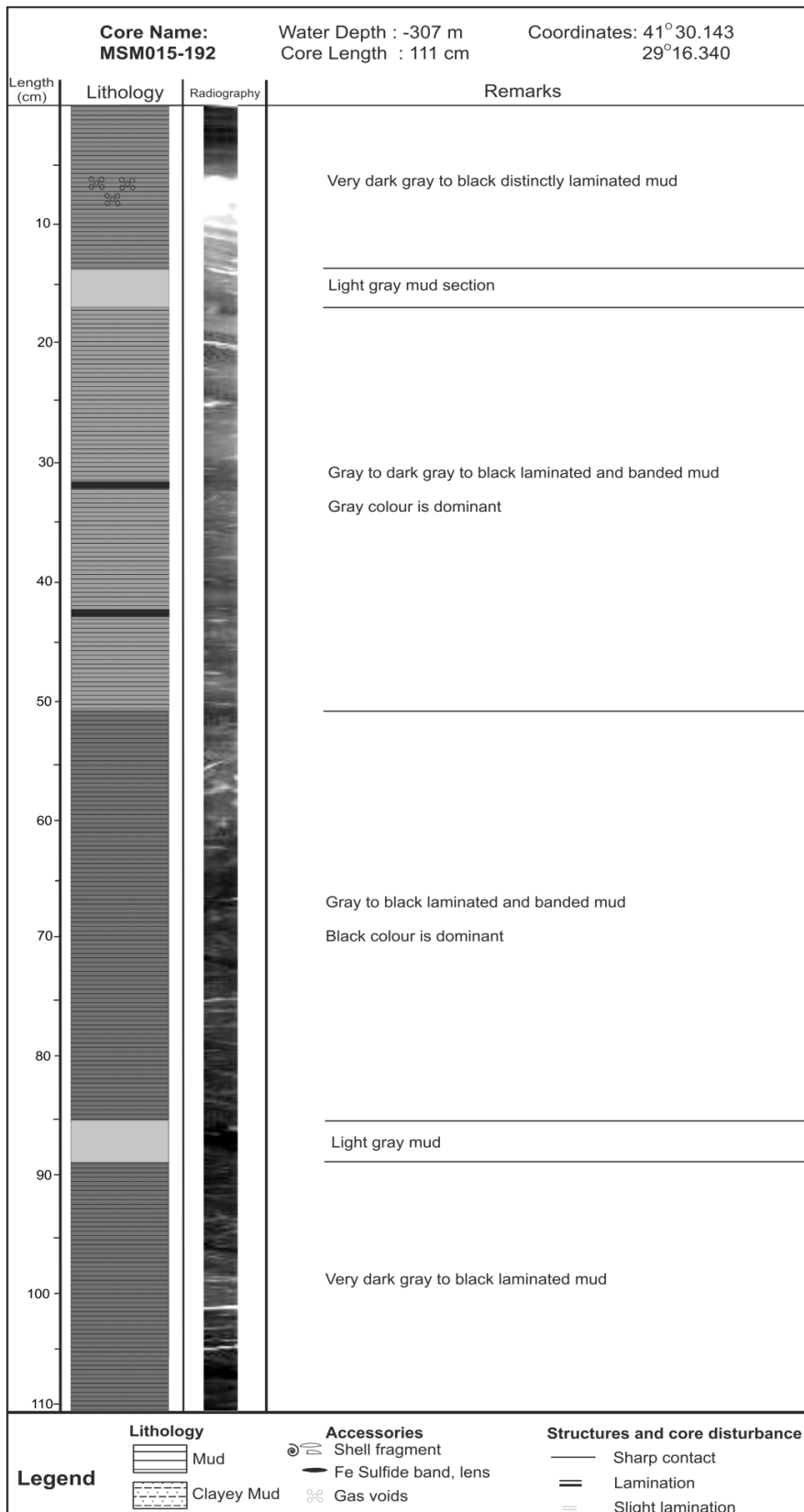


Figure 3.4 :Lithological description and radiographic image of the MSM015-192 core obtained from -307 m at eastern side (SL1) below the present anoxic/oxic boundary showing no sharp lithological change. See Fig. 2.1 for core location.

3.1.2 Seismic Line 8 (SL8) Cores

- HBS09-G18

Core sample HBS09-G18 is obtained during Turkish R/V Arar cruise in 2009. 71.5 cm long core is located on the shelf in oxic zone at -93 m at western side on SL8. It shows the characteristics of Black Sea shelf sediments with green gray mud and euryhaline molluscs. Although there is no abrupt lithological change, there are some colour changes in the sediment (Fig. 3.5). Uncalibrated AMS ^{14}C result is used as for this core obtained from *Cardium sp.* shell giving an age of 505 ± 25 years at 21-23cm depth.

First 3 cm of the core consist of light gray green mud progressively changing colour into darker gray until the 7 cm core depth. 7 cm- 13 cm interval shows very dark gray to black colour. Radiographic image of the core shows light colour indicating less dense material content between these intervals. From 13 cm until the 25 cm core depth sediment is dark gray to dark green gray mud with distinct FeS lenses. From the radiographic image shells are recognized between 17 cm and 20 cm core depth whereas no shells are visible at the surface of split sections. Sediment consists of dark gray mud between the 25–29 cm. Radiographic image indicates distinct shells at around 29 cm core depth.

From 29 cm until the 42 cm depth sediment consists of green gray to dark gray mud with distinct shells and shell fragments. Sieved sample from the 35-37 cm interval contains predominantly the shells of *Cardium sp.*, *Trophonopsis sp.* From 42 cm until the end of the core (71.5 cm), material is gray to dark gray mud with irregular mottles and FeS lenses. Euryhaline bivalves; mainly *Mytilus sp.* and *Cardium sp.* are present at this zone dominantly located at around 42 cm and 60 cm core depth (as observed from the radiographic image). The 42-44 cm interval contains the shells of *Cardium sp.*, *Tellina sp.*, and *Modiolula phaseolina*.

- HBS09-G17B

Core sample HBS09-G17B is obtained during Turkish R/V Arar cruise in 2009. It is located at -120m on the continental shelf at western side on SL8. It is 47.5 cm long and it consists of bioturbated gray green mud. The uppermost 2 cm is very dark gray to black watery mud indicating reducing conditions. From 2 cm to 7 cm depth small shell fragments and shells are visible in green gray mud.

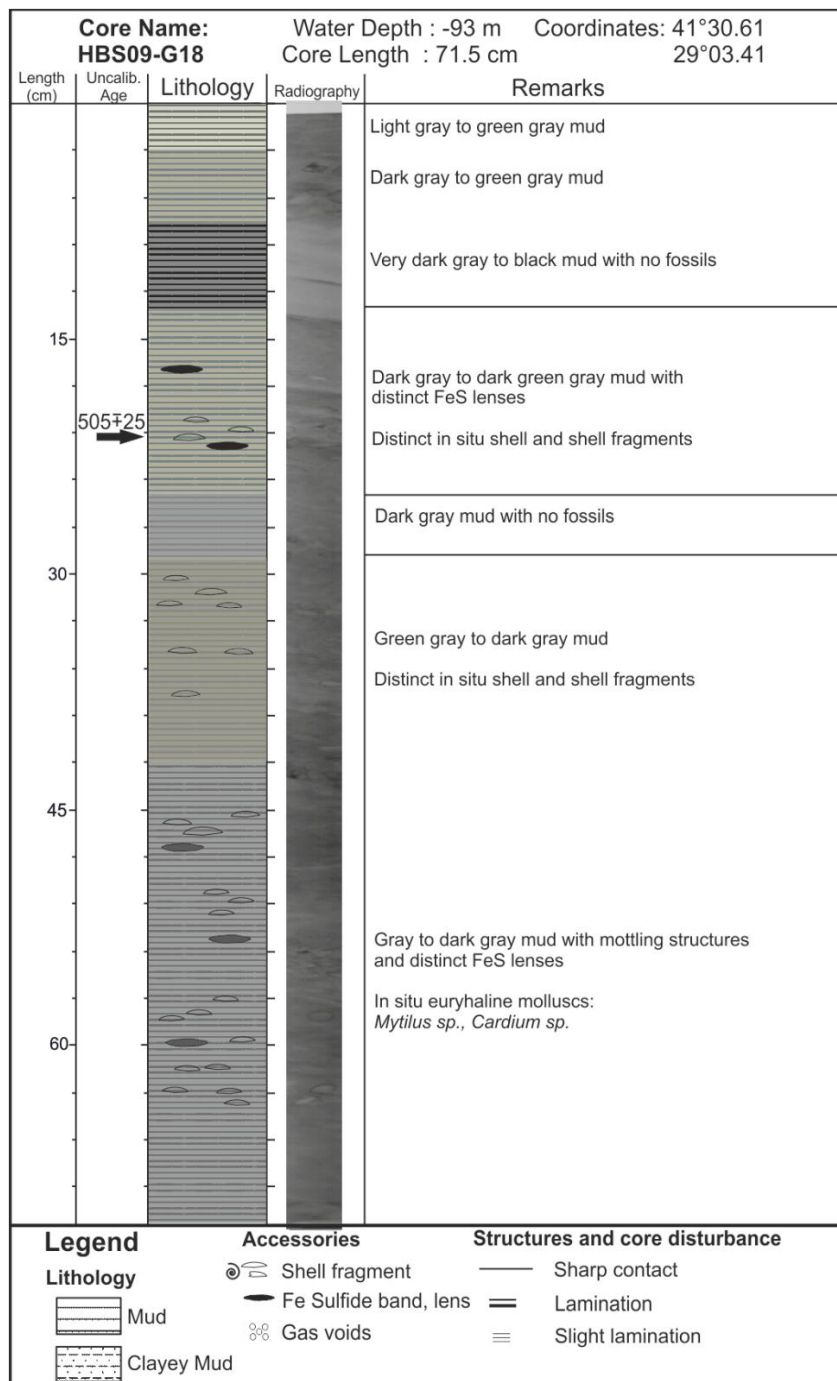


Figure 3.5 :Lithological description and radiographic image of the HBS09-G18 core obtained from -93m at western side (SL8) above the present anoxic/oxic boundary. Decrease in the amount of shells are observed through the top part of the core whereas a distinct change in color is observed. See Fig. 2.1 for core location.

Most of the shell fragments are recognized as *Mytilus sp.* From 7 cm to 30 cm the colour of the material gets grayer and distinct laminations become visible. There are less shells and shell fragments recognized between these depths. Towards to end this

section, shells and shell fragments again begin to appear dominantly consisting of *Mytilus sp.* At 30 cm depth there is a sharp lithological change which is dated using AMS ¹⁴C method and it gives a calibrated age of 6850 BP ± 85 years. Below the 30 cm until the end (47.5 cm), sediment consists of shells and shell fragments dominated mud. The colour of the mud is light green gray to gray green. The water content of this level is much more than the upper levels of the core because of intraparticle porosity. The radiography image of the core shows the bioturbated levels and the shells throughout the core (Fig. 3.6). Material is sieved from 31-33cm, 35-37cm and 42-44cm intervals for mollusc identification. The dominant molluscs of these depths are *Mytilus sp.*, *Trophonopsis sp.* and *Turricaspia lincta*.

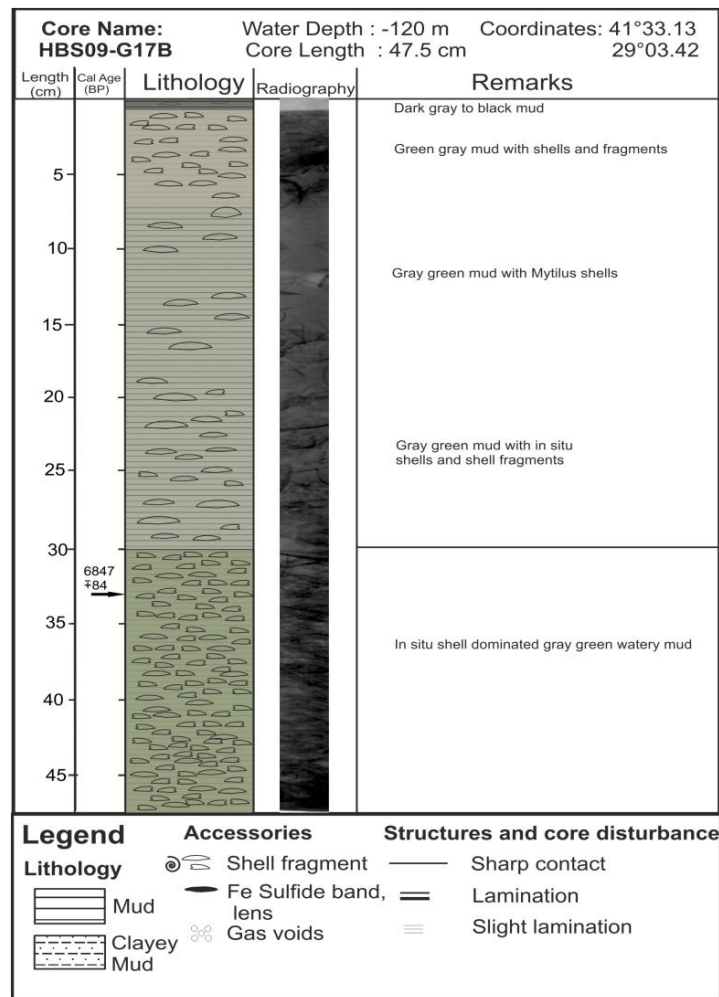


Figure 3.6 :Lithological description and radiographic image of the HBS09-G17B core obtained from -120 m at western side (SL8) above the present anoxic/oxic boundary. Sharp change of the amount of the shells gives an age of 6.8 ka BP. See Fig. 2.1 for core location.

- HBS09-G15B

Core sample HBS09-G15B is obtained during Turkish R/V Arar cruise in 2009. It is located at -160 m at western slope area on SL8. It is a short core with 33.5 cm length (Fig. 3.7). Calibrated ^{14}C age is determined from 26-28 cm core depth giving an age 5550 ± 70 a BP.

Uppermost 4 cm of the core consists of green gray mud with faint lamination containing shells and transported shell fragments of *Dreissena sp.*, *Mytilus sp.* with coarser material. Between 4 cm and 8 cm, sediment shows characteristics of faint reduced black laminated mud; the colour of the material changes to darker colour progressively at this level of the core. Below 8 cm until the end of the core at 33.5 cm, core consists of gray green mud with faint lamination containing whole large *Mytilus sp.* shells at 22 and 27 cm core depth. Radiographic image indicates the density changes and the shell content throughout the core. First 8 cm of the core shows much more dense properties. Small shells are present at the top section of the core. Large (5-7cm long) shells are observed between 20 cm and 30 cm.

- MSM015-311

Core sample MSM015-311 is obtained during the R/V MS Merian cruise Leg 15/1 from the western slope area (SL8) at -307 m. The bottom water conditions of the location are anoxic today. The core shows an abrupt lithological change at 42.5 cm core depth indicating an environmental change during accumulation. The upper unit shows the characteristics of anoxic sedimentation and the lower unit is a typical Black Sea oxic sediment with its gray green colour. Radiographic image of the core shows a great difference in colour (Fig. 3.8). Calibrated ^{14}C dating is obtained from this sharp boundary giving an age of 5325 ± 100 a BP. From every 25 cm, 2 cm thick material is washed and sieved for shell identification (if available). The top of the sediment is successfully preserved with the interface piston gravity coring method and there is not any lost or disturbed material.

First 24.5 cm of the core shows very dark gray to jet black in colour with faint lamination and distinct bands. This very first section of mud contains gas voids. Because of the high gas content, the first shows very high porosity. Gray distinct bands are observed below 10 cm. Between the core depths of 19.5 cm and 24.5 cm, sediment shows predominantly black colour with black laminae.

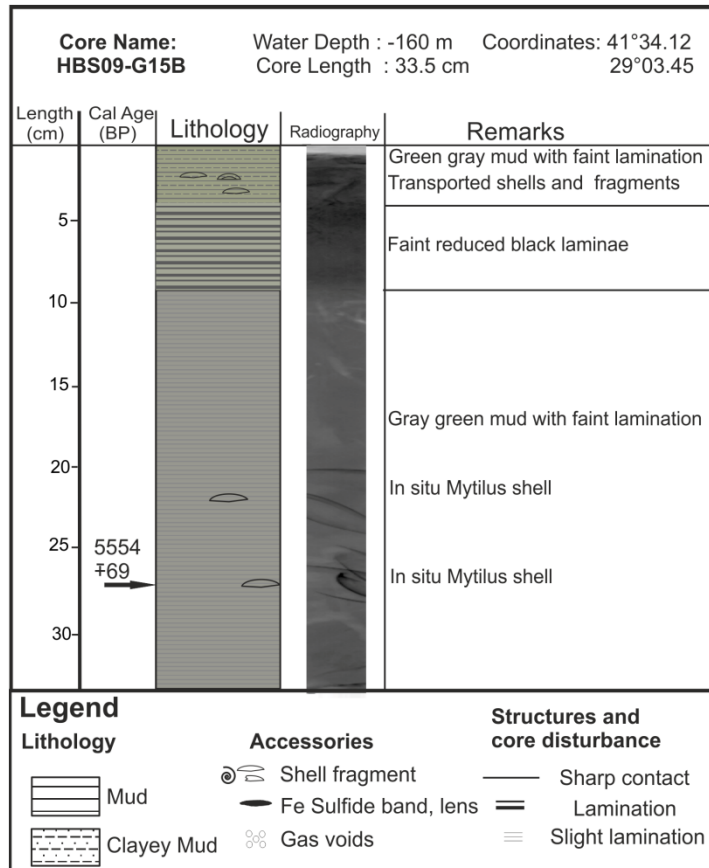


Figure 3.7 :Lithological description and radiographic image of the HBS09-G15B core obtained from -160m at western slope area (SL8) below the present anoxic/oxic boundary. 5.5 ka BP calibrated age determined is shown in the figure. See Fig. 2.1 for core location.

From 24.5 cm until the boundary at 42.5 cm, sediment consists of dark gray to black mud with distinct laminations and gas voids. Below the boundary at 42.5 cm until 52.5 cm depth, there is a transition zone showing properties of green gray to dark gray mud with a 2 cm thick dark gray band at 44 cm. From 52.5 cm until the end of the core at 70.5 cm core consists of olive green to gray green-gray clay mud. This unit is much more dense than the upper unit as seen at the radiographic image of the core. Foraminifera and mollusc types are analyzed as they are good indicators of environmental changes. 23-25 cm interval contains *Ostracoda sp.*, 40-42 cm interval contains predominantly shells of *Ostracoda sp.* followed by *Ammonia sp.*, and *Aubigny perlucida*, 66-68 cm interval contains predominantly diatoms, followed by *Ostracoda sp.*, and *Hyalina baltica*.

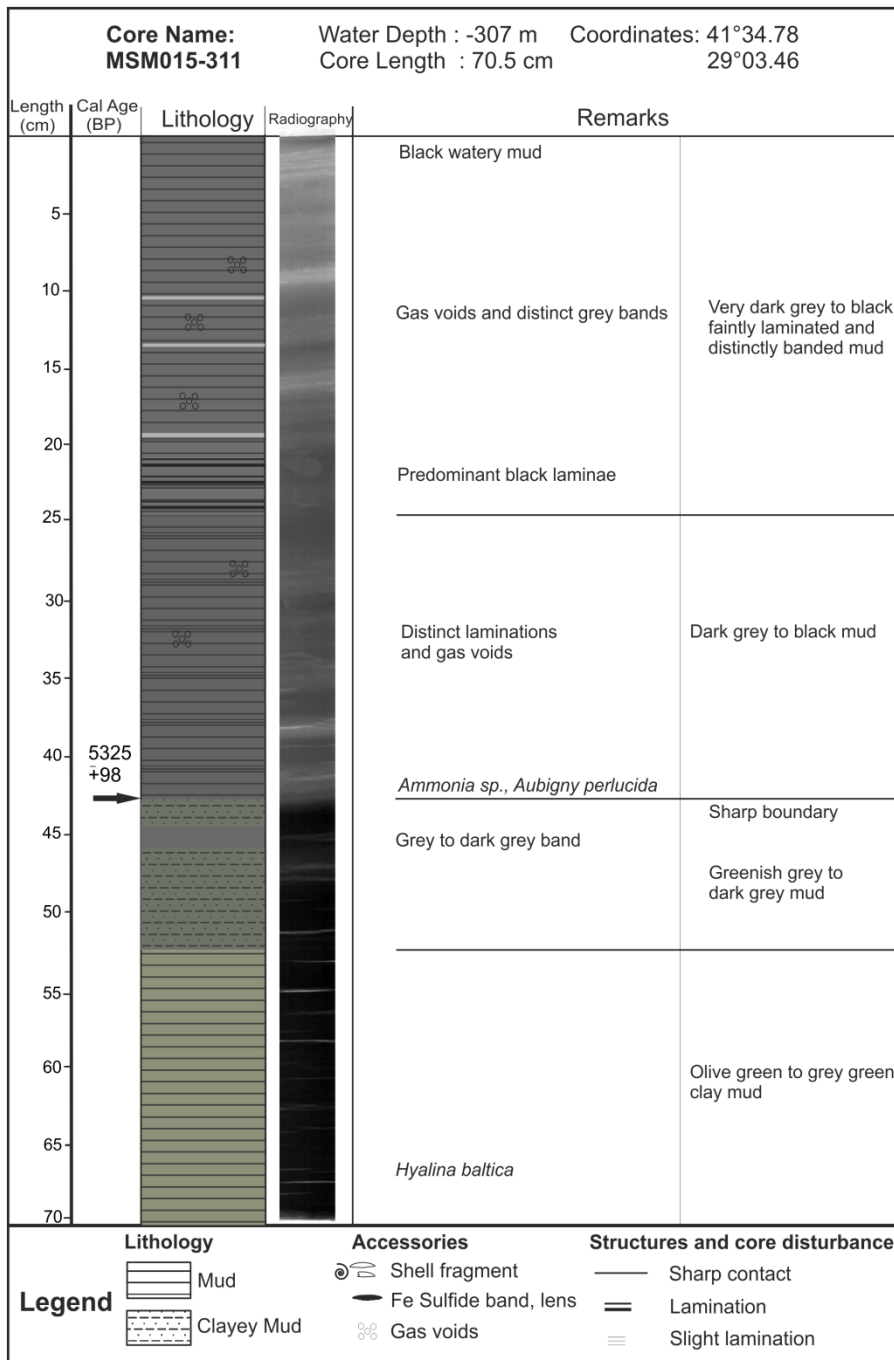


Figure 3.8 :Lithological description and radiographic image of the MSM015-311 core obtained at -307m from western slope area (SL8) below the present anoxic/oxic boundary. Sharp lithological change is dated as 5.3 ka BP. See Fig. 2.1 for core location.

3.2 MSCL Results

Physical properties measured by MSCL are detailed and mentioned in this section. Studied cores are grouped in two parts in order to their locations as mentioned in the previous section (For core locations see Fig. 2.1). Gamma density values with unit of g/cm^3 , magnetic susceptibility values with unit of SI and electric resistivity values with unit of mV of each core are described below.

3.2.1 Seismic Line 1 (SL1) cores

MSCL analysis of the MSM015-300 core show that there is not any abrupt physical change throughout the core (Fig. 3.9). The high values of electrical resistivity in the uppermost part of the core is due to high water content of the fluffy layer. The topmost part of the core shows distinct decrease in all of the profiles as a result of this fluffy layer. Fluctuating electrical resistivity values indicate the changes of porosity and/or pore water salinity levels.

Gamma density fluctuations indicate the lithological changes with different shell content. Higher gamma density values correspond to lower magnetic susceptibility values. Magnetic susceptibility shows a distinct increase at around 40 cm core depth indicating terrestrial input and accumulation of iron-rich material.

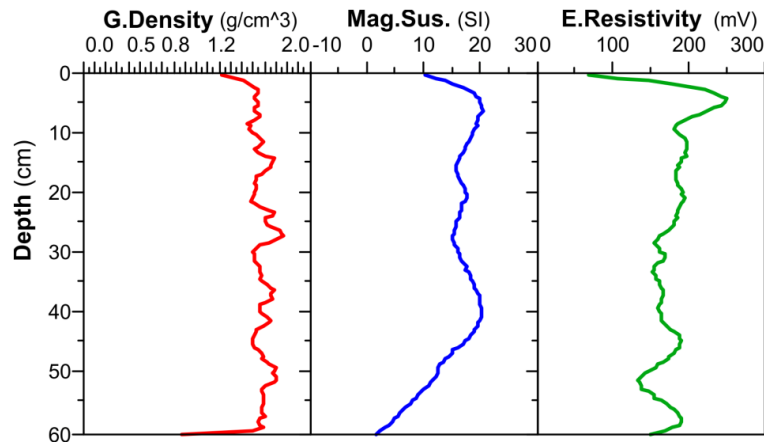


Figure 3.9 :Physical properties (MSCL results) of the MSM015-300 core located at -82m in the eastern side of the area (SL1). See Fig.2.1 for core location.

Physical properties of the core HBS09-G04C are shown in Fig. 3.10. The topmost part of the core shows distinct decrease in all of the profiles as a result of this fluffy layer. Fluctuating gamma density values indicate the different material and shell content in the sediment. Upward increasing values of electrical resistivity values

show the decreasing pore water salinity. The distinct changes of gamma density, magnetic susceptibility and electrical resistivity at 50-55 cm interval indicate terrestrial input.

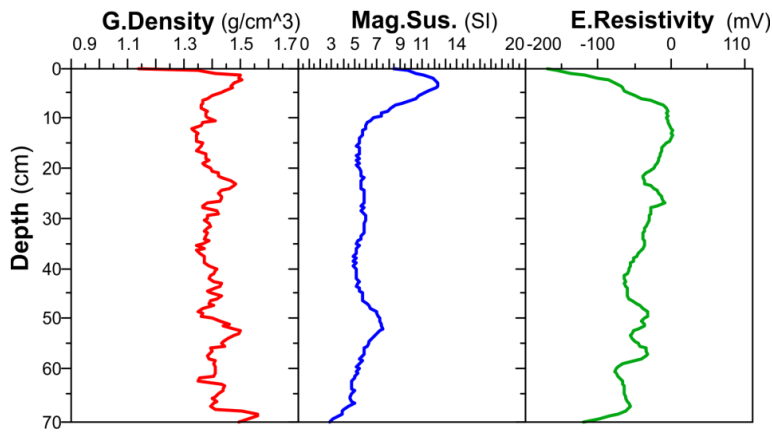


Figure 3.10 :Physical properties (MSCL results) of HBS09-G04C core collected from -120m at eastern side of the area (SL1). See Fig. 2.1 for core location.

Downcore distributions of gamma density, electrical resistivity and magnetic susceptibility properties of core MSM015-245 indicate an abrupt physical change at 45 cm core depth (Fig. 3.11). Distinct increase in gamma density values between 43-48cm shows the changes in mineral composition at this level. In situ shells located below 45 cm resulted distinct changes in the physical properties.

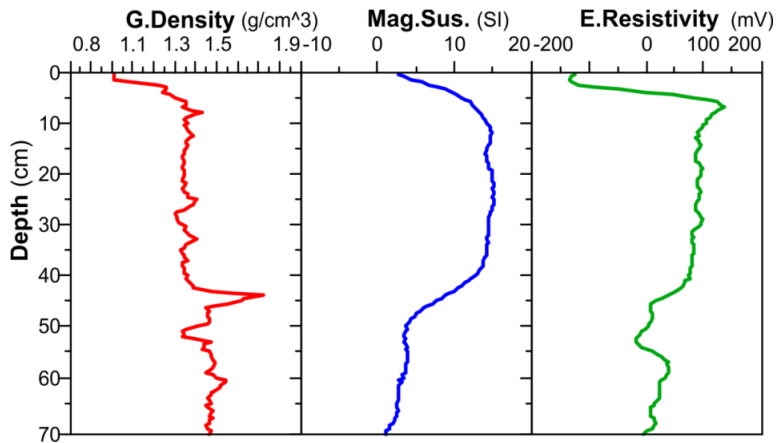


Figure 3.11 :Physical properties (MSCL results) of the MSM015-245 core collected from -152m from eastern slope area (SL1). There is an abrupt change observed at 40-45 cm interval. See Fig. 2.1 for core location.

Magnetic susceptibility values in the top 45cm are twice those of the lower part of the core. Increasing magnetic susceptibility values above the boundary show the increasing amount of iron-rich material in the upper part of the core. Upward

increasing electrical resistivity values indicate the decrease in pore water salinity. The lowest electrical resistivity in the top 5-7 cm is due to high porosity and water content of the sediment.

Physical properties of core MSM015-192 in the Fig. 3.12, show an abrupt decrease at around 5-10 cm core depth; this change is because of the gas content at this level. Released gas from the core created a disturbance zone which measured as lowest values of the properties. Downcore distribution of gamma density and electrical resistivity show uniform trend indicating no abrupt lithological change throughout the core. The slight increase of the magnetic susceptibility values at around 15-30cm, 65-70cm and 100-120cm intervals indicate high content of iron-rich mineral accumulation.

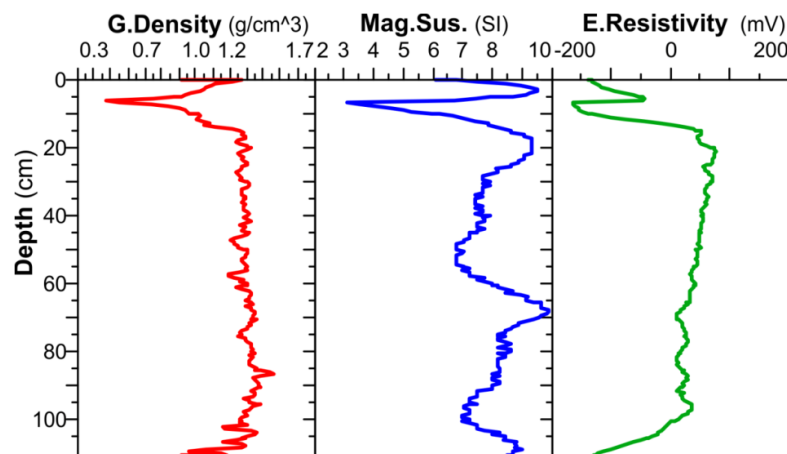


Figure 3.12 :Physical properties (MSCL results) of the MSM015-192 core collected from -307m on eastern slope area (SL1). Uppermost distinct fluctuation is because of the gas (H_2S) content. See Fig.2.1 for core location.

3.2.2 Seismic Line 8 (SL8) cores

Physical properties of core HBS09-G18 demonstrate an upward change throughout the core (Fig.3.13). Above 40 cm core depth gamma density values show an upward decrease indicating the change in the material content. Magnetic susceptibility values show distinct increase at 20-40 cm interval, indicating accumulation of iron-rich

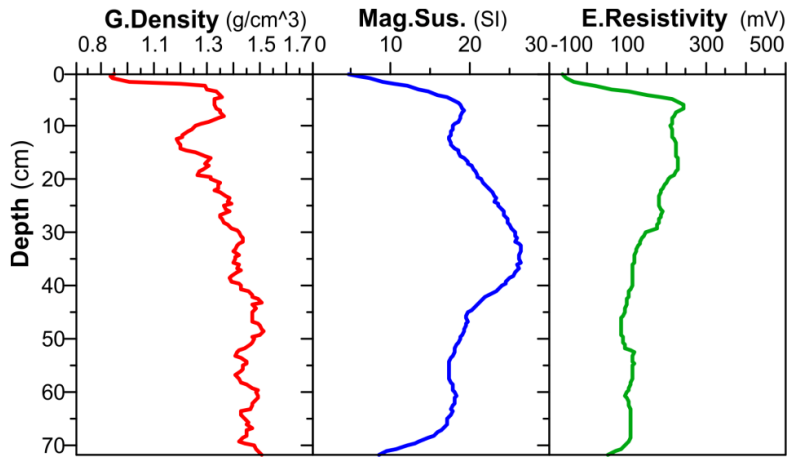


Figure 3.13 :Physical properties (MSCL results) of the HBS09-G18 core collected from -93m at western side (SL8). See Fig.2.1 for core location.

material. Decreased gamma density and magnetic susceptibility in 10-15cm interval show the softer, less iron-bearing material content.

Distinct upward increase in the physical properties of core HBS09-G17B start at about 30 cm core depth (Fig.3.14). Fluctuating gamma density below this depth is due to the abundance of euryhaline shells. As a result of this abrupt shell-rich lithology change, magnetic susceptibility properties show distinct decrease below this depth. Upward increase in the electrical resistivity values indicate decreasing pore water salinity.

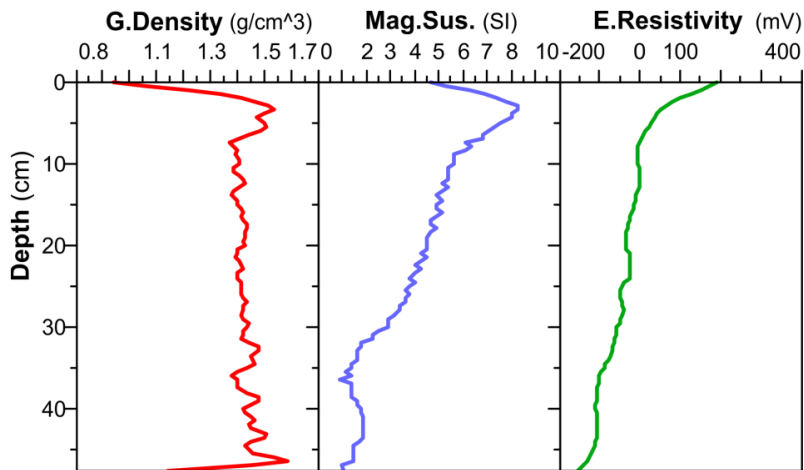


Figure 3.14 :Physical properties (MSCL results) of the HBS09-G17B core collected from -120m at western side (SL8). See Fig.2.1 for core location.

Downcore distributions of physical properties of core HBS09-G15B are shown in the Fig. 3.15. Gamma density fluctuations observed below 20 cm core depth are due to shell content in the sediment. Uniformly upward increasing trend of magnetic

susceptibility indicate a peak at about 5 cm core depth. This peak corresponds a similar peak in the gamma density. The upward decrease in the resistivity starting from about 15 cm depth, is probably due to increase in the porosity (water content) and/or in salinity of the pore waters.

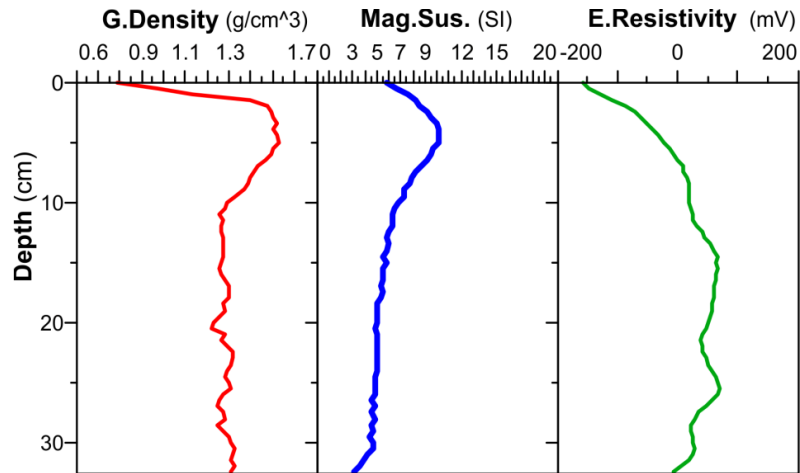


Figure 3.15 :Physical properties (MSCL results) of the HBS09-G15B core collected from -160m at the western slope area (SL8). See Fig.2.1 for core location.

All the physical properties of the Core MSM015-311 show an abrupt change at around 40-45 cm core depth (Fig.3.16). Gamma density and magnetic susceptibility values below this depth show an abrupt increase. On the other hand, the electrical resistivity values show an upward increase starting from about 50cm core depth. This sharp change in the physical properties correspond to sharp lithological change from olive green-green gray mud as described in the previous section.

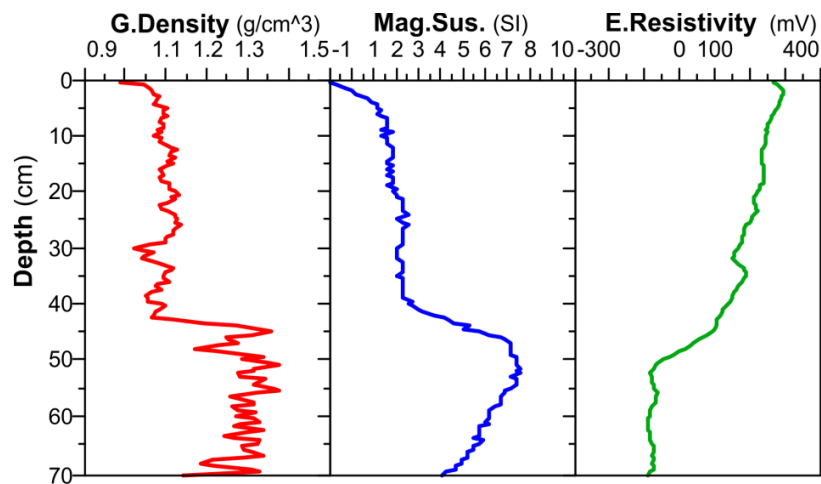


Figure 3.16 :Physical properties (MSCL results) of the MSM015-311 core collected from -307m at western slope area. See Fig.2.1 for core location.

3.3 XRF Results

In this section, elemental XRF analyses of K, Ti, Fe, Mn, Ca, S, Br and I, which are obtained by the Itrax XRF core scanner are described. These elements are used as proxies for clastic input and changing redox conditions. Elemental profiles of the collected along two different depth transects SL1 and SL8 are described below.

3.3.1 Seismic Line 1 (SL1) cores

- MSM015-300

The XRF elemental profiles for this core are summarized in Fig.3.17. The uppermost 1-2 cm of the core show increases in Br and I values whereas the other selected element profiles show minimum values. Bromine profile shows slightly decreasing downcore distribution without any distinct changes, whereas I profile show similar changes to those of Ca.

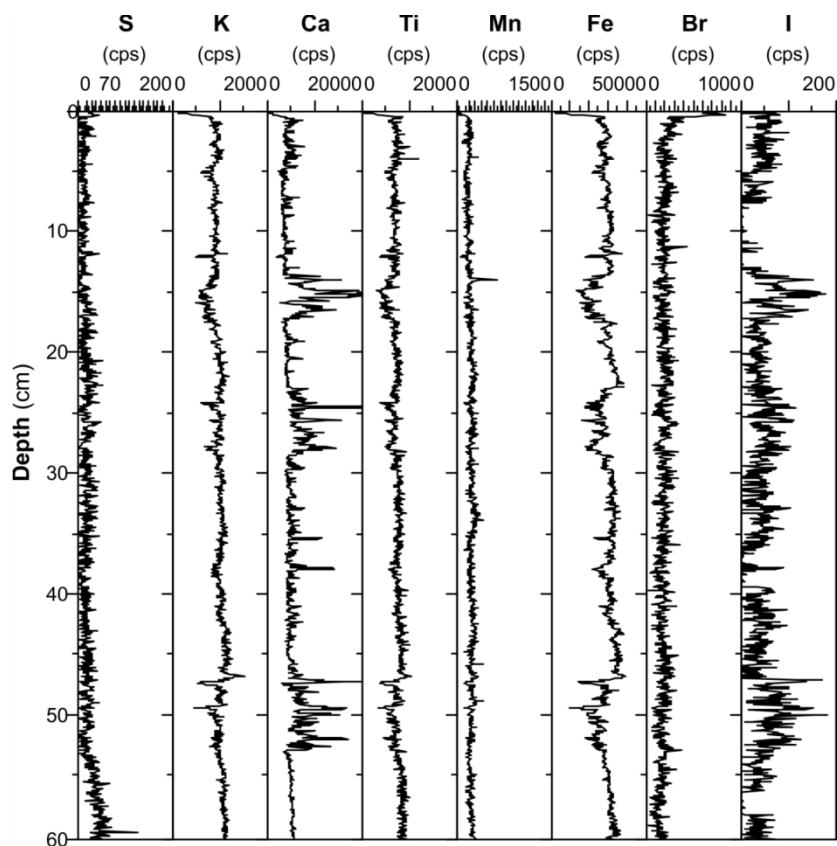


Figure 3.17 :XRF/depth profiles of K, Ti, Mn, Fe, S, Ca, Br and I in the MSM015-300 core located at -82m at eastern side (SL1), Ca peaks are due to shell content and Mn shows no changes. See Fig.2.1 for core location.

Iron, K and Ti profiles show contrasting distributions to those of Ca, being depleted in intervals 13-17 cm, 24-28 cm, 35-37 cm and 47-52 cm because of carbonate dilution effect, where shells and shell fragments accumulated. Manganese and S profiles show similar uniformly low profiles along the core with some increase in S in the lowest 7 cm of the core. Starting from the 52 cm core depth to the end of the core, K, Ti and Fe profiles also show increase where Ca decreases distinctly at the base of the core where sediment becomes dense, darker gray green in colour and devoid of shells.

- HBS09-G04C

The elemental profiles of the core are presented in Fig. 3.18. Manganese profile demonstrates high values in the uppermost 3 cm of the core. Minimum Mn values for this core are observed below 3 cm until 23 cm core depth. Below 23 cm depth, Mn profile shows increasing downcore distribution with a slight decrease at 51-53 cm interval.

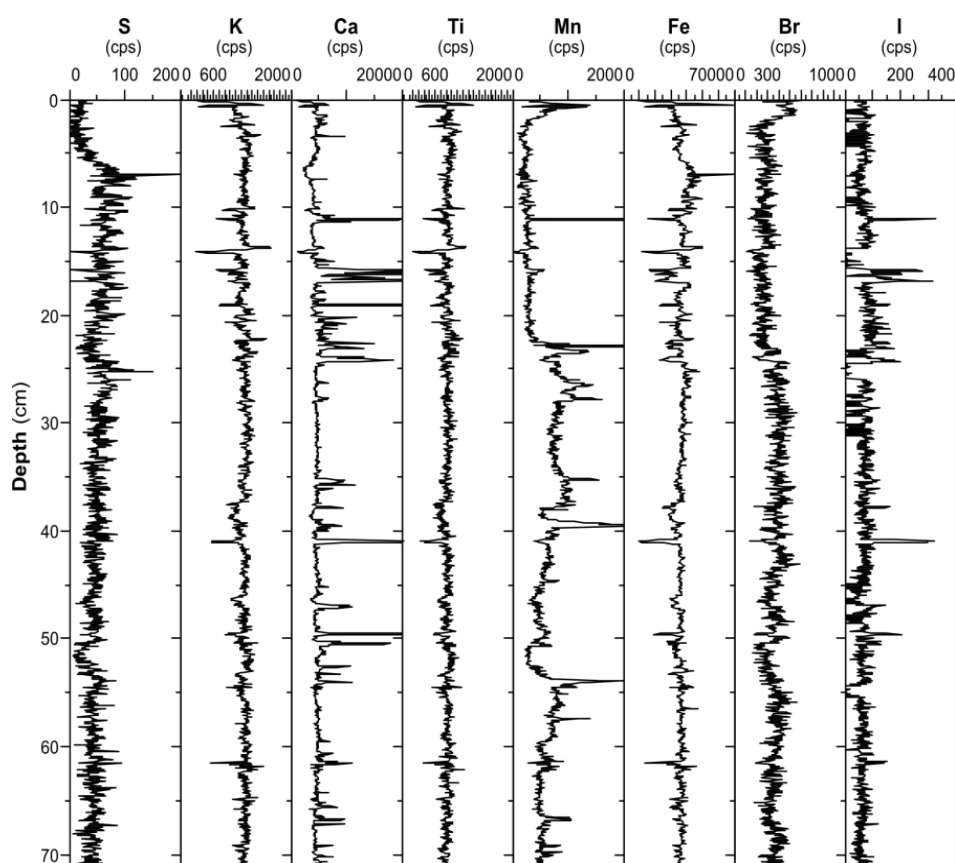


Figure 3.18 :XRF/depth profiles of K, Ti, Mn, Fe, S, Ca, Br and I in the HBS09-G04C located at -120m at the eastern side (SL1), showing Mn decrease above 23 cm core depth in association with increased Fe-S values. See Fig.2.1 for core location.

In contrast to Mn, S shows its minimum values at the uppermost 5 cm of the core. Below this level S profile shows increased values until 20 cm core depth for which interval Fe presents a similar profile. Between 20-23 cm there is a slight decrease in S values where the lithology of the core shows slight change into a lighter colour progressively. Below 23 cm, downcore distribution of S profile does not show distinct changes. The only slight decrease in the profile of S is at 51-53 cm interval where Mn is also depleted, but Ca is enriched. Iron, Ti and K profiles demonstrate a more or less uniform downcore distribution, except in 3-23 cm interval where Fe profile shows a distinct excursions in association with Mn and S. Calcium profile shows positive excursions between 10-23 cm, 33-41 cm, 48-60 cm intervals, where shells and shell fragments are present also observed from the radiographic image. The uppermost 3 cm of the core show increased values of Br. Below 3 cm core depth, Br profile shows slight increase with depth whereas I profile shows separate excursions in the more or less similar intervals as that of Ca profile.

- MSM015-245

The XRF results of the selected elements for this core are shown in the Fig. 3.19. This core shows an abrupt change in elemental data at around 40 cm core depth. Manganese profile demonstrates high values unassociated with Fe and S profiles between 40 and 58 cm. Below 59 cm, Mn profile shows uniform downcore distribution with intermediate values. Downcore S profile shows uniform values until the 40 cm boundary, below this boundary S shows some enrichments and fluctuations. The maximum enrichment of S is observed just below the boundary at 40-45 cm interval Mn values are relatively low. Iron profile, having the same trend with K and Ti, shows uniform distribution with negative excursions corresponding to high values of Ca, showing the carbonate dilution effect. Calcium therefore exhibits a profile that is negatively correlated with those to Fe values with minimum distribution of Fe, K and Ti. The highest amounts of Ca values throughout the core are observed in the 40-60 cm interval. Bromine profile shows increases in the uppermost 3 cm of the core, below which, it shows uniform distribution. Iodine profile shows a similar trend to that of the Ca, being enriched in 40-60 cm interval.

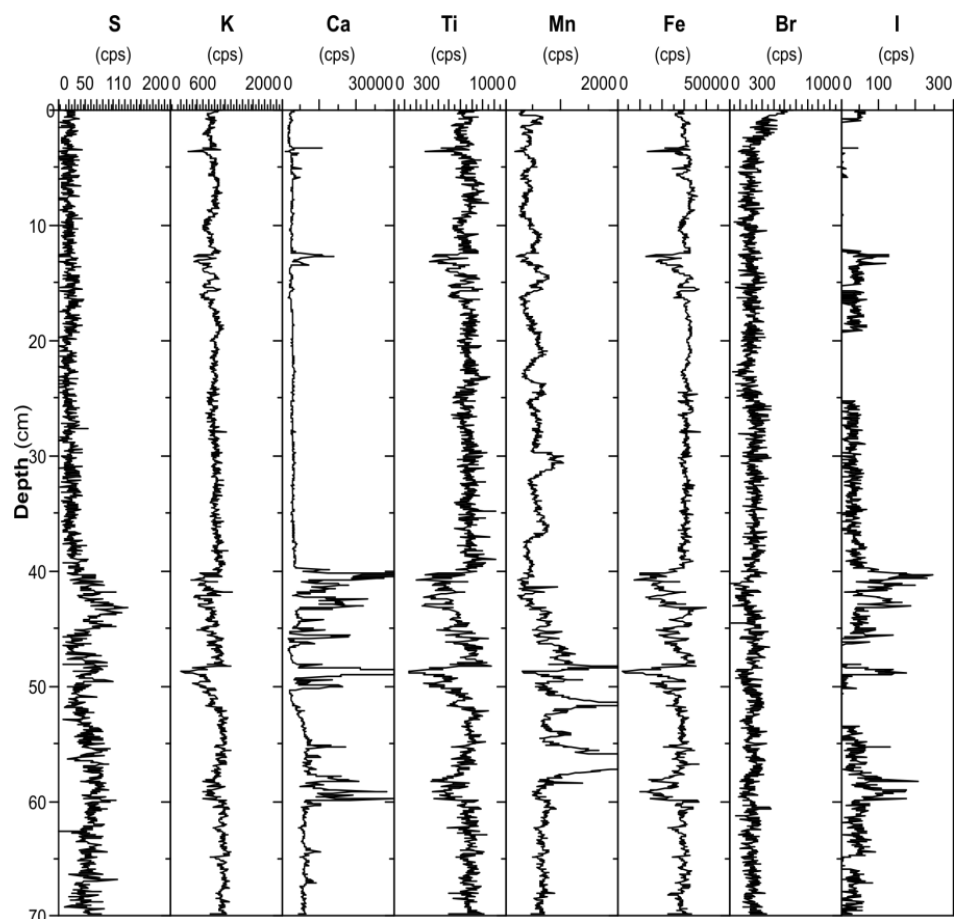


Figure 3.19 :XRF/depth profiles of K, Ti, Mn, Fe, S, Ca, Br and I in the MSM015-245 core located at -152m, at eastern slope area. Sharp change in the amounts of elements at 40 cm core depth indicate presence of two different units. Above the boundary Mn shows fluctuations. See Fig.2.1 for core location.

- MSM015-192

The XRF elemental profiles for this core are summarized in Fig. 3.20. The gas disturbance at around 6 cm core depth possibly affected the XRF data at 6-8 cm interval lowering the values. There are not any significant changes in the downcore distribution of the analyzed elements, except for the Mn profile which shows positive excursions throughout the core, which are unassociated with Fe and S. These excursions occur in 15-19 cm, 32-38 cm, 56-58 cm and 105-108 cm intervals. There are minor decreases of K and Ti values at 8-14 cm interval. Below this level these elements do not show any change in distribution. Sulphur profile shows unchanging trend throughout the core. There is a minor change of S profile at the uppermost part of the core but this change is probably occurred as a result of gas disturbance at this interval. Calcium profile does not show important changes throughout the core. Bromine and I show slight enrichments at the uppermost 15 cm of the core and

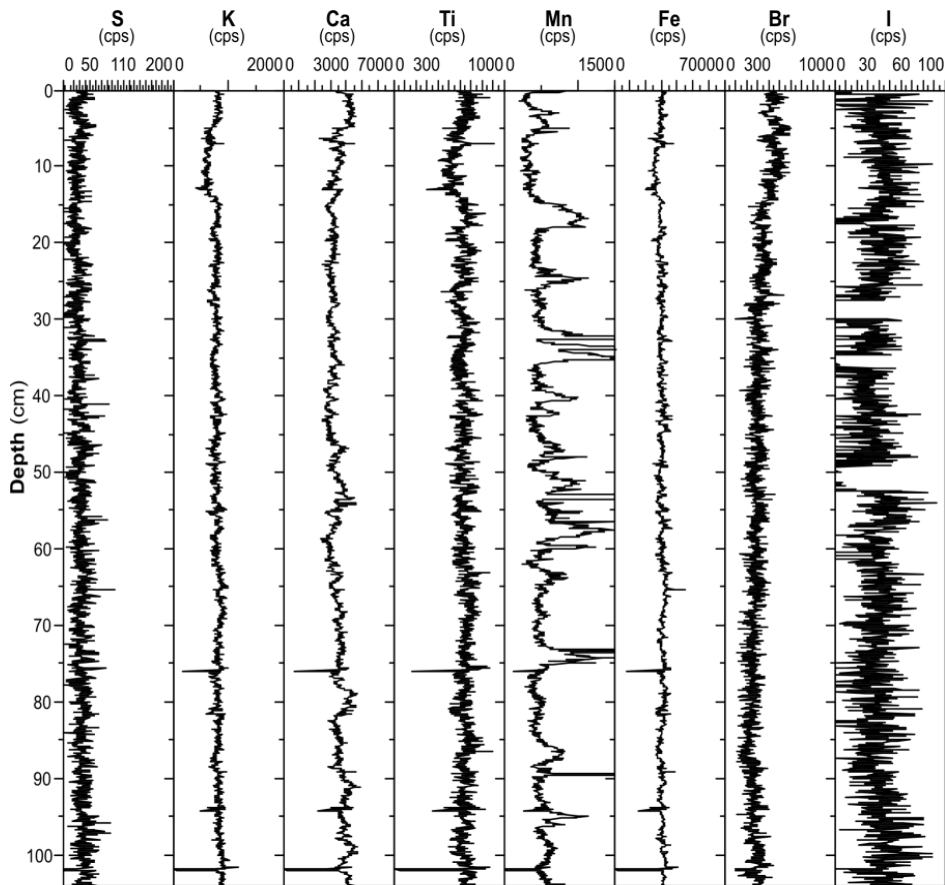


Figure 3.20 :XRF/depth profiles of K, Ti, Mn, Fe, S, Ca, Br and I in the MSM015-192 core collected from -307m at eastern slope area (SL1), Mn shows fluctuations throughout the core beside Mn, the other measured elements do not show distinct changes. See Fig.2.1 for core location.

below this level both I and Br profiles show uniform distribution until the end of the core.

3.3.2 Seismic Line 8 (SL8) cores

- HBS09-G18

The XRF elemental concentrations are plotted in Fig. 3.21. Manganese shows enrichment at 7-13 cm interval where S, Br and I also increase. Iron, K, Ti and Ca values decrease in the same interval but slightly increase downcore. Manganese values fluctuate from the top to the bottom of the core, with a distinct increase at 53-57 cm interval where Ca enrichment is also observed. Calcium values show enrichments in 17 cm, 28 cm, 42-43 cm, and 54-61 cm, and a slight decrease between 30 cm and 40 cm. Sulphur shows a uniform distribution along the core length, except in 7-13 cm interval, as mentioned above.

Bromine shows the highest values at 7-13 cm interval, below this level, there is a decrease in Br content until the core depth of 40 cm. Below 40 cm, and Br profile stays stable until the end of the core. Iodine does not show distinct changes along the core, and is not detected in 26-32 cm interval.

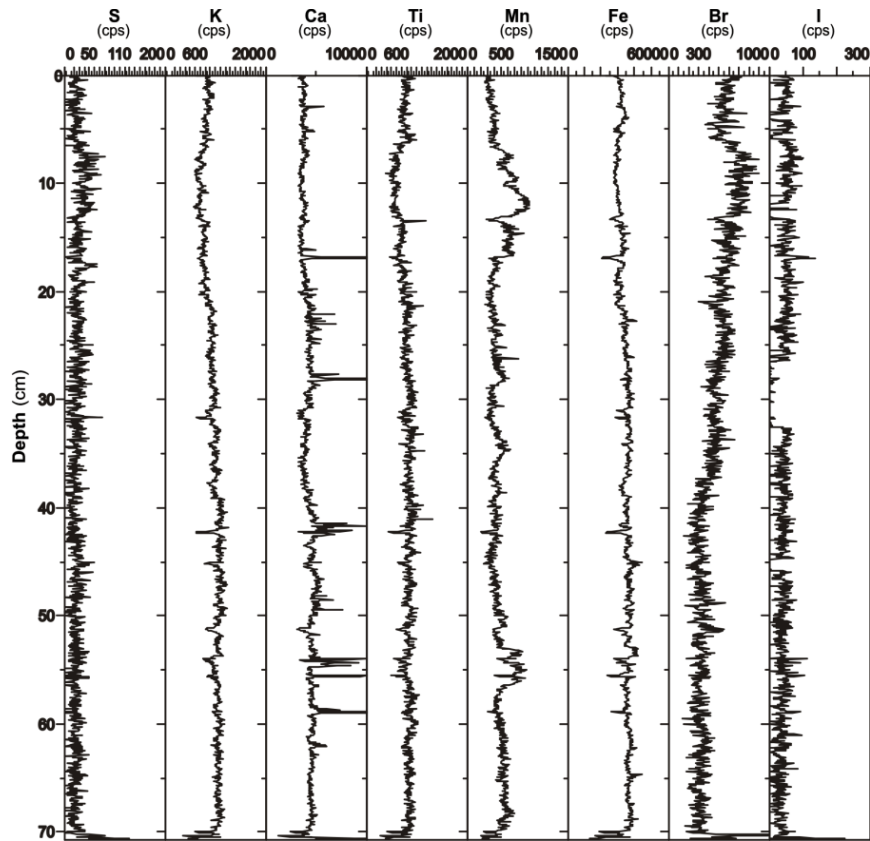


Figure 3.21 :XRF/depth profiles of K, Ti, Mn, Fe, S, Ca, Br and I in the HBS09-G18 core collected from -93m at western side (SL8), show distinct increase in the amount of Mn, S and Br values at 7-13cm interval. See Fig.2.1 for core location.

- HBS09-G17B

The XRF results of the selected elements profiles for this core are shown in Fig. 3.22. This core shows an abrupt change in elemental data at around 30 cm core depth. The 30 cm boundary separates a shell- rich lower part from a shell-poor upper part. Manganese profile shows an increase in the uppermost 3 cm of the core in parallel with Br and I content and shows a decrease in 3-7 cm interval of the core whereas Fe and S profiles show an increase. Manganese profile again shows a general downcore increase until the boundary at 30 cm core depth. Below the boundary Mn profile fluctuates, showing small up and down excursions until the end of the core. Iron and S values are low in the first 3 cm of the core, increase in 3-7 cm

interval, and show uniform trend until the 30 cm boundary with minor changes. Below the boundary both elements show distinct changes. Iron in parallel with S, Ti and K, shows abrupt decrease below the boundary. Calcium enrichment is observed where Fe decreases. Calcium profile has uniform trend until the 30 cm boundary below which it shows an abrupt increase corresponding to the shell rich interval. Bromine and I show enrichment at the uppermost part of the core and their trend does not change much until to the 30 cm boundary. Below the boundary Br shows a decreasing distribution whereas I is enriched similar with the Ca profile. The abrupt changes in all the profiles observed at the intervals of 10.5-12 cm and 42-43 cm are because of voids in the sediment, according to validity values of XRF data, and these data are untrustworthy.

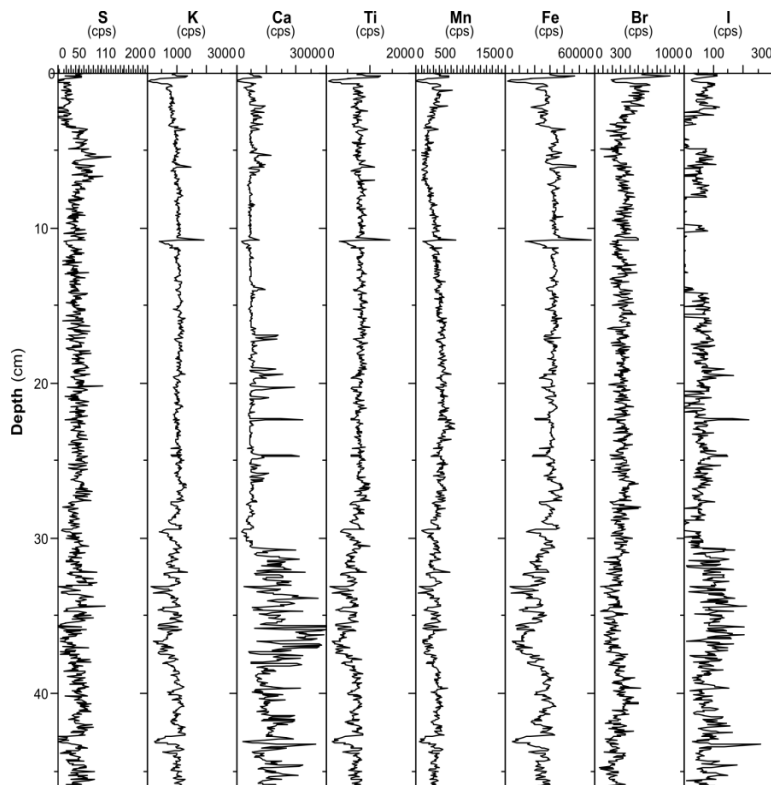


Figure 3.22 :XRF/depth profiles of K, Ti, Mn, Fe, S, Ca, Br and I in the HBS09-G17B core collected from -120m at western side (SL8), show sharp changes at 30 cm core depth and Mn shows distinct decrease at 3-7cm interval in association with Fe-S enrichment. See Fig.2.1 for core location.

- HBS09-G15B

The XRF elemental profiles for this core are presented in Fig. 3.23. The uppermost 8 cm of the core are characterized by low Mn values, the increase dramatically in remaining part of the core. At 3-9 cm interval of the core Fe and S values show

enrichment where sediment shows faint reduced black laminae. Manganese is depleted in parallel with the Fe and S at this interval of the core. Iron and S values show uniform values below 9 cm. Potassium and Ti profiles show a uniform downcore distribution with minimum values in the uppermost 0.5 cm of the core. Calcium also shows uniform distribution throughout the core, except for minor increase in 2.5-6 cm and 21-26 cm intervals. Bromine shows a uniform profile below 1 cm. It is enriched in the uppermost 1 cm. Iodine shows a slight enrichment in the upper 2 cm part of the core. It is below detection in 3-10 cm interval, and below 10 cm, shows a uniform distribution similar to the S profile.

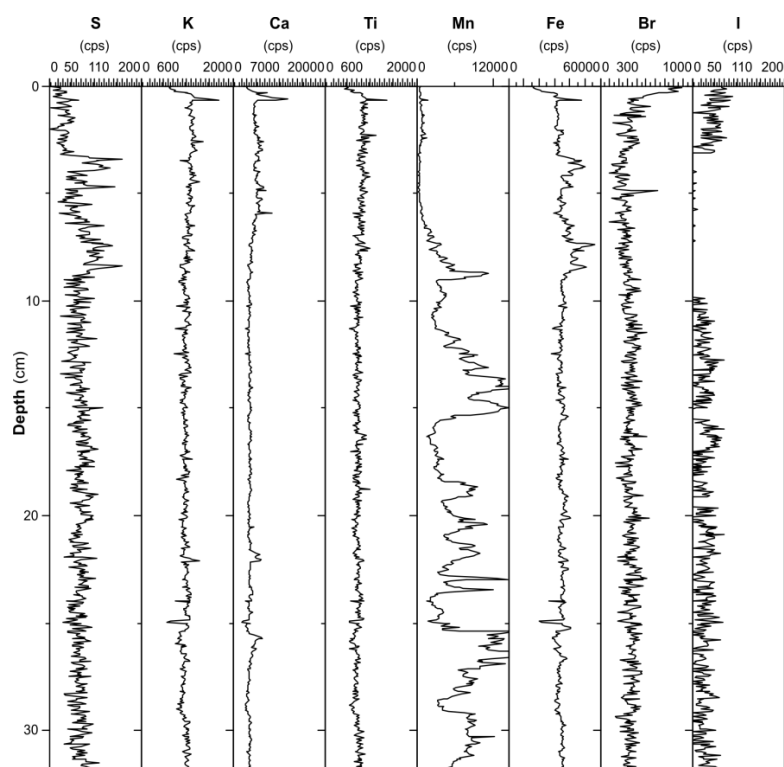


Figure 3.23 : XRF/depth profiles of K, Ti, Mn, Fe, S, Ca, Br and I in the HBS09-G15B core collected from -160m at western slope area (SL8), Mn values fluctuate below the depth of 8 cm, Fe-S enrichments are observed at the topmost 8 cm of the core where Mn is depleted. See Fig.2.1 for core location.

- MSM015-311

The elemental profiles for this core are given in Fig. 3.24. The profiles show a sharp change at around 43 cm core depth also observed in lithological properties changing from olive green gray sediment to dark gray black sediment. Manganese profile shows uniform distribution until 38 cm core depth where Mn shows high peak and decreasing values below this peak. At 38-43 cm interval, Mn starts to increase and

below 43 cm boundary Mn profile shows fluctuations and higher values than the upper parts of the core until the end where sediment is olive green gray in color and denser than the upper unit. Iron, S, Ti, K and Ca profiles show similar downcore distribution with minor decreasing values at 7-9 cm, 14.5-16 cm and 35-38 cm intervals. Below 43 cm core depth, Fe, S, Ti, K and Ca profiles show increasing trends until the end of the core. Bromine shows higher values in the upper part of the core until the boundary at 43 cm core depth, below which it shows a uniform trend. Iodine profile shows a similar trend to Br profile but the difference is not as much as Br values. There is a slight increase in the I values above the boundary.

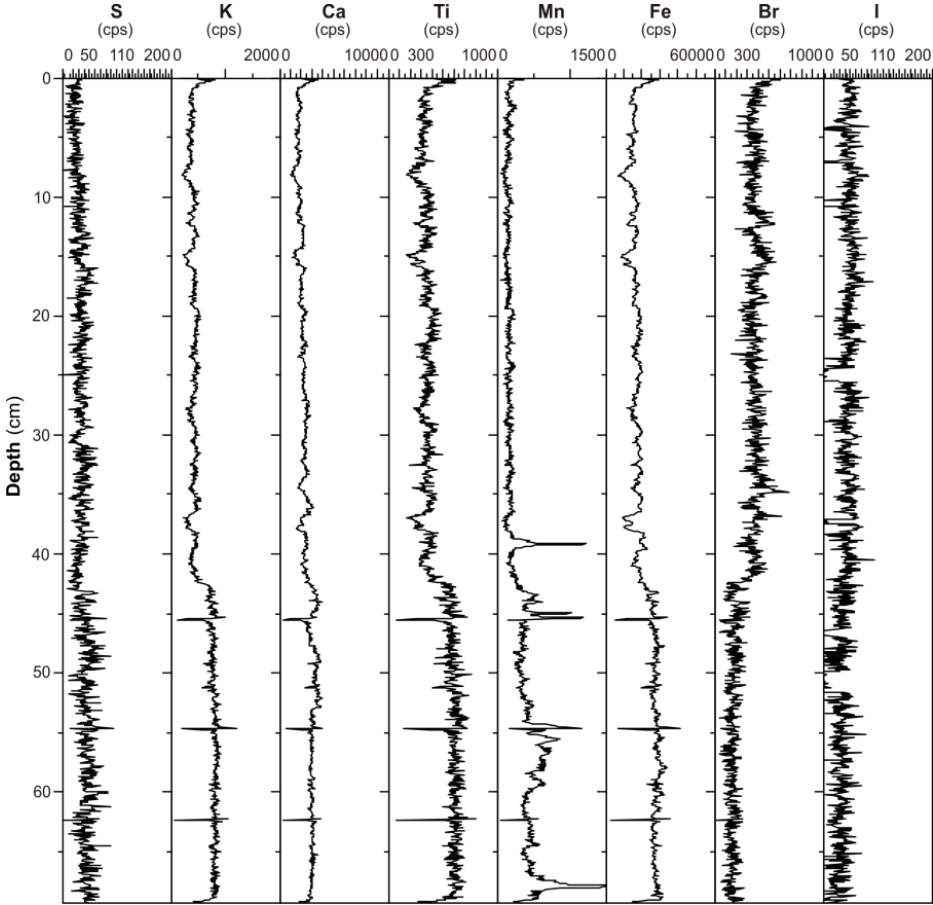


Figure 3.24 :XRF/depth profiles of K, Ti, Mn, Fe, S, Ca, Br and I in the MSM015-311 core collected from -307m at western slope area (SL8), show a sharp change of the elemental data at around 40 cm core depth, Mn depletion observed above the boundary. See Fig.2.1 for core location.

3.4 Total Organic Carbon and Total Inorganic Carbon Results

3.4.1 Seismic Line 1 (SL1) cores

TOC and TIC profiles of core MSM015-300 show fluctuations throughout the core length with highest TIC values (7%) at 15 cm and 50 cm and highest TOC values (2-2.5%) at the uppermost 5 cm part of the core. TOC values show a decreasing trend (2-1%) below 23 cm core depth, continue at its minimum values (1%) until 43 cm core depth, and start to increase (1-2%) below this depth until the end of the core. TIC values show a fluctuating downcore distribution, having 3-4% at the uppermost 9 cm, increasing to 4-7% at 9-14 cm interval, continuing at lower values (2.5-3%) between 14 and 43 cm interval and increasing again to 7% at 50 cm core depth. The lowest values (1%) of TIC are observed at the end of the core at 57 cm core depth (Fig. 3.25a).

TOC and TIC values of the core HBS09-G04C show fluctuating downcore distribution. TOC values vary between 3 and 4% in the uppermost 5 cm, and in the 30-40 cm interval. TOC content decreases to 1-2% in the 5-22 cm interval and at 40 cm core depth, and increases to 2-3% until the end of the core. TIC profile shows a trend around 1-3% throughout the core with high values (3%) at 22 cm, 36-44 cm interval and 64 cm core depth (Fig. 3.25b).

TOC and TIC profiles of the core MSM015-245 show distinct changes below the 40 cm core depth. TOC values reach to 2.5-3% at the uppermost 5 cm of the core and start to decrease downward showing uniform trend with percentage around 1.5% until 40 cm core depth. Below this level, TOC content starts to increase first to 2-2.5% at 50 cm and then to 3-4% at the end of the core. TIC downcore distribution shows an unchanging trend at around 1% until the 40 cm depth, below it starts to increase with a maximum value (4.5%) at 50 cm core depth. Towards the end of the core, TIC values show a uniform trend with decreased values to 2% (Fig. 3.25c).

TOC profile of the core MSM015-192 shows increased values in the top 10-15 cm of the core with a percentages around 3-4%. In 10-20 cm interval, TOC values are between 1.2-2%. The TOC values increase to 3-3.5% in the 30-35 cm interval and to 2-3% below 35 cm until the end of the core. TIC values of this core show fluctuations between 0.7 and 1.6% in the core with a distinct decrease from 22 cm towards the top of the core (Fig. 3.25d).

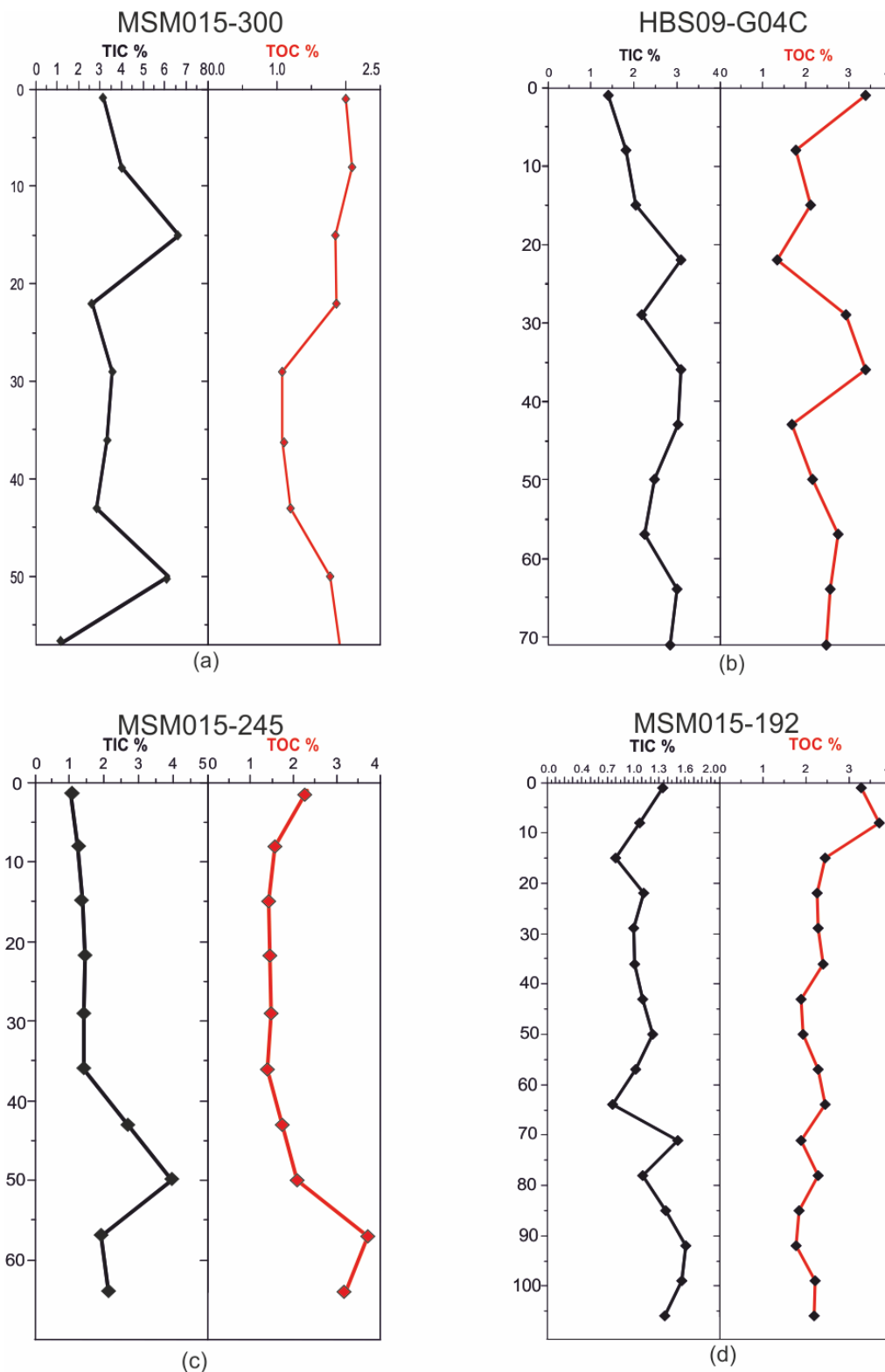


Figure 3.25 :Depth (cm)/TOC and TIC profiles of Seismic Line 1(SL1)cores located at eastern part of the area. (a) MSM015-300 core from -83m, (b) HBS09-G04C core from -122m, (c) MSM015-245 core from -158 m, (d) MSM015-197 core from -307m water depth. See Fig.2.1 for core locations.

3.4.2 Seismic Line 8 (SL8) cores

Downcore TOC distribution of the core HBS09-G18 shows a decreasing downcore trend of TOC content until 45 cm core depth, with values ranging from 2-3% (Fig. 3.26a). Below 45 cm depth TOC shows uniform trend around 1.5% until the end of the core. TIC profile ranges from 1.3% to 2.4% with the maximum value at 44 cm core depth.

TOC and TIC values of the core HBS09-G17B have ranges of 1.8-3.1% and 1.5-7.5%, respectively (Fig. 3.26b). TOC values show decreasing trend in the first 15 cm of the core from 3.1% to 1.8%. Downcore distribution of TOC shows slight fluctuations until the 30 cm depth. Below this depth TOC values show increasing trend to 3-3.5%. TIC content shows a minimum value of 1% at 9 cm core depth. Below this depth, TIC content show an increasing trend with depth, reaching up to 7.5% at 36 cm core depth.

TOC downcore distribution of the core HBS09-G15B shows an increasing trend starting from 2% at 5 cm, increasing up to 4% at 25 cm and decreasing again to 2% at the end of the core (Fig. 3.26c). TIC content fluctuates between 1 and 2% throughout the core except for a distinct increase to 3% at 25 cm core depth.

TOC and TIC profiles of the core MSM015-311 show uniform distributions until about 40 cm core depth, with values 3-4% and 1.3-1.8%; respectively (Fig. 3.26d). The TOC and TIC values drop below about 40 cm to values 2% and 1-1.8%, respectively where lithological and elemental analysis indicate a sharp boundary.

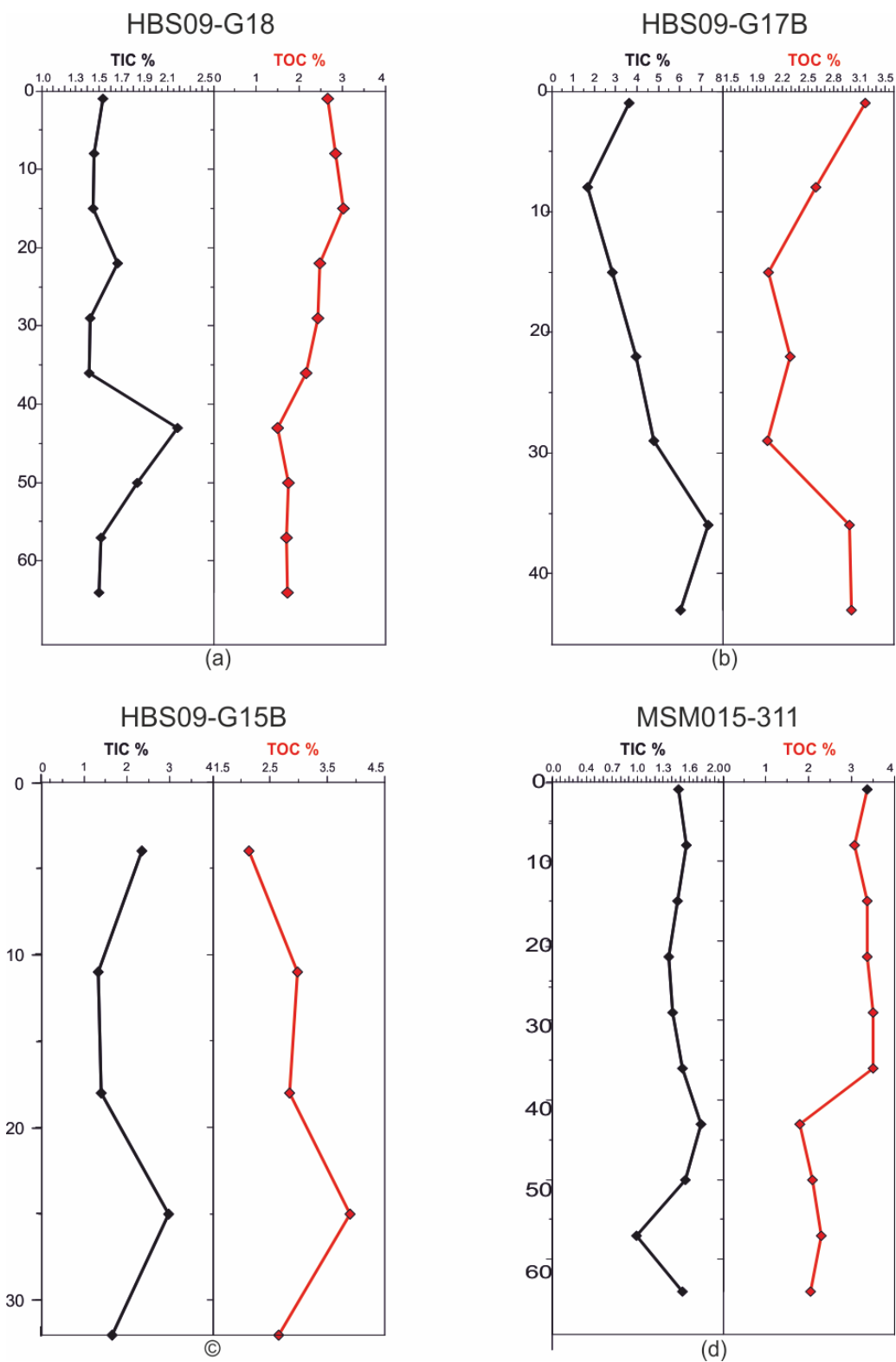


Figure 3.26 :Depth (cm)/TOC and TIC profiles of Seismic Line 8 (SL8)cores located at western part of the area. (a) HBS09-G18 core from -93m, (b) HBS09-G17B core from -120m, (c) HBS09-G15B core from -160m, (d) MSM015-311 core from -307m water depth. See Fig.2.1 for core locations.

4. DISCUSSION

The studied cores located on depth transects, except core MSM015-300, show different water column properties, including the bottom water oxygen conditions and effect of Mediterranean Water (MW). Core MSM015-300 being located at -83m, does not show any major changes regarding to bottom water oxygen condition. Instead, redox-sensitive element profiles and the presence of benthic fauna indicate oxic bottom waters during the deposition of the whole core sequence (Fig. 4.1).

In this chapter, results detailed in the previous chapter are discussed in order to changing conditions of the oxic/anoxic boundary and the MW effect in the study area.

4.1 Changes in the Oxic/Anoxic Boundary

Lithological properties of MSM015-300 core located at -82m at eastern side of the outlet area, suggest an environment in which an active inflow affects the zone bringing material to the area from time to time. When there is abundant material and oxygen, there is high accumulation of benthic faunal and coarser material. In the absence of this inflow sediment shows dark colour with fine grain size and faint banding as indicated in shaded areas in Fig. 4.1. Periodical changes in gamma density, Fe and Ca levels indicate the changing mineral content. Lower density values are indicated by both gamma density values and radiography image of the core. Intervals with high Ca and TIC and low Fe values are characterized by the presence of in situ shells and shell fragments where density shows higher values indicating active inflows. Manganese profile of the core shows uniform trend throughout the core indicating that there has not been any change in bottom water oxic conditions during the deposition of the whole core sequence at -82m on eastern side. Increased TOC values in the upper parts of the core MSM015-300 indicate the increased organic matter production and/or pollutant input above 10 cm core depth.

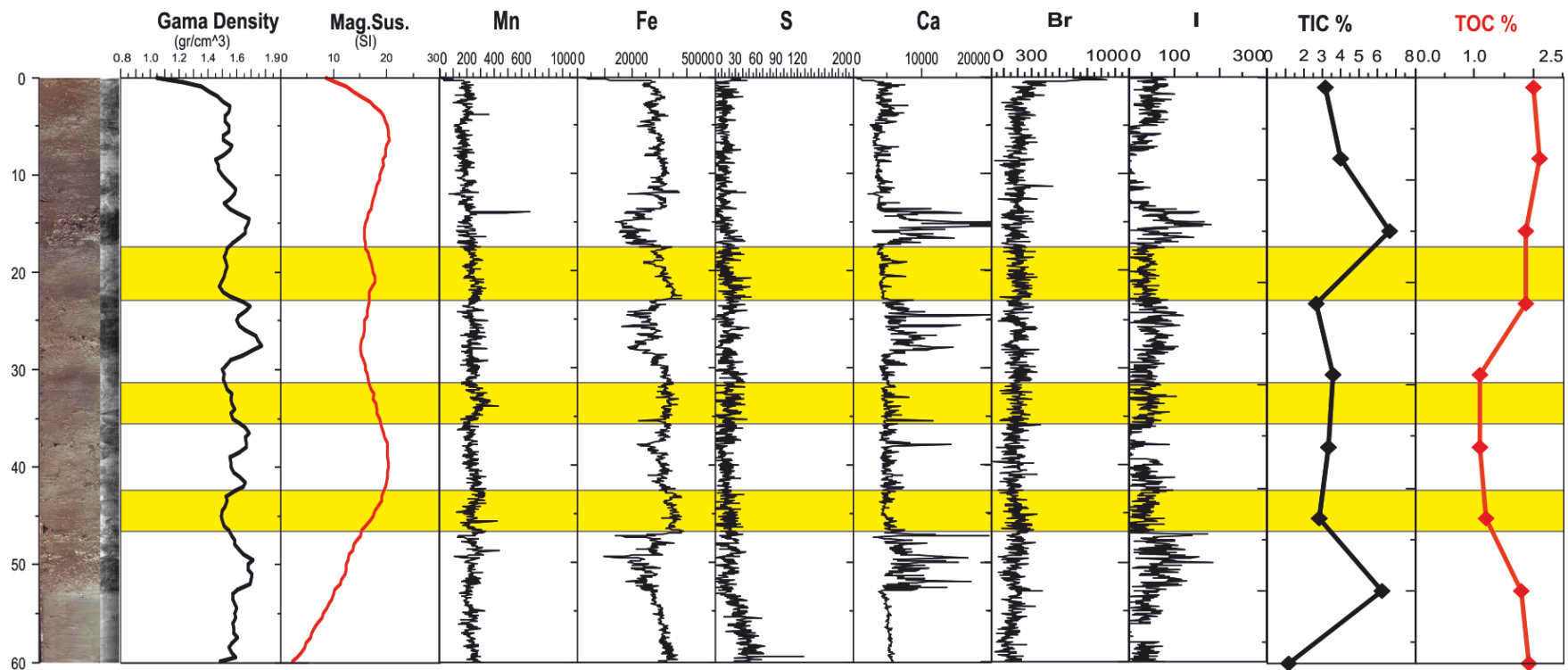


Figure 4.1 : MSCL, XRF and TOC/TIC results of MSM015-300 core collected from -93m in eastern side (SL1) above the present anoxic/oxic boundary. Yellow shaded areas indicate the intervals without shell, shell fragments and transported material. Elemental concentrations are in cps. See Fig. 2.1 for core location.

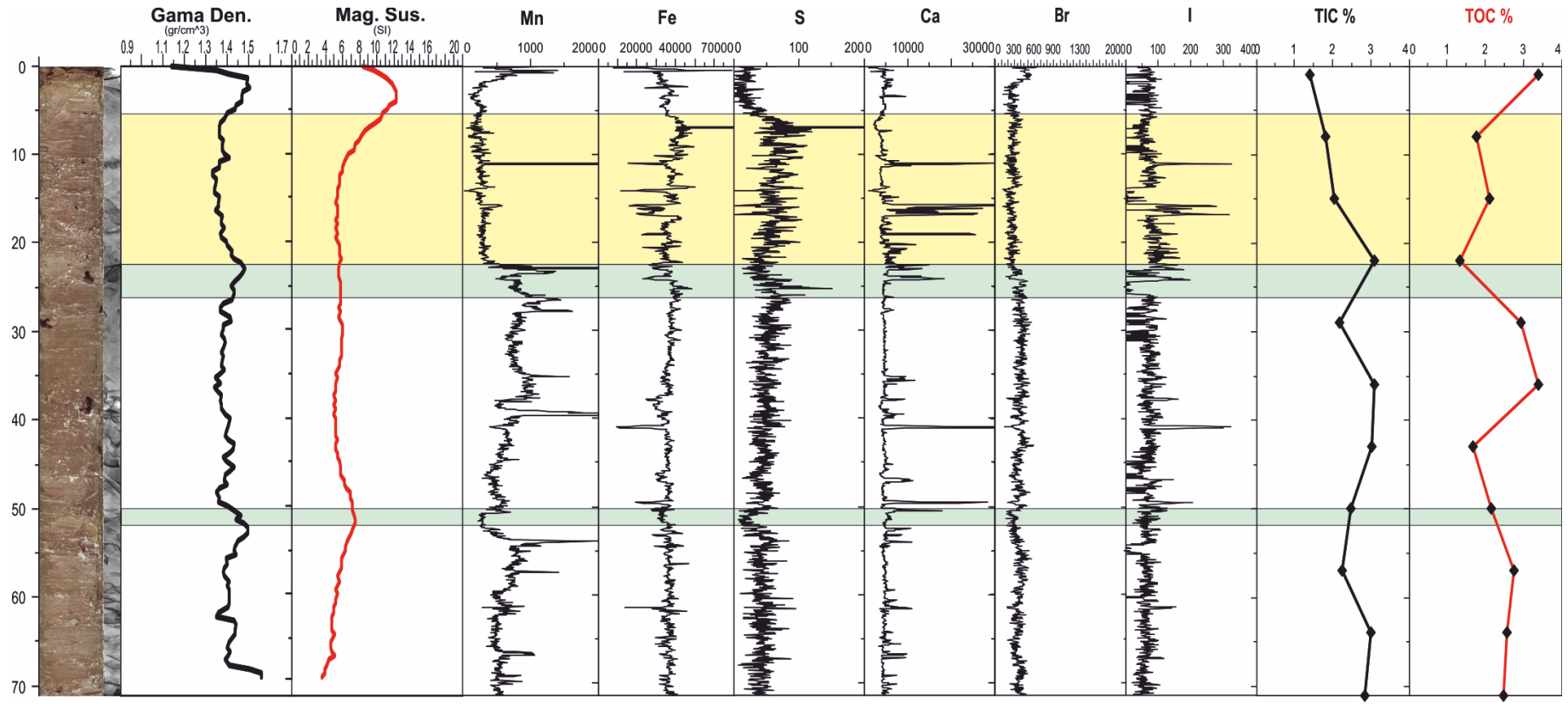


Figure 4.2 : MSCL, XRF and TOC/TIC results of HBS09-G04C core collected from -120m in eastern side (SL1) above the present anoxic/oxic boundary. Green shaded areas indicate the distinct decrease in Mn-Fe-S values, yellow shaded area indicate reducing conditions by depleted Mn and enriched Fe-S values with increasing TOC values. Elemental concentrations are in cps. See Fig. 2.1 for core location.

Core HBS09-G04C collected from -120m on the eastern slope area consists of green-gray mud with in situ euryhaline shells observed both in the sediments and in the radiographic image of the core, indicate the bottom water oxic conditions throughout the core. Fluctuating Mn and Ca data in association with TIC values also support the bottom water oxic conditions in the area (Fig. 4.2). The lithological properties with decreasing amount of in situ shells and decreasing Mn values in association with increased values of Fe and S above 24cm core depth of the core indicate a recent oxygen depletion in the water column during the deposition of the upper part of the sequence above 24cm. The uppermost 5 cm of the HBS09-G04C core is rich in organic carbon content together with the Br content indicating the organic pollution and/or high organic productivity in the last few decades.

Distinct lithological and geochemical changes at 42cm of core MSM015-245, located at -152m on the eastern continental slope area, indicate an abrupt change from oxic to anoxic conditions as a result of oxic/anoxic interface shoaling at 6.8 ka BP as dated by ^{14}C method (Fig. 4.3). Different density values recorded by both gamma density profile and radiographic image of the upper and lower part of the core show the lithological differences of the two units. Prevailing oxic conditions before 6.8 ka BP, are indicated by the colour of the sediment and predominantly in situ large *Mytilus sp.* shells in the lower unit. High values of Ca, TIC and Mn values also support that environment has been suitable for benthic fauna below the boundary so that water column at these depths has been fully oxic. Dark gray to dark green gray mud containing FeS mottlings and lenses and increased magnetic susceptibility values above the boundary show the increased preservation of iron-rich material in the sediment supporting the prevailing reducing conditions in upper unit.

Physical and geochemical data of core HBS09-G17B, located at -120 m on the western slope area, indicate a sharp boundary as observed at MSM015-245 core. Sharp boundary takes place at around 30 cm core depth indicated by lithological, physical and geochemical data (Fig. 4.4). According to the calibrated ^{14}C age results from *Mytilus sp.* shell this sharp boundary corresponds to 6.8 ka BP. As observed from the radiographic image and the lithological description of the core in situ euryhaline shells are dominated below the boundary also indicated by high Ca and TIC values.

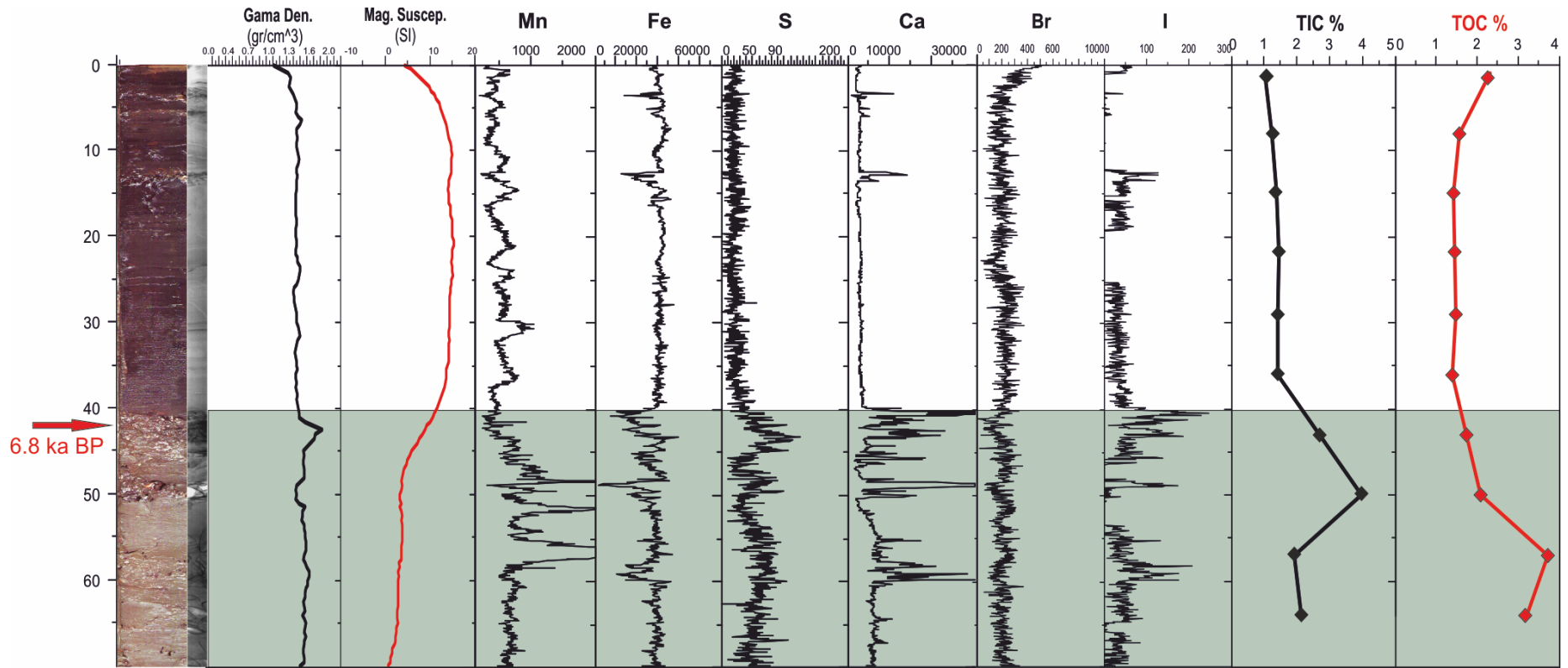


Figure 4.3 :MSCL, XRF and TOC/TIC results of MSM015-245 core collected from -152m in eastern slope area (SL1) below the present anoxic/oxic boundary. Green shaded area indicate bottom water oxic conditons by high values of Mn, Ca and TIC and shell abundance. Sharp boundary is dated as 6.8 ka BP. Above the boundary Mn fluctuations show the MW ventilation effect. Elemental concentrations are in cps. See Fig. 2.1 for core location.

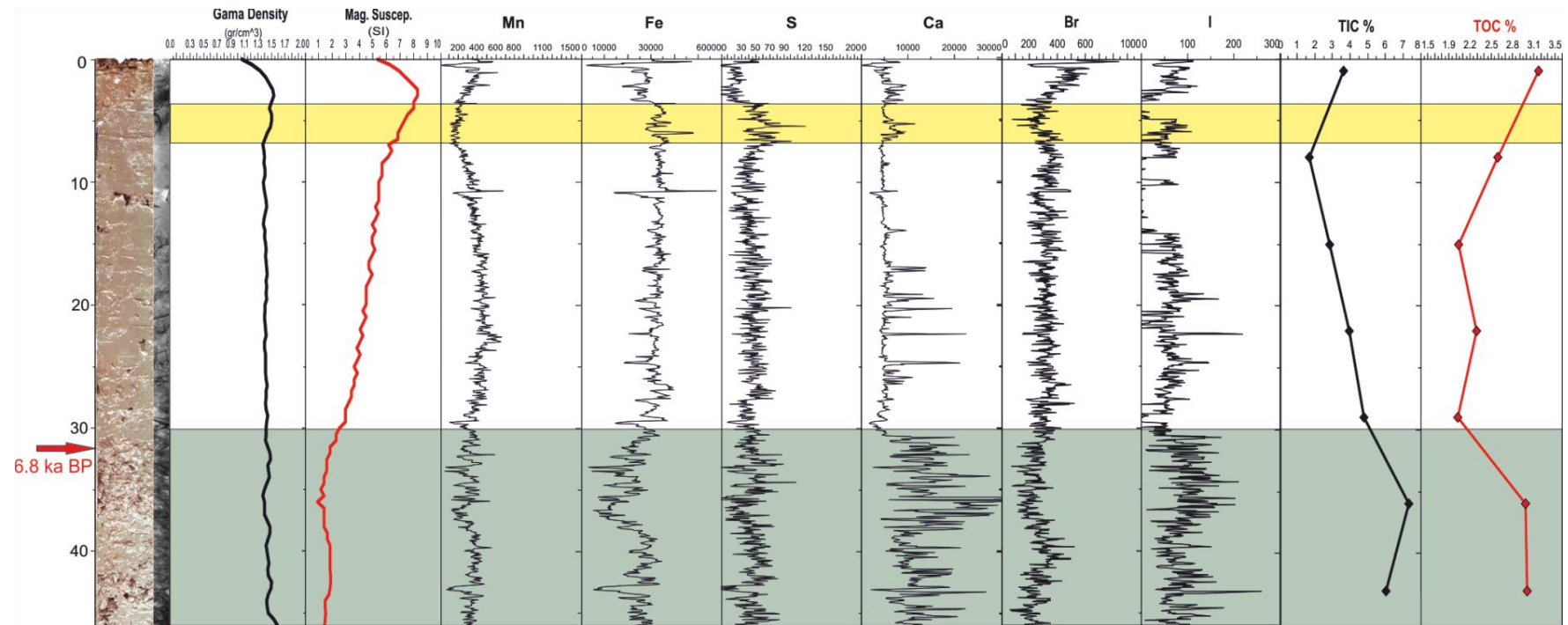


Figure 4.4 :MSCL, XRF and TOC/TIC results of HBS09-G17B core collected from -120m in western side (SL8) above the present anoxic/oxic boundary. Green shaded area indicate a different unit with shell abundant oxygenated bottom water conditions. Sharp boundary is dated as 6.8 ka BP. Yellow shaded area indicate anoxic to suboxic bottom water conditions. Elemental concentrations are in cps. See Fig. 2.1 for the core location.

Fluctuations of XRF data observed below the boundary are because of the abundance of large shells. Iron and S behave in contrast to Ca where magnetic susceptibility values support the lower amounts of Fe related material accumulation below the boundary. Upward decreased values of Ca and the presence of shells above the boundary show that reducing conditions start to prevail as a result of oxic/anoxic interface shoaling at 6.8 ka BP at the whole upper slope area.

Core MSM015-192 located at -307m on the eastern continental slope area, shows the anoxic sediment properties with its laminated and banded dark gray to black soft sediment and high gas content. Gas disturbance is observed from radiographic image and physical properties of the core indicated by white colour and abrupt decreases respectively (Fig. 4.5). No sharp boundary throughout the core is observed from physical and geochemical analysis indicating that this core consists of only Coccolith Unit (Unit 1) (Degens and Ross, 1974; Çağatay, 1999). High TOC values (3-4%) support that environment is suitable for organic matter accumulation and preservation of organic matter indicating anoxic conditions. Bromine data of core is related to organic matter preservation as observed in the Fig. 4.5 and it shows distinct increase as TOC values increase at the uppermost 15 cm of the core.

HBS09-G18 is collected from -93m from the western part of the study area where is located above the oxic-anoxic interface today. Physical properties and TOC/TIC values of the core shown in the Fig. 4.6 indicate upward changes of the water column conditions. Decreased values of density profile supported by radiographic image, the slight upward decrease of Ca and TIC values and decreasing amount of benthic fauna identified from both radiographic image and the lithological properties above 30 cm core depth indicate the progress of reducing conditions in the area. Increasing values of magnetic susceptibility above 30 cm core depth indicate the accumulation of iron-rich material supporting the prevailing reducing conditions. It is assumed that the upward rising of suboxia can be observed throughout the core. Low values of density and magnetic susceptibility where Fe shows a distinct decrease are related to higher TOC values in the interval. Slightly decreasing values of Fe are considered to be effected by terrigenous input so that Fe values are normalized by dividing Fe values by Ti to eliminate the terrigenous Fe and to be able to observe the changing amounts of Fe related to reducing conditions. Distinct enrichment of Mn/Ti, Fe/Ti and S/Ti values at 7-13 cm interval (Fig. 4.7) where the colour of the sediment is

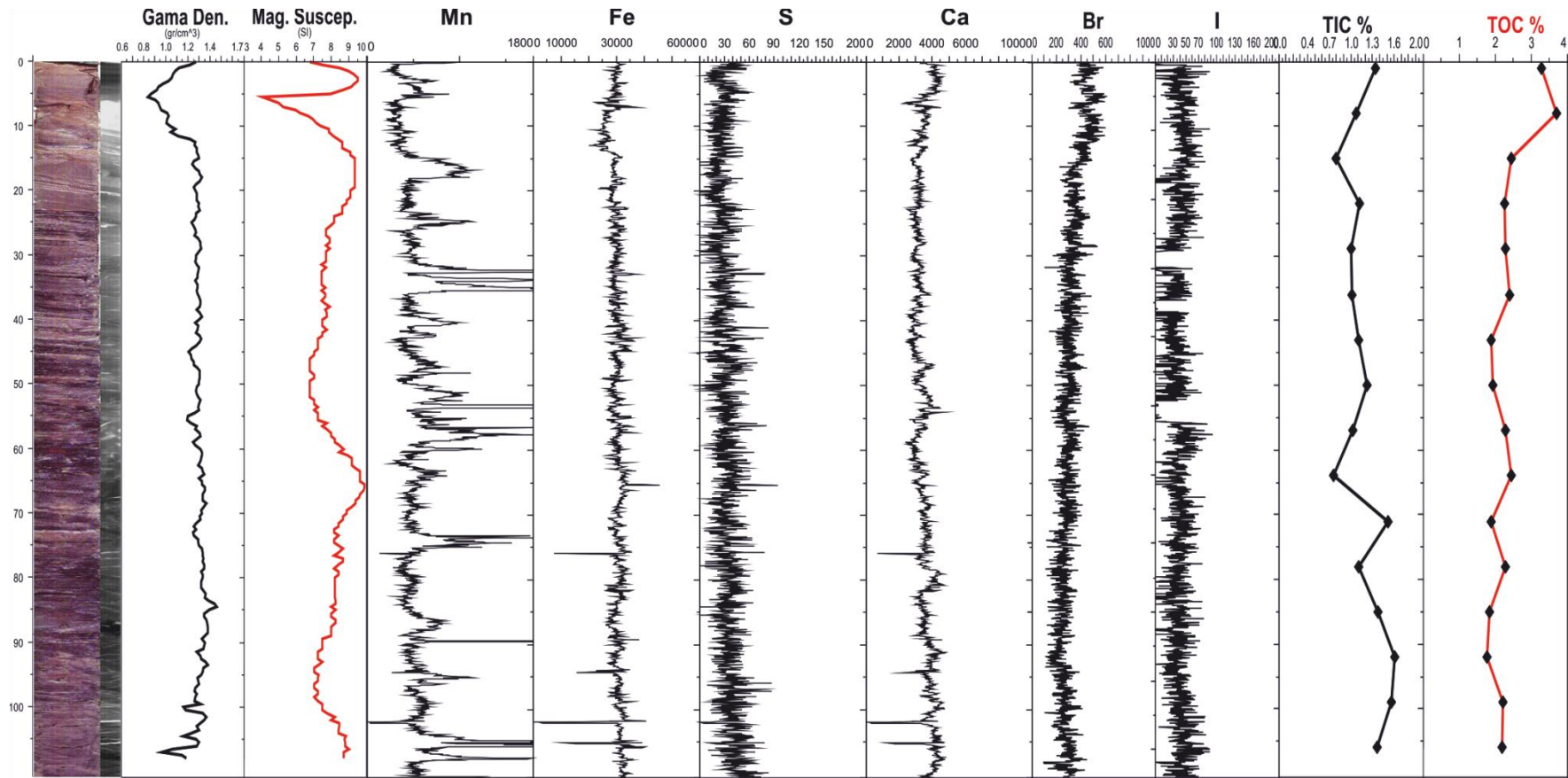


Figure 4.5 :MSCL, XRF and TOC/TIC results of MSM015-192 core collected from -307m in eastern slope area (SL1) below the present anoxic/oxic boundary. MW ventilation effect indicated by Mn fluctuations. Elemental concentrations are in cps. See Fig. 2.1 for the core location.

darker than the rest of the core indicate that oxic/anoxic boundary rose until this depth. Similar results are discussed at a work of Lyons et al., (1993). According to their results, it is indicated that Mn, S and Fe profiles show increased values at the shallow part of the sediment core obtained from the continental shelf area and they indicate that the rise of the interface occurred around 250-300 a BP by extrapolating the Pb-210 based accumulation rate to the depth of the lower Fe-Mn-S peaks. Considering the uncalibrated age (505 a BP) obtained from 21-23cm core depth for the core HBS09-G18, the data presented here supports the findings of Lyons et al. (1993). As a result of this interpretation it is understood that anoxia has reached up to 93m water depth at the SW continental shelf area of the Black Sea basin at around 250-300 a BP.

XRF results of core HBS09-G17B located at -120m at the western slope area, show depletion of Mn values at 3-7 cm interval where Fe-S values show enrichment indicating reducing conditions at that period (Fig. 4.4) Reducing conditions probably correspond the same period as oxic/anoxic interface observed at the 7-13cm interval of core HBS09-G18. When anoxia reaches to -93m, and stayed there, below that depth, water column remained anoxic for a period of time.

HBS09-G15B is a short core located at -160m on the western upper slope area where anoxic conditions prevail today. As observed from the lithological properties and the radiographic image of the core, benthic fauna is absent above 20 cm core depth indicating the prevailing reducing conditions (Fig. 4.8). High Mn values above this depth and following Mn depletion in parallel with Fe and S enrichment in the top part of the core indicate the prevailing anoxic bottom water conditions. Calibrated age determined from in situ *Mytilus sp.* shell at 26-28 cm core depth shows that at around 5.5 ka BP, bottom water were still oxic in the area.

MSM015-311 core is located -307m on the western slope area where the bottom water conditions are anoxic today. Physical, lithological and geochemical properties, as shown in the Fig. 4.9, indicate the presence of two different units with a sharp boundary at around 42 cm core depth. Green gray mud with higher values of density indicated by both gamma density values and the radiographic image of the core show that much more dense material accumulation occurred under oxic bottom conditions containing terrestrial and iron-rich material as indicated by higher magnetic susceptibility values below the boundary. Calibrated ^{14}C age of this boundary is

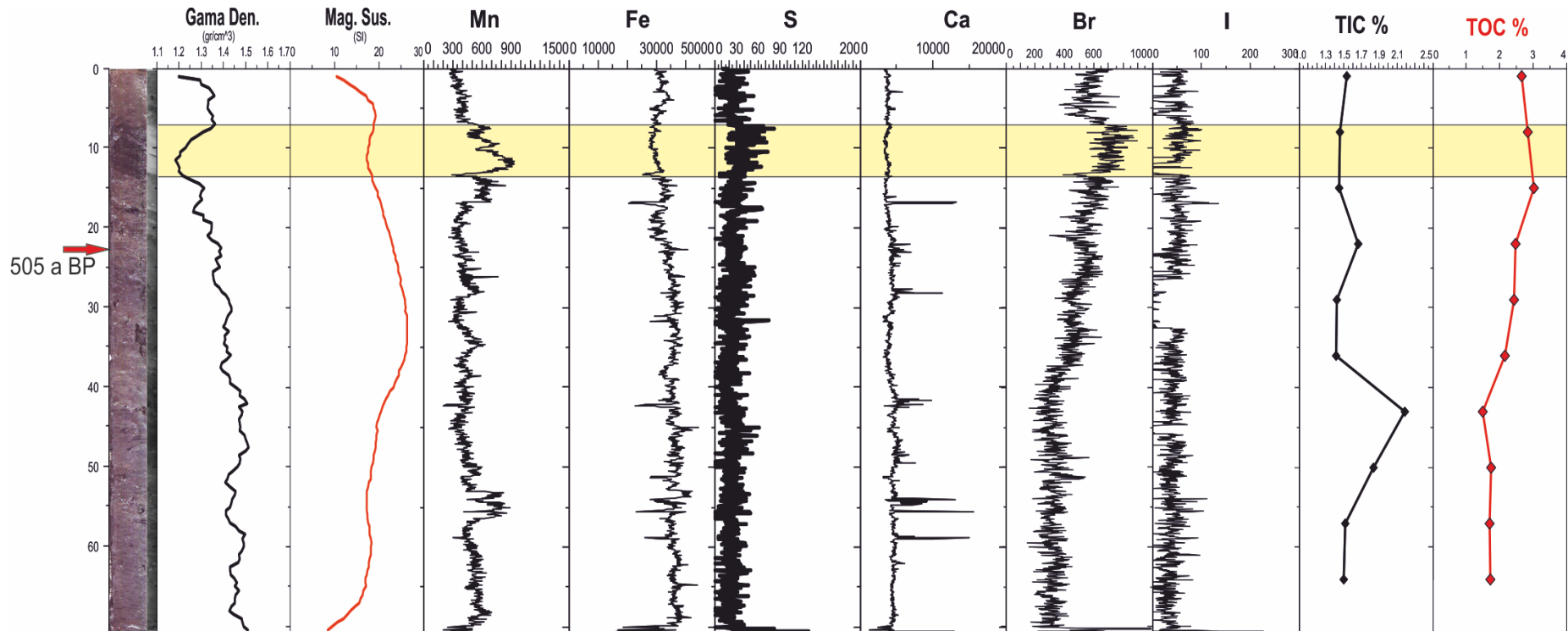


Figure 4.6 :MSCL, XRF and TOC/TIC results of HBS09-G18 core collected from -93m in western side above the present anoxic/oxic boundary. Upward decrease in the amount of oxygen is recorded. Yellow shaded area indicate the recent shoaling of oxitic/anoxic boundary (See also Fig. 4.7). Elemental concentrations are in cps. See Fig. 2.1 for the core location

5.3 ka BP. Higher values of Mn, Fe, and Ca below the boundary indicate the prevailing oxic bottom water conditions and terrestrial input in the area before that time. Foraminiferal data also gives information about the changing water column conditions; *Hyalina baltica* observed at 66-68 cm interval whereas *Ammonia sp.* and *Aubigny perlucida* observed just below boundary indicating the changing conditions from saline and oxic to less saline and suboxic.

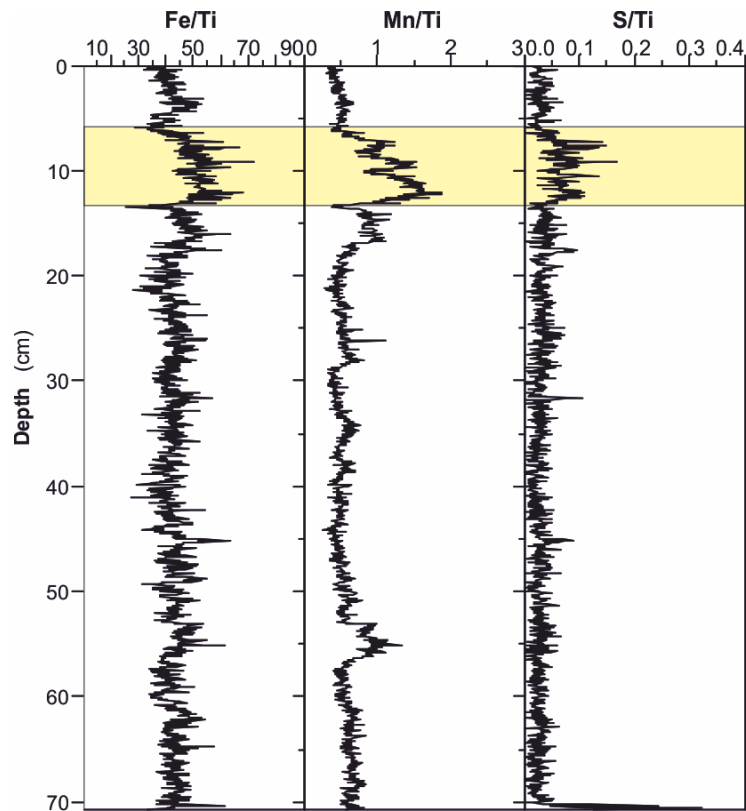


Figure 4.7 :Ti normalized Fe-Mn-S element profiles of HBS09-G18 core located at -93m western side above the present anoxic/oxic boundary. Yellow shaded shows enrichment of Mn-Fe-S record of oxic/anoxic shoaling. Elemental concentrations are in cps. See Fig. 2.1 for the core location.

4.2 Mediterranean Water (MW) Effect

Above the 6.8 ka BP boundary in MSM015-245 core, Mn is depleted as a result of the anoxic/oxic interface shoaling but some high Mn fluctuations are recorded in the upper unit until the topmost part of the core (Fig. 4.3). These Mn fluctuations are unassociated with Fe and S indicating the ventilation effect of MW, started at 6.8 ka BP in the eastern side of the study area where Seismic Line 1 (SL1) is located.

Manganese profile of core MSM015-192, located at -307m on the eastern slope area, shows fluctuations unassociated to Fe and S enrichments (Fig. 4.5), as observed in core MSM015-245 XRF results above the boundary, indicating the active MW ventilation effect in the area. As a result of this preserved Mn values in these cores, it is assumed that MW ventilation is effective today at the continental slope to the depths of at least -300m of eastern side of the study area, starting at 6.8 ka BP.

As indicated in the previous section, the upper part of the -160m western slope HBS09-G15B core shows prevailing bottom water anoxia in the area today but it was still oxygenated at 5.5 ka BP whereas in the eastern slope area shoaling of oxic/anoxic interface occurred at 6.8 ka BP. This oxygenation process is due to the present MW effect in the area at that time. Manganese profile does not show any fluctuations above oxic/anoxic interface observed in the sediment column showing that there is no MW ventilation effect in the area today.

The transition zone from oxic to anoxic bottom water conditions in the western upslope area where MSM015-311 core is located at -307m, indicated by Mn peaks at around 38 cm core depth. Above this sharp lithological and geochemical boundary, TOC values show an upward increase up to 3-4% in association with Br and I content. As observed by high TOC and low Mn values above the boundary, from 5.3 ka BP anoxic bottom water conditions started to prevail at this area. Manganese does not show any fluctuations like observed at MSM015-192 core located at eastern part of the study area on SL1. This comparison combined with the bathymetrical map information (Figure 2.1 :) shows that on the western side of the study area MW has been effective until 5.3 ka BP and today in the area no MW ventilation effect is observed. Direction of MW can also be observed in CTD profiles provided in November 2009 R/V Arar Cruise as shown in Fig.1.6.

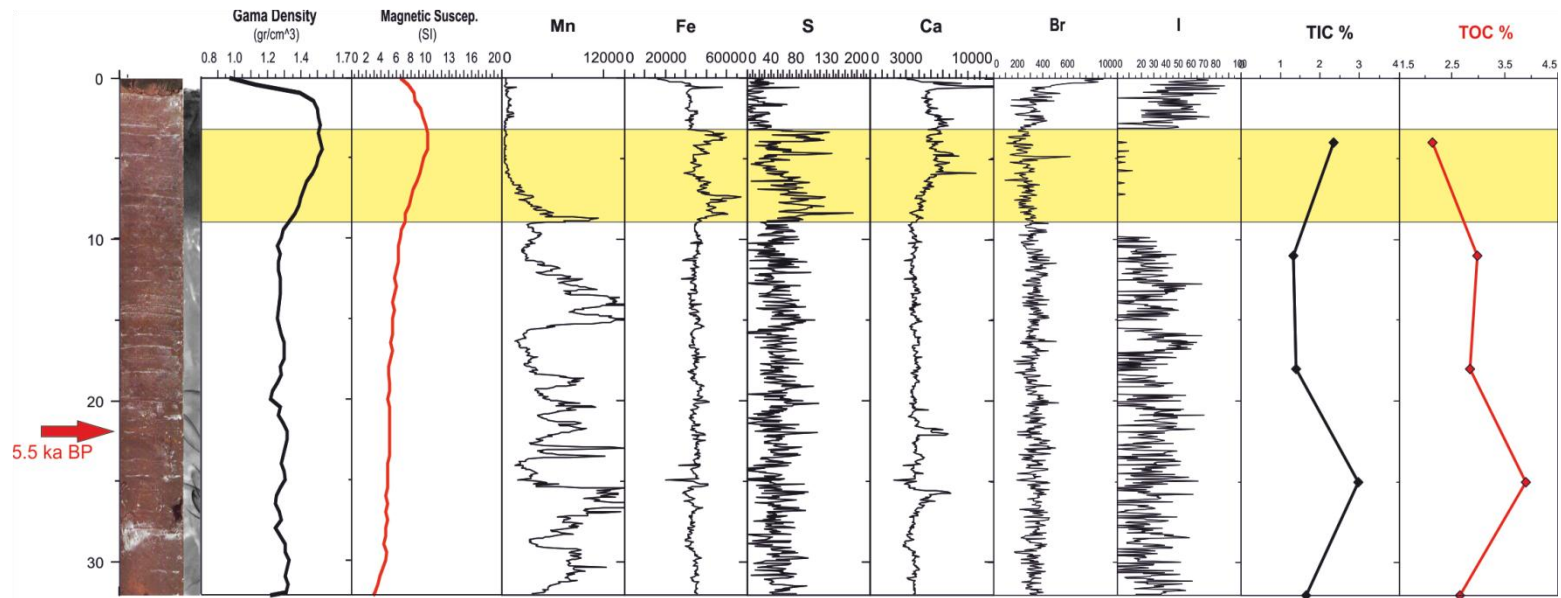


Figure 4.8 :MSCL, XRF and TOC/TIC results of HBS09-G15B core located at -160m western upper slope area below the present anoxic/oxic boundary. Oxidic bottom water conditions prevailed during 5.5 ka BP indicated by in situ shells observed radiographic image below 20 cm. Yellow shaded area indicated the anoxic bottom water conditions with depleted Mn values in association with Fe-S enrichments. Elemental concentrations are in cps. See Fig. 2.1 for the core location.

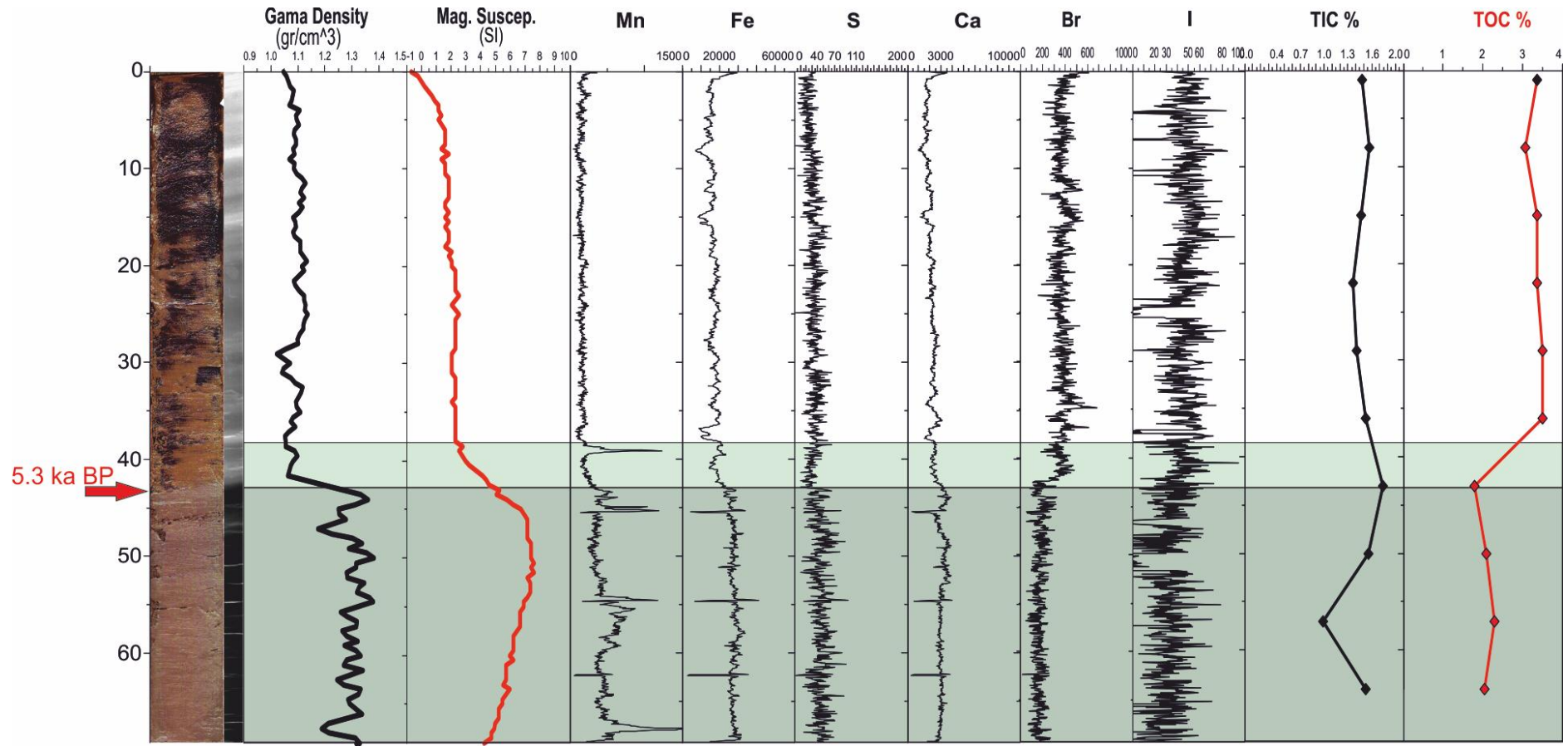


Figure 4.9 :MSCL, XRF and TOC/TIC results of MSM015-311 core located at -307m in western slope area below the present anoxic/oxic boundary. Green shaded area shows the past oxitic bottom water conditions before 5.3 ka BP. Lighter green area shows the transition zone from oxitic to anoxic bottom conditions. Present MW ventilation effect not recorded. Elemental concentrations are in cps. See Fig. 2.1 for the core location.

5. CONCLUSIONS

Outlet area of the Istanbul Strait shows a submarine fan delta with its channel-levée complex that was formed by the Mediterranean Water (MW) which started at 9.4 ka BP (Ryan et al., 2003; Major et al., 2006). Since then MW plays a great role in ventilation of the continental shelf and upper slope areas of the outlet area.

Cores collected from shallower than 150m water depth; consist of green gray mud with in situ euryhaline bivalve shells indicating prevailing oxic conditions. Below this depth cores consist of laminated and banded gray-dark gray to black mud with H₂S gas content indicating prevailing suboxic to anoxic conditions.

Lithological properties and geochemical analysis of the collected cores show an abrupt change in the position of oxic/anoxic interface. According to the redox sensitive element (Mn) profiles and benthic faunal content suboxic-anoxic conditions reached between -120m and -150m depth at 6.8 ka BP over the whole upper slope area.

At the eastern side of the upper continental slope area, at 150m water depth, anoxic conditions started to prevail at 6.8 ka BP, whereas at the western side of the area, at oxic conditions continued until 5.3 ka BP, where oxygen started to be depleted in the water column below 120m as indicated by the decreasing amount of in situ euryhaline bivalves. Furthermore, an abrupt lithological and geochemical change at -300m core on western slope area indicate that the ventilation effect of the MW continued to more than 300m depth until 5.3 ka BP. These results show that MW used the NW oriented main channel until 5.3 ka BP transporting oxygenated water to the area, but changed its course to the east after that date.

On the other hand, the presence of high Mn fluctuations unrelated to Fe-S system at the eastern slope area to depths of at least -300m show that MW ventilation has been active since the shoaling event of oxic/anoxic interface at 6.8 ka BP. This activity in this area continues today according to the CTD results.

A recent rise in the oxic/anoxic interface is determined in a sedimentary core collected at -93m. This rise is indicated by increased values of Mn-Fe-S and high TOC at 7-13 cm interval, corresponding to the intersection of the oxic/anoxic interface with the shelf edge area. 505 ¹⁴C a BP (uncalibrated) date obtained from 21-23cm of this core, correlates with the data of Lyons et al. (1993), which show a similar event dated 250-300 a BP by a radionuclide method.

REFERENCES

- Arthur, M. A., and Dean, W. E.**, 1998. Organic-matter production and preservation and evolution of anoxia in the Holocene Black Sea, *Paleoceanography*, **13**, 4, 395-411.
- Bahr, A., Arz, H., Lamy, F., Wefer, G.**, 2006. Late glacial to Holocene paleoenvironmental evolution of the Black Sea, reconstructed with stable oxygen isotope records obtained on ostracod shells, *Earth and Planetary Science Letters* **241**, 863-875.
- Bahr, A., Lamy, F., Arz, H.W., Major, C.O., Kwiecien, O., Wefer, G.**, 2008. Abrupt changes of temperature and water chemistry in the late Pleistocene and early Holocene Black Sea, *Geochemistry, Geophysics, Geosystems*, **9**, 1, 1-16.
- Baştürk, Ö., Saydam, C. Salihoğlu, I., Ereemeeva, L.V., Konovalov, S.K., Stoyanov, A., Dimitrov, A., Cociasu, A., Dorogan, L. and Altabet, M.**, 1994. Vertical variation in the principle chemical properties of the Black Sea in the autumn of 1991, *Marine Chemistry*, **45**, 149-165.
- Berner, R.A., Raiswell, R.**, 1983. Burial of organic carbon and pyrite sulfur in sediments over phanerozoic time: a new theory, *Geochimica et Cosmochimica Acta*, **47**, 5, 855-862.
- Calvert, S.E.**, 1990. Geochemistry and origin of the Holocene sapropel in the Black Sea. In: V. Ittekkot, S. Kempe, W. Michaelis and A. Spitzzy (Editors), Facets of modern biogeochemistry. Springer-Verlag, Berlin, Federal Republic of Germany, pp. 326-352.
- Calvert, S.E., Pedersen, T.F.**, 1993. Geochemistry of Recent oxic and anoxic marine sediments: Implications for the geological record, *Marine Geology*, **113**, 67-88.
- Chester, R.**, 2000. (Editor) *Marine Geochemistry*, Second Edition, Blackwell, London, 506 pp.
- Canfield, D.E., Raiswell, R., Bottrell, S.**, 1992. The reactivity of sedimentary iron minerals toward sulfide, *American Journal of Science*, **292**, 659-683.
- Codispoti, L.A. Friederich, G.E., Murray, J.W., and Sakamoto, C.M.**, 1991. Vertical variability in the Black Sea: Implications of continuous vertical profiles that penetrated the oxic/anoxic interface, *Deep-Sea Research*, **38**, 2A., 691-710.
- Croudace, I.W., Rindby, A., Rothwell, G.**, 2006. ITRAX: Description and Evaluation of a new Multi-function X-Ray Core Scanner. *New Techniques of Sediment Core Analyses*, Special Publications **267**, 51-63.

- Crusius, J., Calvert, S., Pedersen, T., Sage, D.,** 1996. Rhenium and molybdenum enrichments in sediments as indicators of oxic, suboxic and sulphidic conditions of deposition, *Earth and Planetary Science Letters*, **145**, 65-78.
- Çağatay, M.N.,** 1999. Geochemistry of the Late Pleistocene-Holocene Sediments of the Black Sea: An Overview, Environmental Degradation of the Black Sea: Challenges and Remedies, Eds: S. Beşiktepe et al., 9-22.
- Degens, E.T., Ross, D.A.,** 1974. Recent Sediments of Black Sea. *The Black Sea-Geology, Chemistry and Biology*, 183-199, Memoir 20, Eds. E.T. Degens, D.A. Ross.
- Di Iorio, D., Yüce, H.,** 1998. Observations of Mediterranean flow into the Black Sea. *Journal of Geophysical Research*, **104**, no. C2, 3091-3108.
- Di Iorio, D., Akal, T., Guerrini, P., Yüce, H., Gezgin, E. And Özsoy, E.,** 1999. Oceanographic measurements of the west Black Sea: June 15 to July 5, 1996. *Report SR-305*, Saclantcen; NATO, La Spezia.
- Duman, M., Duman, Ş., Lyons, T.W., Avci, M., İzdar, E., Demirkurt, E.,** 2006. Geochemistry and sedimentology of shelf and upper slope sediments of the south-central Black Sea, *Marine Geology*, **227**, 51-65.
- Flood, R. D., Hiscott, R. N., Aksu, A. E.,** 2009. Morphology and evolution of an anastomosed channel network where saline underflow enters the Black Sea. *Sedimentology*, **56**, 807-839.
- Güngör, E. and Çağatay, M.N.,** 2006. Rapid changes in the ecological conditions of the Black Sea over the last 3 ka. *İTÜ Dergisi/d*, **5**, 4, 23-33.
- Holtappels, M., Lichtschlag, A.,** in prep. Inflow of oxic Mediterranean waters into the anoxic layers of the Black Sea. (CTD profiles obtained during Black Sea cruise).
- Jones, G. A., Gagnon, A. R.,** 1994. Radiocarbon chronology of Black Sea sediments. *Deep Sea Research*, **41**, 3, 531-557.
- Klinkhammer, G.P., Palmer, M.P.,** 1991. Uranium in the oceans: Where it goes and why, *Geochimica et Cosmochimica Acta*, **55**, 1799-1806.
- Lyons, T.W., Berner, R.A., Anderson, R.F.,** 1993. Evidence for large pre-industrial perturbations of the Black Sea chemocline, *Nature* **365**, 538-540.
- Lyons, T.W., Severmann, S.,** 2006. A critical look at iron paleoredox proxies: New insights from modern euxinic marine basins, *Geochimica et Cosmochimica Acta*, **70**, 23, 5698-5722.
- Major, C.O., Goldstein, S.L., Ryan, W.B.F., Lericolais, G., Piotrowski, A.M., Irka, H.,** 2006. The co-evolution of Black Sea level and composition through the last deglaciation and its last paleoclimatic significance, *Quaternary Science Reviews*, **25**, 2031-2047.
- Morford, J.L., Emerson, S.,** 1999. The geochemistry of redox sensitive trace metals in sediments, *Geochimica et Cosmochimica Acta*, **63**, 11/12, 1735-1750.
- Murray, J.W., Jannasch, H.W., Honjo, S., Anderson, S., Reeburgh, W.S., Top, Z., Friederich, G.E., Codispoti, L.A. and Izdar, E.,** 1989.

- Unexpected changes in the oxic/anoxic interface in the Black Sea, *Nature*, **338**, 411-413.
- Oğuz, T., Latun, V.S., Latif, .A., Vladimirov, V.V., Sur, H.I., Markov, A.A., Özsoy, E., Kotovshchikov, B.B., Ereemeev, V.V., Ünlüata, Ü.**, 1993. Circulation in the surface and intermediate layers of the Black-Sea, *Deep-Sea Res. Part I*, **40**, 1597-1612.
- Oğuz, T., Malanotte-Rizzoli, P., Ducklow, H. W., Murray, J. W.**, 2002. Interdisciplinary studies integrating the Black Sea biogeochemistry and circulation dynamics, *Oceanography*, **15**, 3, 4-11.
- Oğuz, T., Tuğrul, S., Kideys, A. E., Ediger, V., Kubilay, N.**, 2005. Physical and biogeochemical characteristics of the Black Sea, *The Sea*, **14**, chapter 33: 1331-1369.
- Özsoy, E., Ünlüata, Ü.**, 1997. Oceanography of the Black Sea: a review of some recent results, *Earth Science Reviews*, **42**, 231-272.
- Özsoy, E., Di Iorio, D., Gregg, M. C., Backhaus, J. O.**, 2001. Mixing in the Bosphorus Strait and the Black Sea continental shelf: observations and a model of the dense water outflow. *Journal of Marine Systems*, **31**, 99-135.
- Plastino, W., Kaihola, L., Bartolomei, P., Bella, F.**, 2001. Background reduction in the radiocarbon measurement by scintillation spectrometry at the underground laboratory of Gran Sasso, *Radiocarbon*, **43** (2A), 157-161.
- Ross, D.A., Degens E. T. and MacIlvaine, J.**, 1970. Black Sea: recent sedimentary history. *Science*, **170**, 163-165.
- Ryan, W.B.F., Major, C.O., Lericolais, G., Goldstein, S.L.**, 2003. Catastrophic flooding of Black Sea, *Annual Review of Earth and Planetary Sciences*, **31**, 525-554.
- Siani, G., Paterne, M., Michel, E., Sulpizio, R., Sbrana, A., Arnold, M., Haddad, G.**, 2001. Mediterranean Sea Surface Radiocarbon Reservoir Age Changes Since the Last Glacial Maximum, *Science*, **294**, 5548, 1917-1920.
- Thomson, J., Higgs, N.C., Croudace, I.W., Colley, S., Hydes, D.J.**, 1993. Redox zonation of elements at an oxic/post-oxic boundary in deep-sea sediments, *Geochimica et Cosmochimica Acta*, **57**, 579-595.
- Thomson, J., Higgs, N.C., Wilson, T.R.S., Croudace, I.W., De Lange, G.J., Van Santvoort, P.J.M.**, 1995. Redistribution and geochemical behaviour of redox-sensitive elements around S1, the most recent eastern Mediterranean sapropel, *Geochimica et Cosmochimica Acta*, **59**, 17, 3487-3501.
- Tuğrul, S., Baştürk, Ö., Saydam, C., Yılmaz, A.**, 1992. Changes in the hydrochemistry of the Black Sea inferred from water density profiles, *Nature*, **359**, 137-139.
- URL, webpage of Geotek MSCL:** <http://www.geotek.co.uk/products/mscl-s>. Retrieved in 15/03/2011.

- Wilkin, R.T., Arthur, M.A., Dean, W.E.,** 1997. History of water column anoxia in the Black Sea indicated by pyrite framboid size distributions, *Earth and Planetary Science Letters*, **148**, 3-4, 517-525.
- Wilkin, R.T., Arthur, M.A.,** 2000. Variations in pyrite texture, sulfur isotope composition, and iron systematics in the Black Sea:evidence for Late Pleistocene to Holocene excursions of the O₂-H₂S redox transition, *Geochimica et Cosmochimica Acta*, **65**, 9, 1399-1396.
- Yarincik, K.M., Murray, R.W., Lyons, T.W., Peterson, L.C., Haug, G.H.,** 2000. Oxygenation history of bottom waters in the Cariaco Basin, Venezuela, over the past 578,000 years: Results from redox-sensitive metals (Mo, V, Mn and Fe), *Paleoceanography*, **15**, 6, 593-604.

APPENDICES

APPENDIX A.1 : The detailed information about the sediment cores

Table A.1 : The detailed information about the sediment cores.

Seismic Line	Core Name	Location		Water Depth (m)	Length (cm)	AMS C14		
		N	E			Core Depth	Type	Cal Age BP
SL1	MSM015-300	41°22.31	29°08.34	82	61.5	-	-	-
	HBS09-G04C	41°28.68	29°14.81	122	71.5	-	-	-
	MSM015-245	41°28.91	29°15.07	152	70.5	42-44 cm	Mytilus	6810±84
	MSM015-192	41°30.14	29°16.34	307	111	-	-	-
SL8	HBS09-G18	41°30.61	29°03.41	93	71.5	21-23 cm	Cardium	505±25*
	HBS09-G17B	41°33.13	29°03.42	120	47.5	31-33 cm	Mytilus	6847±83
	HBS09-G15B	41°34.12	29°03.45	160	33.5	26-28 cm	Mytilus	5554±69
	MSM015-311	41°34.78	29°03.46	307	70.5	42-44 cm	Ammonia sp.	5325±98

*Uncalibrated ¹⁴C age.

CURRICULUM VITAE



Zeynep ERDEM

Address : Çamli Sok. Dostlar Apt. No:7/17 34740 Suadiye Istanbul Turkey
GSM : +90(533) 343 53 93
Home number: +90(216) 372 89 01
E-Mail : erdemz@itu.edu.tr

Personal Details:

Nationality : Turkish
Place of birth : Istanbul
Date of birth : 26/05/1985

Education:

MSc : Istanbul Technical University, Eurasian Institute of Earth Sciences,
2011
BSc : Istanbul Technical University, Department of Geological
Engineering, 2004 - 2008
High School :Kadıköy Anadolu Lisesi, Istanbul 1996 – 2004
Liceo Scientifico Ettore Majorana, Latina, Italy, 2002 - 2003

Foreign Languages:

English/Advanced
Italian/Upper Intermediate
French/Beginner

Research Interests:

Marine sciences
Geochemistry
Biogeochemistry
Paleoclimatology
Systematics of molluscs and foraminifers

Computer & Lab Skills:

Microsoft Office programs
CorelDraw and related image programs

MATLAB (beginner)
ArcGIS (beginner)

ITRAX XRF Core Scanner
Geotek (MSCL) Multi Sensor Core Logger
Schimadzu TOC Analyzer
Freeze Dryer

Trainings and Seminars:

2011 HYPOX Project 2nd Annual Meeting – Oral Presentation: Bosphorus area (and beyond). Basin history and past oxygen availability in the Black Sea: new findings from x-ray core scanning.
2011 64th Geological Congress of Turkey – Oral Presentation: Abstract: Effect of Mediterranean Inflow on Redox Conditions of the Istanbul Strait Outlet Area of the Black Sea.
2011 EGU – Oral Presentation: Abstract: Effect of Mediterranean Inflow on Redox Conditions of the Istanbul Strait Outlet Area of the Black Sea.
2010 HYPOX Project 1st Annual Meeting (Modelling Workshop)
2009 and 2010 Geological Congress of Turkey (62nd and 63rd)
2008 (France), 2009 (Turkey), 2010 (Hungary) European AFS volunteer summit and trainings
2002 – 2003 AFS Intercultural Student Exchange Program (study in Italy 10 months)

Internships:

2007 DSİ (State Hydraulic Works) XIV. Region Headquarters
2006 Eastern Mediterranean Centre for Oceanography and Limnology (EMCOL) laboratories

Thesis:

Sedimentary Record of Mediterranean Inflow Effect on Redox Conditions of the Istanbul Strait Outlet Area of the Black Sea, MSc. Thesis, ITU Eurasian Institute of Earth Sciences, Climate and Ocean Sciences, 2011.

Geology of Kilyos (Northern İstanbul) and The Sedimentological Properties of dunes in the region, BSc. Thesis, ITU, Faculty of Mines, Geology department, 2008.

Projects:

ICDP: PALEOVAN Project. 2010, TÜBİTAK (108Y279), Coordinator: Namık Çağatay.

In situ Monitoring of Oxygen Depletion in Hypoxic Ecosystem of Coastal and Open Seas and Land-locked Water Bodies (HYPOX), 2009, EC 7th Framework, ITU
Coordinator: Namık Çağatay

Research:

Researcher; laboratory, ICDP: PALEOVAN Sampling Party of Lake Van cores, 12-31 January 2011, MARUM, IODP-ICDP Core Repository, Bremen, Germany.

Researcher; URANIA 2010 Italian R/V Urania, Geophysical and geological studies in Sea of Marmara, 11 – 13 October 2010.

Researcher; laboratory, ICDP: PALEOVAN Lake Van, Turkey, 12 – 25 August 2010

Researcher; MSM-15/1 German R/V M.S.Merian, Geological and Geophysical Studies in Black Sea (Bosphorus Outlet Area), HYPOX project. 11 – 19 April 2010.

Researcher; Turkish R/V Arar, Geological and Geophysical Studies in Black Sea (Bosphorus Outlet Area), HYPOX project 9 – 20 November 2009.

Others:

Since 2007 Part time librarian in a private library

2007 - 2009 AFS Volunteer Association İstanbul region board member

2006 - 2008 ITU Geological Engineering Student Club board member